Modeling and Statistical Assessment of Fluid Migration Response in the Above Zone Monitoring Interval of a Geologic Carbon Storage Site

Submitted in partial fulfillment of the requirements for
the degree of
Doctor of Philosophy
in
Department of Civil & Environmental Engineering

Argha Namhata

B.Tech., Civil Engineering, National Institute of Technology, Durgapur, INDIA
M.S., Civil & Environmental Engineering, Carnegie Mellon University, USA

Carnegie Mellon University
Pittsburgh, PA 15213

August, 2016

Abstract

Carbon dioxide (CO_2) capture and storage (CCS) into geological formations is regarded as an important strategy for achieving a significant reduction in anthropogenic CO_2 emissions. An increasing emphasis on the industrial-scale implementation of CO_2 storage in geological formations has led to the development of whole-system models to evaluate the performance of candidate geologic storage sites and the environmental risk associated with them. The United States Department of Energy (DOE), through its National Risk Assessment Partnership (NRAP) Program, is conducting research to develop science-based methods to quantify the likelihood of risks associated with the long-term geologic storage of CO_2. A key component of this research is the development of an Integrated Assessment Model (IAM), which simulates the geologic storage system by integrating the primary sub-system components of the system for the purpose of elucidating the relationship between CO_2 injection into the subsurface and the short- and long-term containment of the stored CO_2. The sub-system components of that engineered geologic storage system include the storage reservoir, overlying aquitards (primary caprock and secondary seals) and aquifers (including the above zone monitoring interval, or AZMI, which directly overlays the primary seal), and potential leakage pathways including wells, fractures, and faults, to name a few. The subsystems are modeled using simplified reduced order models (ROMs), which are then coupled together to characterize the entire storage system. The construction of the IAM permits the quantification and assessment of the storage risks in a more computationally efficient manner as compared to the use of full physics-based models.

This Ph.D. research was initiated with a review of the IAM development efforts of NRAP and an assessment of the current status of the ROMs for each of the sub-system components of the storage system. In addition, gaps in the development in the IAM structure were identified. The research also investigated

the potential migration of subsurface fluids (i.e., CO_2 and formation brine) in geologic storage sites. Leakage of CO_2 and brine through the primary seal to the overlying porous and permeable formations, such as the AZMI, may occur due to the intrinsic permeability of the seal and/or the presence of natural fractures or induced perforations or fractures. Pressure modeling of the AZMI provides a useful source of information regarding seal performance and the subsurface pressure response to CO_2 leakage from the reservoir. As part of this research, a ROM for the AZMI, a missing component of the current IAM of NRAP, was developed. This AZMI ROM simulates fluid flow above the primary seal and predicts spatial changes in pressure over time due to this fluid migration from the reservoir. The performance of the AZMI ROM was verified using full physics-based models of the zone. A data-driven approach of arbitrary Polynomial Chaos (aPC) Expansion was then used to quantify the uncertainty in the pressure predictions in the AZMI based on the inherent variability of the different geologic parameters such as the porosity, permeability, and thickness of the AZMI, and the caprock permeability and thickness. The aPC approach, which represents the models as a polynomial-based response surface, was then used to perform stochastic model reduction. Finally, a global sensitivity analysis was performed with Sobol indices based on the aPC technique to determine the relative importance of the different system parameters on pressure prediction. The research results indicate that there can be substantial uncertainty in pressure prediction locally, around the leakage zones, and that the degree of the uncertainty depends on the quality of the site-specific information available for analysis. The research results confirm the need for site-specific data for the efficient predictions of risks associated with geologic storage activities. Lastly, the research investigated the use of the AZMI model outputs as a basis for the Bayesian design of a monitoring framework for this zone of a geologic carbon storage system. Monitoring of reservoir leakage requires the capability to intercept and resolve the onset, location, and volume of leakage in a systematic and timely manner. The results of this research suggest that an optimal monitoring system with these capabilities can be designed based on the characterization of potential CO_2 leakage scenarios that are determined using an assessment of the integrity and permeability of the caprock inferred from pressure measurements in the AZMI.

Acknowledgements

This work was primarily supported by the National Energy Technology Laboratory's Regional University Alliance (NETL-RUA) under the RES contract 1000025 (2013/ 14) and the Oak Ridge Institute for Science and Education (ORISE) doctoral research fellowship at NETL (2015/ 16). Additional support for tuition and research was provided by the Carnegie Mellon University (CMU) Dean's Fellowship (2013/14) and the Bertucci Graduate Fellowship (2014/15). Travel support to conferences was provided through Fenves travel grant and the Graduate Student Assembly travel fellowships.

I would like to thank my advisors Prof. Dr. David Nakles and Prof. Dr. Athanasios Karamalidis for their constant support and encouragement through the course of my graduate studies at CMU. I have had the liberty of dropping by their offices for brainstorming sessions to address questions that I've had. From them I've learnt the importance of being organized, committed, and professional in research, teaching, and professional service. I hope to carry forward these lessons for the rest of my career. I would also like to thank my NETL mentor and committee member, Dr. Robert Dilmore, for taking me in and showing me the ropes at NETL. Without Bob's support and research ideas this research would not have been possible. I would also like to thank my other committee members Prof. Dr. Mitchell Small and Prof. Dr. Sergey Oladyshkin for their insightful comments, ideas, and suggestions to improve my work. Despite his busy schedule, Mitch always made time to meet and discuss my work, which has been of enormous help in honing my statistics and modeling skills. I would especially like to thank Sergey, as well as Prof. Dr. Wolfgang Nowak and Prof. Dr. Holger Class of the University of Stuttgart for giving me an opportunity to attend the University of Stuttgart for a semester and collaborate with their research group. I had an inspiring learning experience during my research stay. I would also like to thank Prof. Dr. David Dzombak, Head of the Civil & Environmental Engineering

(CEE) Department for his constant encouragement and financial support from the department when required.

A part of the work presented in this thesis was conducted in collaboration with scientists at NETL and other Department of Energy laboratories through the National Risk Assessment Partnership. In particular, I would like to thank Dr. Seth King, Dr. Grant Bromhal, Dr. Ernest Lindner and Dr. Mark McKoy for their help during my appointment at NETL. I would also like to thank Dr. Haruko Wainwright, Dr. Erika Gasperikova and Dr. Tom Daley of the Lawrence Berkeley National Laboratory for providing some significant data used in this research as well as Dr. Rajesh Pawar of Los Alamos National Laboratory for helping me get started with Goldsim and CO_2 storage modeling during the initial phase of my Ph.D.

I am extremely grateful to my colleagues at CMU and NETL for their help during various stages of my Ph.D.: Dr. Liwei Zhang for his help in almost every aspect of my Ph.D. from explaining the theory to help with modeling, Dr. Ya-Mei Yang for her help with making me understand monitoring design and optimization concepts and Dr. Nick Azzolina and Dr. Zan Wang for providing research support when I needed. I would like to thank my friends at CMU especially, Aditya, Agniv, Arka, Arvind, Ashesh, Pranav, Prathamesh, Prashant, Subhro, and Vaibhav and Miaolei at NETL for their support. I have met a lot of interesting people over the past 4 years and have learnt something of value from each of them. I am grateful to all my friends in Pittsburgh, and India who've made this experience special. Apart from those mentioned above, I would like to thank Maxine Leffard and the CEE staff. Their hard work and effort have made international students like me feel at home at CEE.

I am thankful to my friends from high school and college especially Arghya, Arnab and Rahul who have been always by my side. Finally, I would like to thank my family - my sister, brother-in-law and my parents, who have made every effort possible to ensure my wellbeing and, Chandreyee, for her unconditional love and support and faith in me.

This page is intentionally left blank

Contents

List of Figures

List of Tables

Chapter 1

Introduction

Significant changes in average temperature around the globe over the past century have raised concerns regarding the stability of the earth's ecosystem. Projections of recent emission trends, assuming a business-as-usual scenario, suggest that potential temperature increases between 1.1 – 6.3 ^{o}C by the end of the 21st century (Bachu, 2008; IPCC, 2013). Increases in the atmospheric concentration of carbon dioxide (CO_2) and other greenhouse gases (GHGs) are considered one of the major causes of this rise in temperature (IPCC, 2013). An International Energy Agency (IEA) study indicates that CO_2 emissions will increase by 130% by 2050 in the absence of new policies or supply constraints because of increased fossil fuel usage (IEA, 2008; IEA, 2013). Addressing climate change through the reduction of anthropogenic greenhouse gas emissions is one of the most significant challenges of our time.

CO_2 capture and storage (CCS) is one of a portfolio of solutions for the reduction of anthropogenic greenhouse gas emissions to the atmosphere. This process involves separating CO_2 from the gaseous emissions of large industrial sources, compressing the CO_2 to form a liquid phase, transporting the liquid CO_2 via pipeline to an injection site, and injecting it into deep geologic formations. Specifically, underground formations such as depleted oil and gas reservoirs and deep saline formations are two of the targets most commonly considered for the

subsurface storage of CO_2 (IPCC, 2005). However, there are outstanding regulatory, market, and environmental hurdles to overcome before CCS can be widely deployed at a commercial scale.

The increasing emphasis on the commercialization and full-scale implementation of CCS has led to the development of mathematical models for the quantitative assessment of the performance of potential geologic storage sites and associated risks. The United States Department of Energy (DOE), through its National Risk Assessment Partnership (NRAP) Program (NETL, 2011), has been involved in this research, focusing on the development of modeling strategies for the geologic storage system, including sub-system component models and integrated assessment models (IAMs) for these applications (Pawar et al., 2016). The IAM for a geologic storage system couples predictive models of the primary sub-system components of the storage system (i.e., storage reservoir; caprock seal; migration pathways including wellbores, faults and fractures; groundwater aquifers; and the atmosphere), with the goal of assessing the long-term CO_2 storage security and environmental risk performance of the system. NRAP quantitative risk assessments consider multiple risks, including potential impairment of underground sources of drinking water and potential leakage of CO_2 to the atmosphere. The integration of complex models of the individual subsystem components of a geologic storage system to form an IAM would yield a model that is computationally expensive, requiring potentially hundreds of hours to run a single realization of the system performance. To circumvent this limitation, NRAP has elected to develop an IAM for the geologic storage of CO_2 by constructing computationally efficient reduced order models (ROMs) for the primary subsystem components for integration into the IAM. All of the ROMs

are developed and/or calibrated based on results from detailed, physics-based numerical models. Several types of ROMs have been developed, including simple correlations, look-up tables, analytical expressions, simple regressions, reduced physics models, and surrogate models (Zhang and Pau, 2012; Bromhal et al., 2014; Soeder et al., 2014). In all cases, the ROMs represent abstractions, when appropriate, and are based on detailed physical and chemical descriptions of the key subsystem components at the sites (Pawar et al., 2013).

Figure 1-1 presents a schematic of a typical geologic storage system. This research reviewed the status of the ROM development efforts of NRAP, examined their role in the CO_2 storage modeling research, highlighted the current issues and barriers to their development, and identified the outstanding gaps in the current model development efforts. This effort identified the need for a ROM to address the above zone monitoring interval (AZMI) of a geologic storage system, which is the zone that lies just above the caprock seal. Currently, the IAM of NRAP does not model the fate of CO_2 or brine in the AZMI or the region above it that lies between it and the nearest USDW; rather, it directly connects any leakage through the caprock to the nearest USDW using ROMs for well leakage and/or faults.

The primary focus of this research is on the development of a ROM for the above-zone monitoring interval (AZMI) of the geologic storage system to fill this gap in the NRAP modeling efforts. A combination of literature analysis, mathematical modeling, and statistical analysis is used to address this gap.

The thesis has four specific objectives. These objectives and the related

questions for which they provide answers are listed below:

Objective 1: Review and identify gaps in the CO_2 storage modeling efforts of NRAP.

a) What is the basic IAM structure being developed by NRAP? How does it address the geologic CO_2 storage system?

b) What are the different leakage pathways from the storage reservoir to critical human and environmental receptors?

c)What ROMs for the IAM framework currently exist in the literature or are under development?

d) What ROMs are still required to complete the NRAP IAM framework for a geologic storage system?

Objective 2: Develop a model to characterize fluid migration through above zone monitoring interval (AZMI) of a geologic storage system.

a) What is AZMI and how is it important in modeling the fate of fluid migration in a geologic storage system?

b) What is the mathematical formulation required to model fluid flow migration in the AZMI?

c)What geological properties of the AZMI play an important role in the model development?

d) What is the predictive ability of the AZMI ROM compared to a full physics simulator of the AZMI?

Objective 3: Quantify the uncertainty of the AZMI model predictions and identify the most critical parameters affecting the model outputs.

a) What is the uncertainty in the predictions of the AZMI ROM?

b) How does the model predictive behavior change over time and space?

c)What is the relative importance of model input parameters on its output?

Objective 4. Bayesian design of an above zone pressure monitoring program to detect leaks from the reservoir

a) What are the requirements of a monitoring framework for CO_2 storage?

b) How can the AZMI ROM results be used to statistically quantify potential leaks from the reservoir?

c)How will the AZMI ROM help provide a foundation for a Bayesian design of a subsurface monitoring program for a geologic storage system?

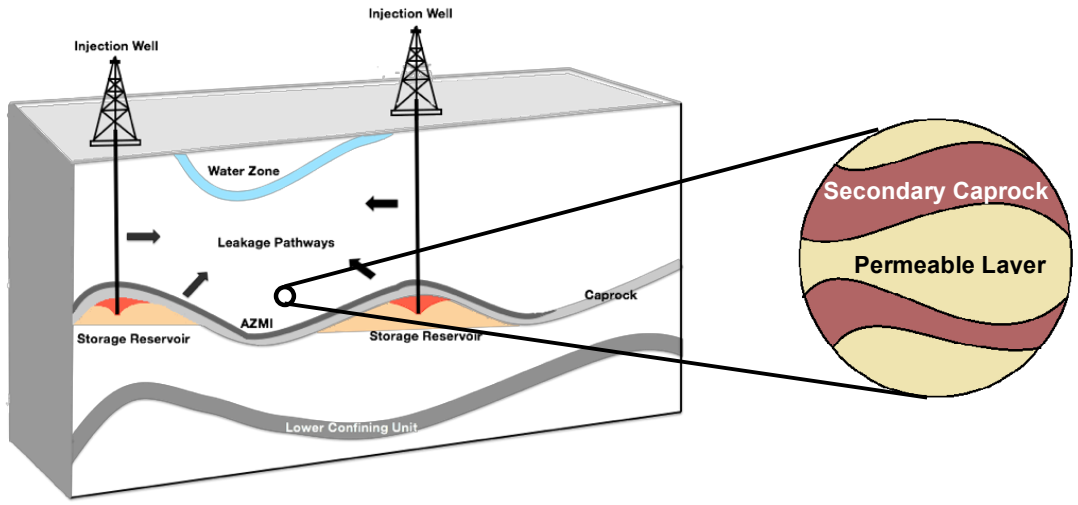

Figure 1-1: Schematic representing a typical geologic storage system. Components of the engineered geologic system include the storage reservoir, overlying aquitards (primary caprock and secondary seals) and aquifers (including the above zone monitoring interval, or AZMI, directly overlying the primary seal), and potential leakage pathways which include wells, fractures, and faults.

In addition to this introductory chapter, this dissertation consists of five chapters and three appendices. The main content of the thesis is presented in Chapters 2 to 5, which comprise materials submitted to, or in preparation for publication, in peer-reviewed journals and conference proceedings. Chapter 6 provides a summary of the major research findings. A brief description of each of these chapters as well as the three appendices follow.

Chapter 2 presents a literature review of the IAM development efforts being conducted by NRAP for the geologic storage of CO_2 storage. This chapter analyses the present components of the IAM and identifies technical gaps which represent future areas of research. These results have been published in the Proceedings of the Geological Society of America, Annual Meeting, 2015 under the title: *Development of an Integrated Assessment Model for CO_2 Storage: Overview and Areas of Future Development.* Mr. Argha Namhata was the primary author of this work with co-authors Dr. Athanasios K. Karamalidis, Dr. Robert M. Dilmore and Dr. David V. Nakles.

Chapter 3 presents a ROM that was developed to address a current gap in the NRAP IAM efforts for a geologic storage system. The new ROM was developed to characterize the migration of fluids and associated pressure and gas saturation changes in the Above Zone Monitoring Interval (AZMI) of a geologic carbon storage site. This model development effort was submitted for publication to the peer-reviewed journal, International Journal of Greenhouse Gas Control, under the title: *Modeling Pressure Changes due to Migration of Fluids into the Above Zone Monitoring Interval of a Geologic Carbon Storage Site*, and is currently under review. This manuscript was authored by Mr. Argha Namhata

and co-authored by Dr. Liwei Zhang, Dr. Robert M. Dilmore, Dr. Sergey Oladyshkin and Dr. David V. Nakles.

Chapter 4 describes an uncertainty quantification assessment of the AZMI ROM of Chapter 3. A data-driven approach of arbitrary Polynomial Chaos (aPC) Expansion is used to quantify the uncertainty in the above zone pressure predictions of the AZMI ROM based on the inherent uncertainties of different geologic parameters of the AZMI and caprock seal. Global sensitivity analysis is also performed with Sobol indices based on the aPC technique to determine the relative importance of these different parameters on pressure prediction. As part of this effort, the AZMI model was used to simulate pressure profiles in the AZMI of the Kimberlina geologic storage site in California, USA. The results of this uncertainty and sensitivity analysis have been incorporated into a manuscript titled, *Probabilistic Assessment of Above Zone Pressure Predictions at a Geologic Carbon Storage Site*, and was submitted to the peer-reviewed journal, Scientific Reports, and is currently under review. This manuscript was authored by Mr. Argha Namhata and coauthored by Dr. Sergey Oladyshkin, Dr. Robert M. Dilmore, Dr. Liwei Zhang and Dr. David V. Nakles.

Chapter 5 investigates the use of pressure measurements in the AZMI for the purpose of designing an AZMI monitoring system for the detection of leaks from the storage reservoir. Using Bayesian methods, the calculations of the time required to distinguish AZMI pressure outcomes and the associated leakage scenarios that produce them are presented. The results of this monitoring design assessment is being incorporated into a manuscript titled, *Bayesian Inference for Caprock Permeability Based on Above Zone Pressure Monitoring*, which will be

submitted to the peer reviewed journal, International Journal of Greenhouse Gas Control. This manuscript is being authored by Mr. Argha Namhata and coauthored by Dr. Mitchell J. Small, Dr. Robert M. Dilmore and Dr. David V. Nakles.

The last chapter of this dissertation, Chapter 6, summarizes the major findings of the research and identifies the specific contributions of the research to improving the understanding of subsurface fluid migration and environmental risks associated with the geologic storage of CO_2 storage. A brief discussion of the broader impact of the research beyond the geologic storage of CO_2 is also provided.

Appendices A, B and C provide supporting information for Chapters 2, 3 and 5, respectively.

Chapter 2

Overview and Gaps of the NRAP CO_2 Storage Modeling

The primary focus of this chapter is to review and summarize the existing literature of the modeling efforts of NRAP regarding the geologic storage of CO_2 and to present a preliminary assessment of the developing IAM framework. Given the spatial extent and complex heterogeneity of CO_2 subsurface storage sites, the development of a science-based IAM for risk assessment is challenging. The standard approach being used by NRAP, which is designed to support a quantitative environmental risk assessment, is to treat the overall system as a set of coupled subsystem components, each of which embodies a unique set of physical and chemical characteristics and processes. This approach assumes that these subsystems can be treated independently (i.e., the feedback between system components can be neglected), with their coupling occurring explicitly within the IAM (Pawar et al., 2013, 2016). The environmental risks considered by NRAP are the potential impact to overlying receptors, i.e., changes in groundwater quality in response to possible leaks of CO_2 and/or brine and CO_2 leakage to the atmosphere, and the potential to induce seismic response. NRAP considers risk proxies (or midpoint indicators of human health impact or ecosystem impact), such as amount of CO_2 leaked or volume of groundwater impacted by composition change, rather than endpoint indicators of human health impact or

ecosystem impact. In this chapter, we are considering only the leakage-related ROMs and not the ROM related to induced seismicity.

The IAMs are system-based models that simulate the response, through time, of the engineered geologic system to large-scale CO_2 injection by coupling the primary subsystem components of the system, i.e., storage reservoir formation, migration pathways (i.e., seals, wellbores, faults and fractures), and the overlying aquifers. The overall goal of the IAM is to elucidate the relationship between effective CO_2 storage and short- and long-term security. A simplified schematic of the conceptual IAM structure and the corresponding risk assessment and management framework are shown in Figure 2-1. ROMs have been developed for each of the sub-system level components of the IAM. The description of the existing ROMs is discussed in § 2.1.–2.3. Table 2-1 shows the development efforts of different ROMs in NRAP.

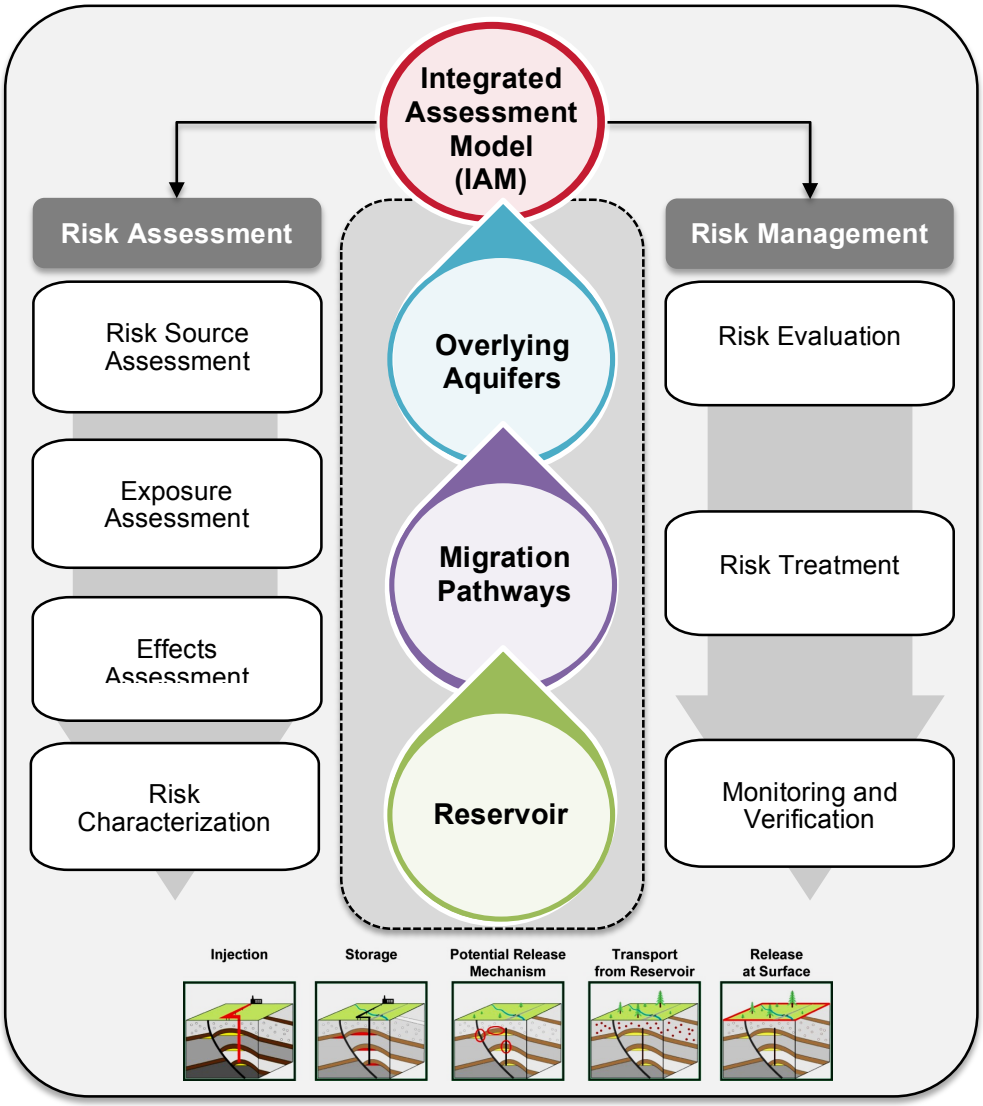

Figure 2-1: Schematic structure of the conceptual Integrated Assessment Model. The IAM is assumed to comprise of three primary components: reservoir, migration pathways and the overlying aquifers.

Table 2-1: Summary of ROM development efforts of NRAP as reported in publicly available literature as of January 2016.

Component	Primary Reporting Organization	Name of the Model	Model Outputs
Reservoirs	NETL	Polynomial Chaos Expansion (PCE) ROM	Pressures and Saturations over time
		Grid Based Surrogate Reservoir Model (SRM)	Pressures and Saturations over time
	LBNL	Brine Reservoir ROM for Kimberlana site	Pressure, CO_2 and brine saturations over time.
Migration Pathways (Wellbores, Faults and Seals)	NETL	NSealR	CO_2 and Brine mass flux with time.
		Wellbore Cement ROM	Change in cement porosity and permeability with time
	LANL/LLNL	Wellbore ROM	CO_2 and Brine flow rate
	LBNL	Wellbore ROM	CO_2 and Brine flow rate
	LLNL	Fault ROM	CO_2 and Brine flow rate
Groundwater	LLNL/LBNL	High Plains Aquifer ROM	Changes in pH, TDS, trace metal and organic concentration profiles and CO_2 leakage rate out of aquifer.
	LANL/PNNL	Edwards' Aquifer ROM	Changes in pH, TDS, trace metal and organic concentration profiles and CO_2 leakage rate out of aquifer.

** NETL : National Energy Technology Laboratory, LBNL: Lawrence Berkeley National Laboratory, LANL: Los Altmos National Laboratory, LLNL: Lawerence Livermore National Laboratory, PNNL: Pacific Northwest National Laboratory*

2.1 STORAGE RESERVOIRS

Reservoirs are usually classified either on the basis of the types of fluids occupying the pore space, by whether they are on or off structure, or by the type of geologic formation. NRAP has been focused on developing reservoir ROMs for the three major types of fluid-filled formations: saline, oil, and gas reservoirs. The outputs of the reservoir ROMs are predictions of CO_2 and formation fluid pressures and saturations over time at the reservoir-seal interface. Typical input parameters include porosity, permeability, and injection rates, pressures and durations. The reservoir ROMs are being used to conduct sensitivity analyses of these input parameters and their impacts on pressure and saturation responses as a means of identifying the key variables for further detailed analysis. To date, five types of ROMs have been evaluated: (1) Look-up tables; (2) Response surfaces; (3) Polynomial chaos expansion or PCE; (4) Surrogate reservoir models, or SRM (artificial intelligence and data mining) and (5) Gaussian process regression. A description on each of the individual ROMs is provided in Appendix A.1.

2.2 RELEASE AND TRANSPORT (Wellbores, Seals, Faults and Fractures)

NRAP has developed ROMs to simulate and compute the flow of CO_2 and formation brines through different potential migration, or leakage, pathways from the reservoir. These leakage pathways include seals, wellbores, and other anthropogenic and natural features of the storage system. These ROMs can efficiently model fluid flow from the reservoir to environmental receptors of interest in risk assessments such as drinking water aquifers or the atmosphere.

The ROMs use site-specific input parameters including information on the seals, wellbores, faults and fractures, geological properties of the subsurface and chemical and physical properties of the subsurface fluids.

2.2.1 Wellbore ROMs

The wellbore ROM developed within the NRAP framework is called the Well Leakage Analysis Tool (WLAT) (Huerta and Vasylkivska, 2015). The WLAT is a standalone tool that contains four reduced-physics models or reduced-order models (ROMs) for well leakage. These tools assesses the behavior of a leaky well given different assumptions, well geometries, and leakage scenarios. These tools can be used to help quantify the uncertainty associated with geologic CO_2 storage and to develop strategies to reduce the risk associated with these operations. The WLAT generates leakage rates of CO_2 and other reservoir fluids over time through the wellbore. These ROMs receives inputs of pressure and saturation from the reservoir ROMs and generates outputs that report to thief zones in the overburden and/or come into contact with receptors such as groundwater sources of drinking water and/or the atmosphere. The four wellbore models which WLAT comprises are the cemented wellbore, multi-segmented wellbore, open wellbore and the brine leakage model (See Appendix A.2 for more details).

2.2.2 Seal ROMs

NRAP has developed a ROM for seals, NSealR (Lindner, 2015), which can be used to model possible flow of CO_2 and other reservoir fluids over time

through the caprock overlying a reservoir as well as other seals within the geologic storage site. NSealR receives inputs of pressure and saturation from the reservoir ROMs and will generate outputs based on a uniform permeability assigned to the seal, a single leaking fracture or fault, or a multiple fracture network within the seal. This seal integrity ROM is more portable than reservoir ROMs and will help to operationalize storage by providing efficient modeling of fluid flow from the reservoir-seal interface upward to various environmental receptors in the overburden zone of interest in risk assessments.

NSealR provides for the simulation of CO_2 flow through the seal barrier horizon, a rock formation that is assumed to be a relatively impermeable, rock unit initially saturated with a saline groundwater. A two-phase, relative permeability approach and Darcy's law are used for one-dimension (1-D) flow computations of CO_2 through the horizon in the vertical direction (See Appendix A.3 for more details).

2.2.3 Fault and Fracture ROMs

Fractures represent a common pathway for vertical flow in a CO_2 storage system and the current ROMs use both discrete fracture (partially transferable, specific to depth of reservoir and depths of receptors) and fracture-network (fully transferable) approaches. The transmissive fault ROM has been built using simulations of discrete fracture flow under varying geo-mechanical conditions to predict fluid migration through a fault between the reservoir and a groundwater aquifer. The fracture network model uses simplified physics models for flow through a fractured caprock, using up-scaled parameters for transmissivity and

has been tested against discrete fractured network flow models (e.g., NSealR). These current ROMs can be applied to seals of varying depths and sets of reservoir conditions.

2.3 GROUNDWATER ROMs

The groundwater tool developed within the NRAP framework is called the Aquifer Impact Model (AIM) (Bacon et al., 2014). The AIM tool comprises of groundwater ROMs that have been developed using data and modeling results for two different aquifers:

a) An unconfined sandstone in a reducing environment (High Plains Aquifer),
b) An unconfined limestone in an oxidizing environment (Edward's Aquifer).

Together, these aquifers broadly represent conditions found in 60% of the aquifers in the United States. Additionally, a "no impact" threshold criterion has been established as a benchmark against which to compare calculated, site-specific impacts to an aquifer for TDS, pH, select metals and select organics (NETL, 2014b).

The ROM developed from the High Plains Aquifer is summarized in Carroll et al., (2014). The groundwater ROMs have been designed to predict the evolution of several groundwater metrics over time in response to impacts from the leakage of CO_2 and/or formation brine. The ROMs are based on simulations from continuum-scale reactive transport simulations in which the inherent

uncertainties in the groundwater system were propagated throughout the predictive process. The focus was on assessing a variety of conditions including the magnitude of trace element source terms, the impact of leakage from multiple sources and aquifer heterogeneity, to name a few. Potentially variable parameters that were considered included aquifer heterogeneity, permeability, porosity, regional groundwater flow, and CO_2 and total dissolved solids (TDS) leakage rates over time.

The next steps in groundwater ROM development involve adapting the ROMs to various leakage scenarios, particularly those with multiple sources; the consideration of ROMs for additional aquifer types; the validation of flow predictions based on coupled groundwater/wellbore ROMs; and potentially the expansion of the "no impact" threshold technique to other aquifer types. (NETL, 2014b).

2.4 AREAS OF DEVELOPMENT

The current IAM directly connects leakage from the reservoir, through wellbores, seals or other migration pathways, to the environmental receptors of interest such as drinking water aquifers and/or the atmosphere. These direct linkages bypass the heterogeneous overburden that lies between the interval just above the seal and these primary risk receptors. Since the zone overlying the seal consists of sequences of high permeable and low permeable geologic systems, a more accurate prediction of leakages to the groundwater resources requires the detailed modeling of this intermediate vadose zone, which can be conceptualized as a stack of several low permeable seal models with some high permeable zones

in between them. The first such zone, immediately above the primary seal, is defined as the Above Zone Monitoring Interval, or, AZMI (see Figure 1-1 for AZMI location in the geologic system).

Development of a ROM for migration of gases through the AZMI is the second primary objective of this research. Chapter 3 describes the development and numerical formulation of this ROM. The development of this ROM will permit the creation of an IAM that more realistically links the reservoir and wellbore/seal ROMs to the groundwater ROMs.

Chapter 3

Characterization of Pressure and Gas Saturation due to Fluid Migration into the Above Zone Monitoring Interval

This chapter presents a ROM developed to predict pressure changes due to migration of fluids into the above zone monitoring interval (AZMI), which is an important component of the IAM. A flux aggregation approach is developed and applied in the ROM to significantly reduce the computational time of the model without compromising the accuracy of the model predictions.

In its simplest form, a geologic storage system can be considered to be made up of three components: (1) the porous/permeable storage reservoir formation where the CO_2 is injected and stored; (2) a relatively impervious rock layer designated as the seal or caprock, which overlays the reservoir; and (3) a heterogeneous geologic zone, which extends from above the caprock to the deepest underground source of drinking water. The caprock overlying the reservoir has an intrinsic permeability through which CO_2 may leak; in a good candidate storage site, that intrinsic caprock permeability will be quite low. These sealing layers may also contain natural faults or fractures and other

leakage pathways (e.g., legacy wells), all of which may represent potential conduits for the vertical migration of injected CO_2 and connate brine to overlying formations and potentially to overlying receptors of concern. To verify storage permanence and understand the extent of potential unwanted fluid migration in the subsurface, it is important to design approaches to effectively and efficiently monitor the performance of these engineering systems. One way to detect such leakage is the use of atmospheric or near-surface monitoring technologies; however, these techniques may not identify leaks until after receptors of concern have been impacted. It may be useful to couple near-surface measurement to verify that those receptors of concern are not endangered, with direct or indirect deep subsurface monitoring techniques to detect potential unwanted conditions near the storage reservoir. Ideally, these deep monitoring techniques will have the capability to identify and resolve the onset, location, and volume of leakage from the reservoir in a systematic and timely manner. The monitoring of pressure changes, as an indication of leakage, represents one such approach (Azzolina et al., 2014; Jung et al., 2013; Sun and Nicot, 2012; Wang and Small, 2015). Recent studies (Nicot et al., 2009; Hovorka et al., 2013) show the potential utility of monitoring to detect and estimate leakage and pressure changes above the caprock.

There have been numerous studies about numerical simulation of geologic CO_2 storage (e.g., Oldenburg et al., 2001; Nordbotten et al., 2004; Pruess, 2004; Xu et al., 2004; Bielinski, 2007; Bryant et al., 2008; Jiang, 2011; Pruess and Nordbotten, 2011; Cihan et al., 2012, Vilarassa et al., 2013; Heath et al., 2014). These models range from simplified analytical approaches to three-dimensional (3D) multi-phase and multi-component models. U.S. DOE (2009) provides an

extensive list of 20 numerical codes that have been applied to understand the geologic CO_2 storage performance. Numerical models that couple physics, chemistry, and/or geomechanics can generate high quality, technically credible and defensible results. These models are, however, computationally expensive, often requiring tens of hours to calculate a single realization; this limits their utility for rapid scenario evaluation, sensitivity analysis, and uncertainty quantification, which could call for the calculation of hundreds or thousands of realizations. The aim of this study is to develop a ROM to simulate the pressure and CO_2 saturation response over time in the geologic interval directly above the primary seal of the geologic storage confining system, termed the above zone monitoring interval (AZMI), which results from fluid migration from the storage reservoir. The construction of a computationally efficient ROM for the AZMI represents a useful addition to the NRAP M for CO_2 storage because it allows consideration of the AZMI response to potential CO_2 leakage from the storage interval, and exploration of how that signal can be used for deep subsurface monitoring and early detection of unexpected leakage through the seal. A generalized schematic of the IAM framework into which the AZMI ROM will be integrated is shown in Figure 3-1. The figure outlines the hierarchy of sub-system level ROMs as they reside within a proposed IAM framework, and how information is passed betwee en them. Stated simply, in that hypothetical IAM framework the results from storage reservoir ROM (pressure and saturation at the reservoir/seal interface) are passed on to the primary seal ROM which then passes the information to the AZMI ROM, and so on, capturing important fluid flow and pressure response through the system. In the present study, development of a ROM that predicts changes in pressure in the AZMI due to fluid leakage from the reservoir and CO_2 flow through brine saturated geologic

formations is targeted. This chapter provides a description of the AZMI model formulation (§ 3.1), discusses a baseline case study of its application (§ 3.2), and summarizes the base case study results and the verification of the ROM performance based on comparison with comparable results from a detailed numerical model - TOUGH2 (Pruess, 2005).

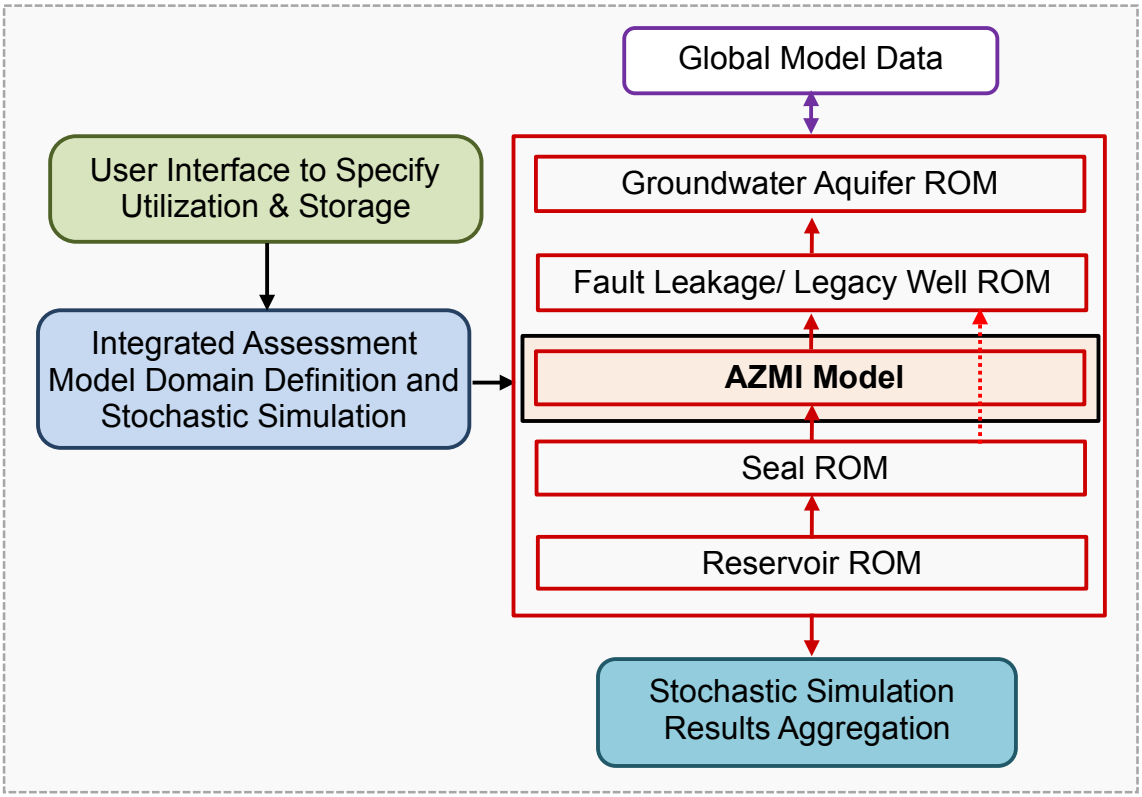

Figure 3-1: Integrated Assessment Model (IAM) structure showing position of AZMI ROM in the systems level hierarchy. The model structure acts as a basis to the IAM modeling algorithm where the user defines the storage scenarios, geologic conditions and simulation properties. Each ROM (in red box) passes input to the overlying receptors.

NOMENCLATURE

Symbol	[dimensions]	Parameter
α	[–]	Fluid phase: CO_2 and brine
S_α	[–]	α – phase saturation
ρ_α	[ML^{-3}]	Fluid density in the α – phase
ϕ	[–]	Porosity
t	[T]	Time
$\boldsymbol{q}_\alpha$	[LT^{-1}]	Darcy flux of the α – phase
S_e	[–]	Effective saturation
S_{rb}	[–]	Residual brine saturation
k	[L^2]	Intrinsic permeability
$k_{r\alpha}$	[–]	Relative permeability of the α – phase
μ_α	[$ML^{-1}T^{-1}$]	Viscosity of the α – phase
P_α	[$ML^{-1}T^{-2}$]	Pressure of the α – phase
g	[LT^{-2}]	Gravitational acceleration constant
z	[L]	Vertical coordinate
$Q_\alpha^{(j)}$	[L^3T^{-1}]	Total flux flow in α – phase for j^{th} cluster
j	[–]	Cluster number and j = {1,2,...,k}
$q_{\alpha,i}$	[L^3T^{-1}]	Flux flow in α – phase for i^{th} cell
m	[–]	Number of cells in j^{th} cluster
$\boldsymbol{B}$	[L]	Thickness of AZMI
b	[L]	Thickness of CO_2 plume
r	[L]	Radius of CO_2 plume
λ	[$M^{-1}LT$]	Total mobility
$\overline{p}$	[$ML^{-1}T^{-2}$]	Vertically averaged pressure governing flow of composite fluid
δ	[L^{-2}]	Dirac delta function
X_{well}	[–]	Distance to the location of k-means centroid or the "pseudo injection points" from corresponding point.

Dimension abbreviations are as follows: L = length, T = time, and M = mass.

3.1 ABOVE ZONE MONITORING INTERVAL (AZMI) ROM

As described in the previous section, the AZMI is the porous and permeable geologic interval directly above the primary seal of the geologic storage confining system, i.e., the geologic structure immediately overlying the impermeable caprock layer. The AZMI ROM divides the model domain into 10,000 uniformly sized grid blocks (100 by 100 gridblock array), with the dimensions of each grid block dictated by the size of the domain required to represent site-scale geologic storage. The 100 by 100 grid system is selected to match that prescribed for reservoir resolution in NRAP's IAM (for potential integration at a later stage), though the AZMI ROM is designed as a stand-alone ROM. As can be seen from the hypothetical systems level hierarchy (Figure 3-1), the flux output from the seal ROM is the primary input for the AZMI model, which it receives for each time step. In the present study, CO_2 and brine flux are used as input. TOUGH2 is used to create these flux inputs from the seal. However, the AZMI model can accept input from any seal model as long as those inputs are consistent with the AZMI modeling structure.

3.1.1 AZMI ROM Assumptions

There are certain theoretical assumptions that underlie, and are embedded within, the AZMI ROM. The AZMI model assumes that the subsurface layer of interest is situated at a sufficient depth to ensure that free CO_2 remains in the supercritical state (i.e., the depth of the AZMI should be more than $\sim$735 m). In addition, it is assumed that the AZMI is initially saturated with brine, with open lateral and vertical boundaries. For computational purposes, only vertical one-

dimensional flow is considered for the flux, and geomechanical impacts on the AZMI response are neglected. Flow is also considered laminar, permitting the application of Darcy's law. It is assumed that the flux entering the AZMI from the caprock seal is comprised of two phases - CO_2 and brine (Nordbotten and Celia, 2006; Lindner, 2015). The impact of CO_2 dissolution in brine within the AZMI is neglected. In this system, CO_2 is considered the non-wetting fluid and brine is considered the wetting fluid.

3.1.2 Governing Equations for Two-Phase Flow

The AZMI ROM predicts changes in pressure and CO_2 saturation responses over time and space within the AZMI. This predictive capability provides an assessment of the extent of fluid migration from the reservoir in cases of heterogeneous caprock permeability. It also helps in understanding the subsurface response, and implications of that response, for diagnostic purposes of seal integrity, plume disposition, pressure based monitoring and related uncertainties. The ROM is also able to predict the gas saturations above the AZMI.

The widely employed mass and momentum conservation equations are used to describe two-phase flow in the AZMI. As part of the momentum balance, Darcy's law is extended to multi-phase flow using the additional constraint:

$$S_{brine} + S_{CO_2} = 1 \tag{3.1}$$

For laminar flow, Darcy's law for fluid α (under the assumption of negligible capillary pressure) is expressed as:

$$\mathbf{q}_\alpha = -\frac{k k_{r\alpha}}{\mu_\alpha} \nabla (p - \rho_\alpha g z) \tag{3.2}$$

The mass conservation equation for CO_2 and brine is then expressed as:

$$\frac{\partial}{\partial t} \phi \rho_\alpha S_\alpha + \nabla \cdot \mathbf{q}_\alpha = 0 \tag{3.3}$$

The relative permeability of phase α is defined as:

$$k_{r\alpha} = \frac{k_\alpha}{k} \tag{3.4}$$

3.1.3 Closure Relations

Relative permeability has important implications for fluid flow in subsurface geological systems. The two most widely used models developed to formulate relative permeability are the Brooks-Corey (Krevor at al., 2012; Saadatpoor et al., 2010) and van Genuchten (Bielinski, 2007; Lucier et al., 2006) models. In this study, the Brooks-Corey Model is used to define relative permeability in the AZMI ROM.

According to Brooks and Corey (1966), the relative permeability for brine ($k_{r,brine}$) and CO_2 ($k_{r,CO2}$) can be represented as:

$$k_{r,brine} = {S_e}^{[\frac{2+3\beta}{\beta}]} \tag{3.5}$$

$$k_{r,CO_2} = 1 - {S_e}^2[1 - S_e^{[\frac{2+3\beta}{\beta}]}] \tag{3.6}$$

where, the Brooks-Corey parameter β is related to the distribution of pore sizes and the effective saturation (S_e) is defined as the normalized wetting phase saturation adjusted to define two-phase flow in the different zones of interest (Lindner, 2015; Luckner et al., 1989). In the case of low wetting phase saturations, there exists a zone where the flow of the wetting phase does not remain coherent and is defined as the residual wetting phase (the brine in this study) saturation. Similarly, at high wetting phase saturations, there exists a zone where the flow of the non-wetting phase (the CO_2 in this study) does not remain coherent and is defined as residual non-wetting phase saturations. Since both CO_2 and brine exhibit coherent flow, the effective saturation is defined in the AZMI ROM as:

$$S_e = \begin{cases} (\frac{S_{brine} - S_{r,brine}}{1 - S_{r,brine} - S_{r,CO_2}}), & if, S_{r,brine} < S_{brine} < (1 - S_{r,CO_2}) \\ 0, & if, S_{brine} \leq S_{r,brine} \\ 1, & if, S_{brine} \geq (1 - S_{r,CO_2}) \end{cases} \tag{3.7}$$

When two immiscible phases exist within the same pore space, there is an interfacial tension between the two phases that results in a pressure differential, which must be overcome to initiate flow. The pressure differential between the two phases (i.e., wetting and non-wetting phase) is called the capillary pressure (P_c). Capillary pressure highly influences the flow processes and can also prevent

the upward migration of CO_2 in geologic storage formations (Lindner, 2015; Chalbaud et al., 2010; Nielsen, 2012).

With CO_2 and brine as the two phases, capillary pressure is defined as:

$$P_c = P_{CO_2} - P_{brine} \tag{3.8}$$

The experimental findings of Brooks and Corey established that capillary pressure can be related to effective saturation using a power law:

$$P_c = \left[\frac{P_b}{(S_e)^{\frac{1}{\beta}}}\right], if\ 0 < S_e \leq 1 \tag{3.9}$$

where, P_b is a material constant, termed as the bubbling pressure. This constant is essentially a curve fitting parameter for the Brooks and Corey relative permeability model.

3.1.4 k-means Clustering

As described previously, the AZMI model is constructed to accommodate 100 by 100 grid blocks, receiving flux input from the seal model for each of the individual blocks. Rather than manage each of these fluxes individually, which can become computationally intensive, a flux aggregation approach using k-means spatial clustering is used to describe the CO_2 and brine fluxes of the entire space. The following section explains the pressure response calculation performed using this approach.

To increase the computational efficiency of the AZMI ROM, the system space is aggregated into a few clusters with similar properties/features (In this research, the seal property, permeability, was used). The spatial clustering is based on a widely accepted cluster analysis methodology in data mining known as k-means clustering (MacQueen, 1967). The concept of k-means clustering aims to partition a given set of n data, $\{x^{(1)}, x^{(2)},\ldots\ldots, x^{(n)}\}$, into a few "cohesive" k clusters in which each data point belongs to the cluster with the nearest mean, serving as a prototype of the cluster.

A flux-based aggregation approach, in which the fluid flux coming from the seal in each grid block present in the individual clusters is used to compute the total CO_2 and brine flow in each of these clusters, was developed for this research. The total incoming flux is assumed to enter the AZMI from the centroid of the individual clusters. Mathematically, total incoming volumetric flux flow of the a – phase for the j^{th} cluster (among "k" number of clusters) containing "m" number of grid blocks can be represented as:

$$Q_\alpha{}^j = \sum_{i=1}^{m} q_{\alpha_i}^j \tag{3.10}$$

In the current model, for a set of 10,000 data points (each grid in the 100 by 100 grid block system represents a data point), five clusters have been used for the simulations since the seal permeability has five high permeable regions. The user can also use the model for different sets of clusters as intended. With a greater number of clusters, the prediction will more accurately match that of the detailed numerical simulation; however, at the same time, the computational time will also increase.

3.1.5 Analytical Solution

The AZMI ROM uses the analytical solution for CO_2 plume movement in the storage formation derived by Nordbotten et al. (2005) to quantify pressure changes in the zone overlying the caprock due to the leakage of CO_2 through the caprock. The solution for CO_2 flow in a brine-saturated formation developed by Nordbotten et. al., was modified slightly to account for differences in formation thickness and the possibility of occurrence of a CO_2 front during the flow. With this conceptual framework and other assumptions based on the Nordbotten solution, the following equation, which governs the flow of composite fluid over the entire AZMI thickness, was derived:

$$-kB\nabla \cdot (\lambda \nabla \bar{p}) = {Q_\alpha}^j \delta(X - X_{well}) \tag{3.11}$$

The individual phase mobility is defined as the relative permeability of the phase to that of fluid viscosity, $\lambda_\alpha = k_{r\alpha} / \mu_\alpha$.

A general schematic of this flow system is shown in Figure 3-2. The continuous solution to Eq. (3.11) is as follows:

$$P(r,t) - P_0 = -\frac{{Q_\alpha}^j}{2\pi\lambda_{brine}k} \int_{r_{well}}^{R} \frac{dr}{r[(\lambda - 1)b(r) + B]} \tag{3.12}$$

$$\int_0^B \phi\pi r^2 db = \int_0^t {Q_\alpha}^j(t)\, dt = V(t) \tag{3.13}$$

The thickness b of CO_2 plume was derived as a function of radial distance, as shown below:

$$\frac{b(r,t)}{B} = \frac{1}{\lambda_{CO_2} - \lambda_{brine}} \left[\sqrt{\frac{\lambda_{CO_2}\lambda_{brine}V(t)}{\phi\pi B r^2}} - \lambda_{brine} \right] \tag{3.14}$$

where ,

$$\lambda = \frac{b}{B}\lambda_{CO_2} + \frac{(B-b)}{B}\lambda_{brine} \tag{3.15}$$

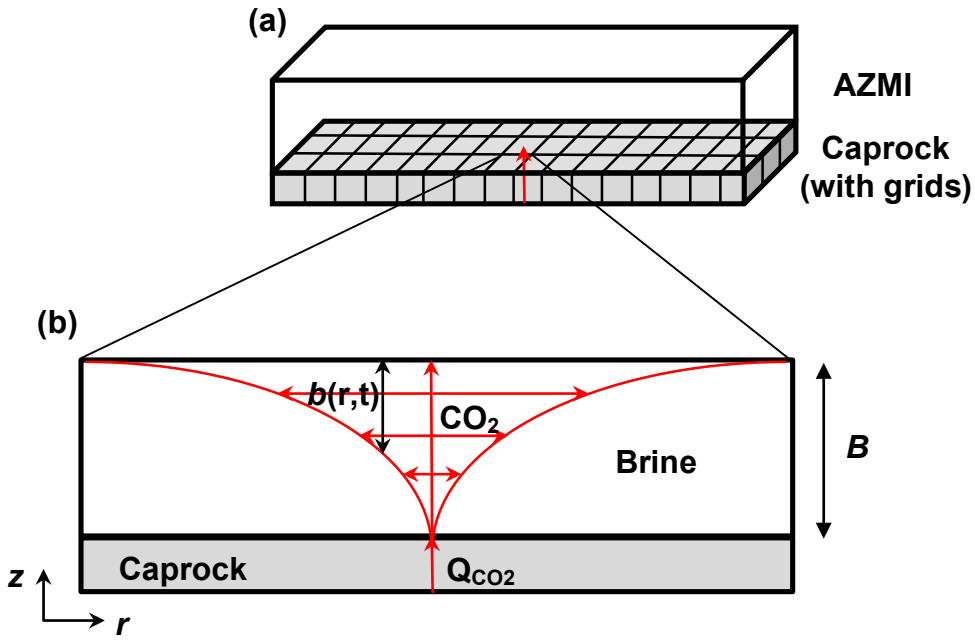

Figure 3-2: Schematic diagram showing: (a) aggregated CO_2 flux at j^{th} cluster (in red) containing *"m"* number of grid blocks (in grey); (b) a typical profile of CO_2 region denoted by b(r,t) in AZMI.

To reduce the computational time of the model, e non-linear, second order ordinary differential form of the solution was broken into a step-wise form. Thus,

the solution to Eq. (3.11) can be represented, as shown below, to predict CO_2 pressure response:

$$\left|P_{CO_2}(r,t)-P_0\right|^j = \begin{cases} -\frac{{Q_{CO_2}}^j}{2\pi KB}\left\{\frac{1}{\lambda_{CO_2}}\ln\left(\frac{r}{a_2}\right)+\left[\frac{B}{b\lambda_{CO_2}+(B-b)\lambda_{brine}}\right]\ln\left(\frac{a_2}{a_1}\right)+\frac{1}{\lambda_{brine}}\ln\left(\frac{a_1}{R}\right)\right\}, & r_{well}<r<a_2, \\ -\frac{{Q_{CO_2}}^j}{2\pi KB}\left\{\left[\frac{B}{b\lambda_{CO_2}+(B-b)\lambda_{brine}}\right]\ln\left(\frac{r}{a_1}\right)+\frac{1}{\lambda_{brine}}\ln\left(\frac{a_1}{R}\right)\right\}, & a_2<r<a_1, \\ -\frac{{Q_{CO_2}}^j}{2\pi KB}\left\{\frac{1}{\lambda_{brine}}\ln\left(\frac{r}{R}\right)\right\}, & a_1<r<R. \end{cases} \tag{3.16}$$

where,

$$a_1=\sqrt{\frac{\lambda_{CO_2}V(t)}{\phi\pi(b\lambda_{CO_2}+(B-b)\lambda_{brine})}} \qquad a_2=\sqrt{\frac{\lambda_{brine}V(t)}{\phi\pi(b\lambda_{CO_2}+(B-b)\lambda_{brine})}} \tag{3.17}$$

Eq. (3.16) calculates the changes in pressure from fluid migration into the AZMI for the j^{th} cluster. We then use superposition of the pressure change response vectors resulting from the flux aggregation of each of the clusters to compute the cumulative pressure change in the AZMI.

$${\Delta P_{CO_2}}^j=\left|P_{CO_2}(r,t)-P_0\right|^j \tag{3.18}$$

$$\Delta P_{AZMI}=\sum_{j=1}^{k}{\Delta P_{CO_2}}^j \tag{3.19}$$

3.1.6 Fluid Properties

Fluid properties such as density and viscosity play an important role in the quantification of fluid flow in a porous media. These properties of CO_2 are functions of temperature and pressure of the formation, which in turn are functions of its depth. The density and viscosity of brine are functions of salinity as well. Therefore, to compute the fluid properties, the temperature and pressure for the formation were assumed to have a gradient of 0.025^{o}C/m and 0.01 MPa/m, respectively (Raza, 2009; Szulczewski and Juanes, 2009). These fluid property variations with depth were incorporated into the AZMI ROM as detailed in Appendix B, Section B-1. Since the impact of CO_2 dissolution in brine has been ignored in this work, its impact on the density of brine does not play a role (Meng and Jiang, 2014).

3.2 BASE CASE ANALYSIS

3.2.1 AZMI Model Base Case Setup

A hypothetical AZMI system was defined and is used as the subject of the base case analysis. This system consists of AZMI layer overlying a 10 m thick primary seal and 100 m thick storage reservoir. The reservoir is located at a depth of 1000 m. The areal extent of the subsurface storage system is defined as 10 kms $\times$ 10 kms. The reservoir and seal features used in this study are shown in Table 3-1. CO_2 is injected into the storage aquifer at a rate of 1 MT per year for a period of 30 years. CO_2 and brine flux from the seal are simulated for a period of 30 years of injection and 170 years of post-injection using TOUGH2. It is

assumed that the AZMI layer has a porosity of 0.1 and a permeability of 10.5 mD. The residual CO_2 and brine saturations were set at 0.01 and 0.02 respectively and the bubbling pressure was set to equal 0.01 MPa. The reference CO_2 and brine viscosities, and CO_2 and brine density corresponding to the AZMI were calculated from the lookup tables as described in § 3.1.6 (Appendix B, Section B-1). The study addresses two different AZMI scenarios of varying thickness: Scenario I is based on a 3 m thick AZMI and Scenario II is based on a 90 m thick AZMI. Figure 3-3 describes the geologic profile of these benchmark storage scenarios.

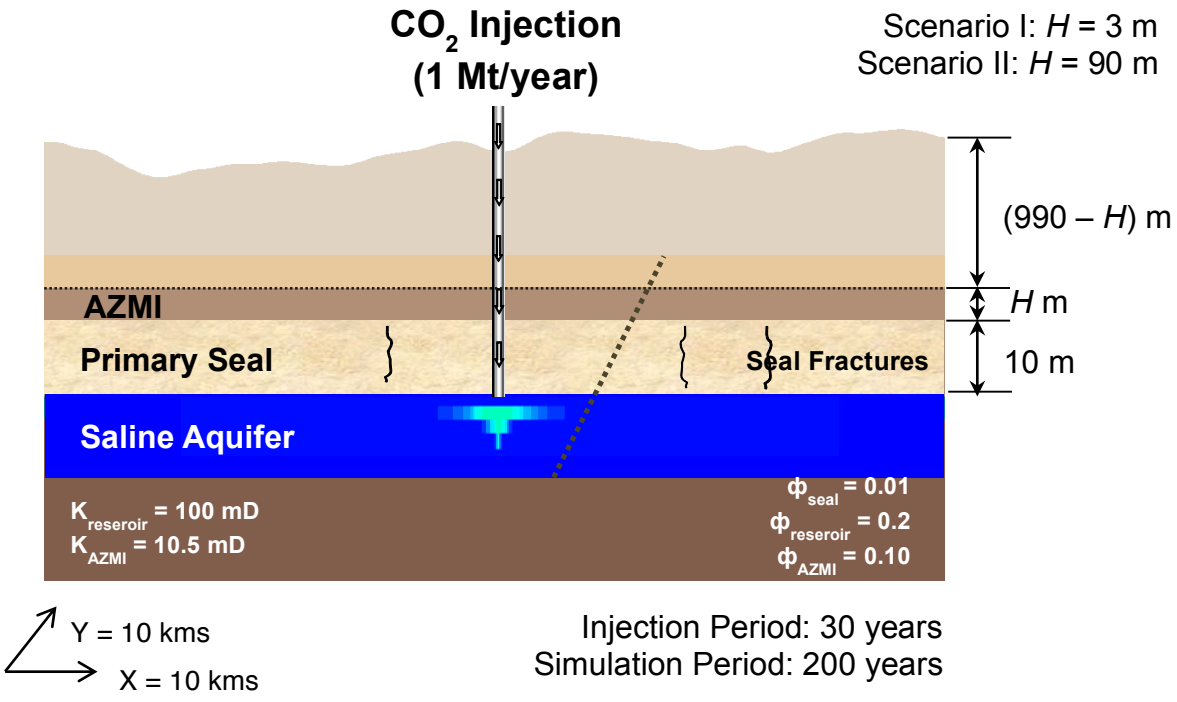

Figure 3-3: Geological profile of the base case CO_2 storage site representing two different AZMI thickness scenarios (*not to scale*).

Table 3-1: Storage reservoir and caprock features

Parameters	Value
Density of rock	2600 kg/m^3
Initial pressure at depth =1000 m	10 MPa
Pressure gradient	10^4 Pa/m
Average temperature at caprock	50 ^oC
Horizontal permeability (storage formation)	10^{-13} m^2 (0.1 D)
Vertical permeability (storage formation)	10^{-14} m^2 (0.01 D)
Horizontal permeability (non-fractured caprock)	10^{-19} m^2 (10^{-7} D)
Vertical permeability (non-fractured caprock)	10^{-20} m^2 (10^{-8} D)
Horizontal permeability (fractured caprock)	10^{-19} m^2 (10^{-7} D)
Vertical permeability (fractured caprock)	10^{-17} m^2
Salt (NaCl) mass fraction in brine	0.08
Porosity (storage formation)	0.1
Porosity (caprock)	0.05
CO_2 residual saturation	0.1
CO_2 injection period	30 years
Maximum simulation time	200 years
Domain size	10 ×10 km
Boundary condition	Open boundary

3.2.2 TOUGH2 Model Description

The AZMI ROM takes its input in the form of fluid flux from the underlying seal. Any full-scale reservoir simulator such as TOUGH2 (Pruess et al., 2012) or ROM such as NSealR (Lindner, 2015) can be used to generate these fluid flux inputs for the AZMI ROM. In this study, we use a detailed TOUGH2 simulation to compute the flux output from the seal and used the outputs as an input to the AZMI ROM.

TOUGH2 is a multi-phase flow transport code that has been widely applied to simulate subsurface migration of CO_2 and brine under geologic carbon storage conditions (Pruess et al., 2012; Pruess and Nordbotten, 2011; Zhou et al., 2010; Rohmer and Seyedi, 2010). In this study, a 3-D TOUGH2 model was developed to simulate the injection of CO_2 into a deep saline reservoir, as well as CO_2 and brine leakage through the seal based on its intrinsic permeability. The model was constructed with five vertically stacked horizontal intervals (Figure B-5 in Appendix B). Moving from bottom to top, these intervals were comprised of a lower boundary, the CO_2 storage reservoir, the seal, the AZMI and an upper boundary. The dimensions of the modeling domain were either 10,000 m × 10,000 m × 133 m (Scenario I) or 10,000 m × 10,000 m × 220 m (Scenario II). The upper and lower boundary intervals had very low permeabilities (10^{-19} m^2 for horizontal permeability and 10^{-20} m^2 for vertical permeability), and a thickness of 10m each. Adding together the upper and lower boundaries (20m), the storage formation (100m), the seal (10m), and the AZMI thicknesses of 3m and 90m yields thicknesses of 133 and 220 m for Scenario I and II, respectively.

The CO_2 was injected into the CO_2 storage reservoir, which was 100m thick. The interval above the CO_2 storage reservoir was the seal interval, which is 10m thick. The portion of the seal blocks representing a non-fractured seal had a horizontal permeability of 10^{-19} m^2 and a vertical permeability of 10^{-20} m^2; the portion of the seal blocks representing a fractured seal had an identical horizontal permeability but a vertical permeability of 10^{-17} m^2. The interval above the seal was designated as the AZMI, which had a porosity of 0.1 and a horizontal permeability of 10.5 mD. In the central region surrounding the CO_2 injection well, small grid blocks were assigned to capture the complex two-phase transport behavior that would take place close to the injection well. Grid blocks with larger sizes were assigned in other regions outside the central region. The model had 23,328 active grid blocks in total for Scenario I and 37,908 active grid blocks in total for Scenario II.

3.3 RESULTS

For demonstration purposes, a credible, but arbitrarily selected, heterogeneous seal permeability was used for the model input of the base case as represented graphically in Figure 3-4. The higher permeable zones in the test case have permeabilities that are three orders of magnitude greater than those of the low permeable zones of the seal. The higher permeability zones in the seal are taken to be representative of leaky zones. It is expected that fluid will migrate preferentially through these high permeable zones, as would also be expected in fractured zones of a caprock. The fluids migrating out of the seal through the high permeable zones then move through the overlying porous and permeable formation (the AZMI), driven by pressure gradients and buoyancy, resulting in

an increase in pressure in the region.

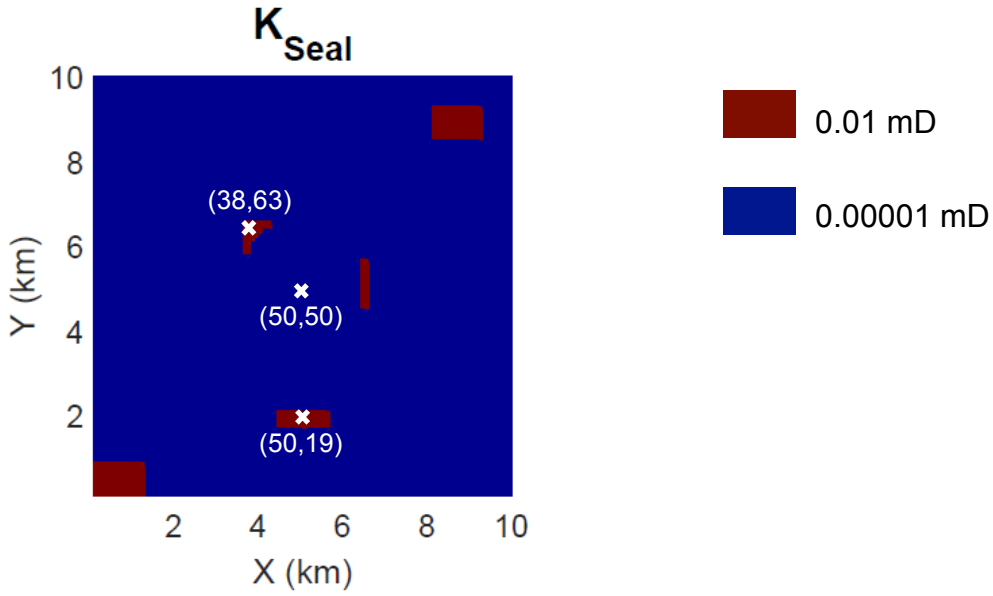

Figure 3-4: Map view of seal permeability used for the benchmark CO_2 storage site showing coordinates of injection well location (50,50) and centroids of two high permeable zones (38,63) and (50,19).

Figures 3-5 and 3-6 present the changes in pressure responses in the AZMI over time for Scenarios I and II, respectively, as generated using flux from the seal (TOUGH2 results) for the simulation periods previously discussed. For both scenarios, the highest increase in pressure is observed at the centroids of the high permeable zones at the end of injection (i.e., 30 years), with the maximum increase in pressure being about 0.49 MPa and 0.20 MPa for Scenario I and II, respectively. The change in pressure gradually fades away from the centroids of the high permeable zones to the simulation domain boundaries for both of the scenarios. After CO_2 injection stops, the rate of increase in pressure gradually decreases and normalizes over time by the end of the simulation (i.e., following a post-injection period of 170 years). Figures 3-5 and 3-6 also show that the change in pressure decreases as the thickness of the AZMI increases. The pressure change

in the thick AZMI scenario is smaller because the total pore volume into which the additional fluid is moving is significantly greater, so there is more capacity for attenuation of the fluid within the system.

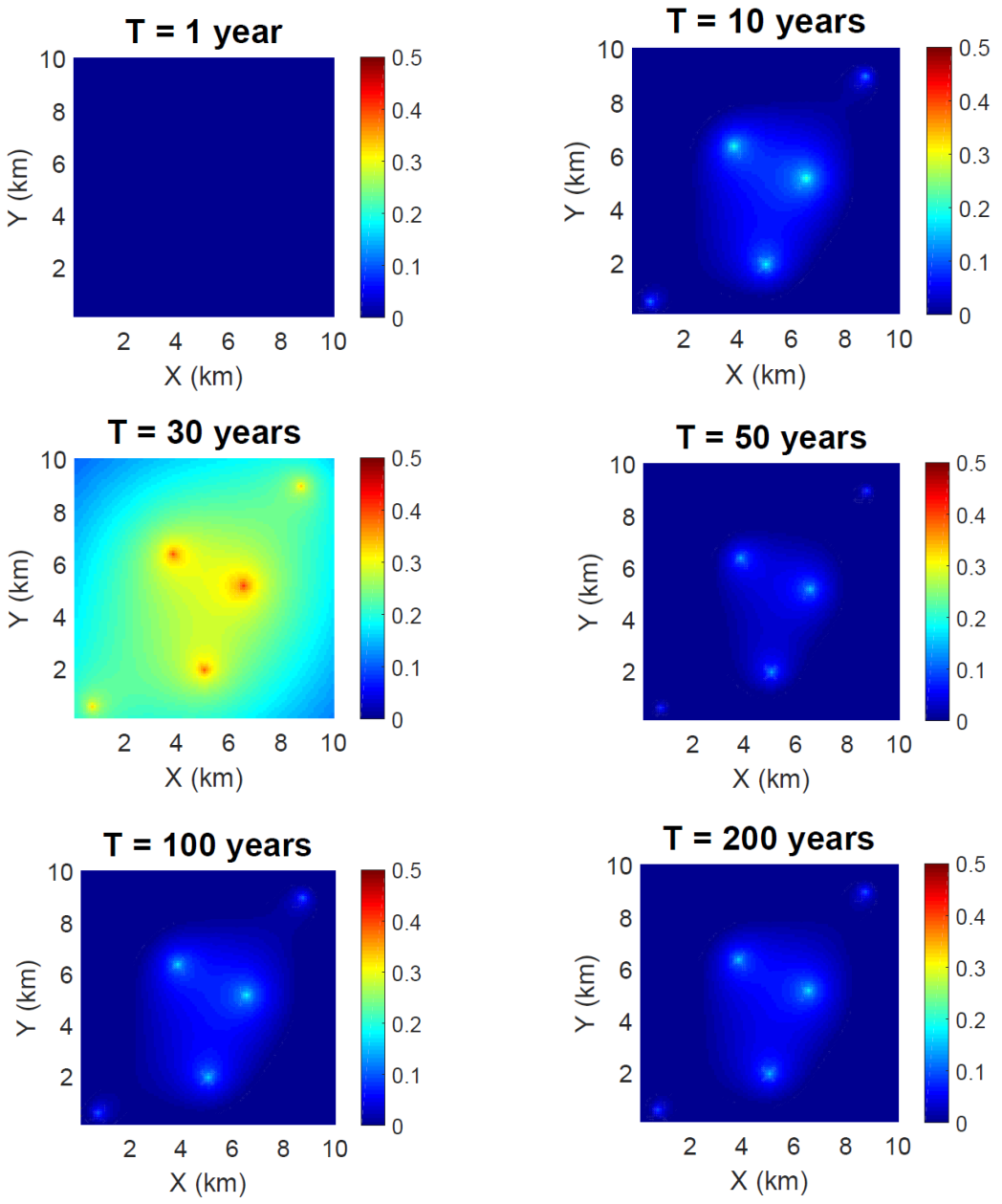

Figure 3-5: Change in pressure response (in MPa) at the top of AZMI for Scenario I (thickness of 3 m) through 200 years of total performance (including 30 years of injection).

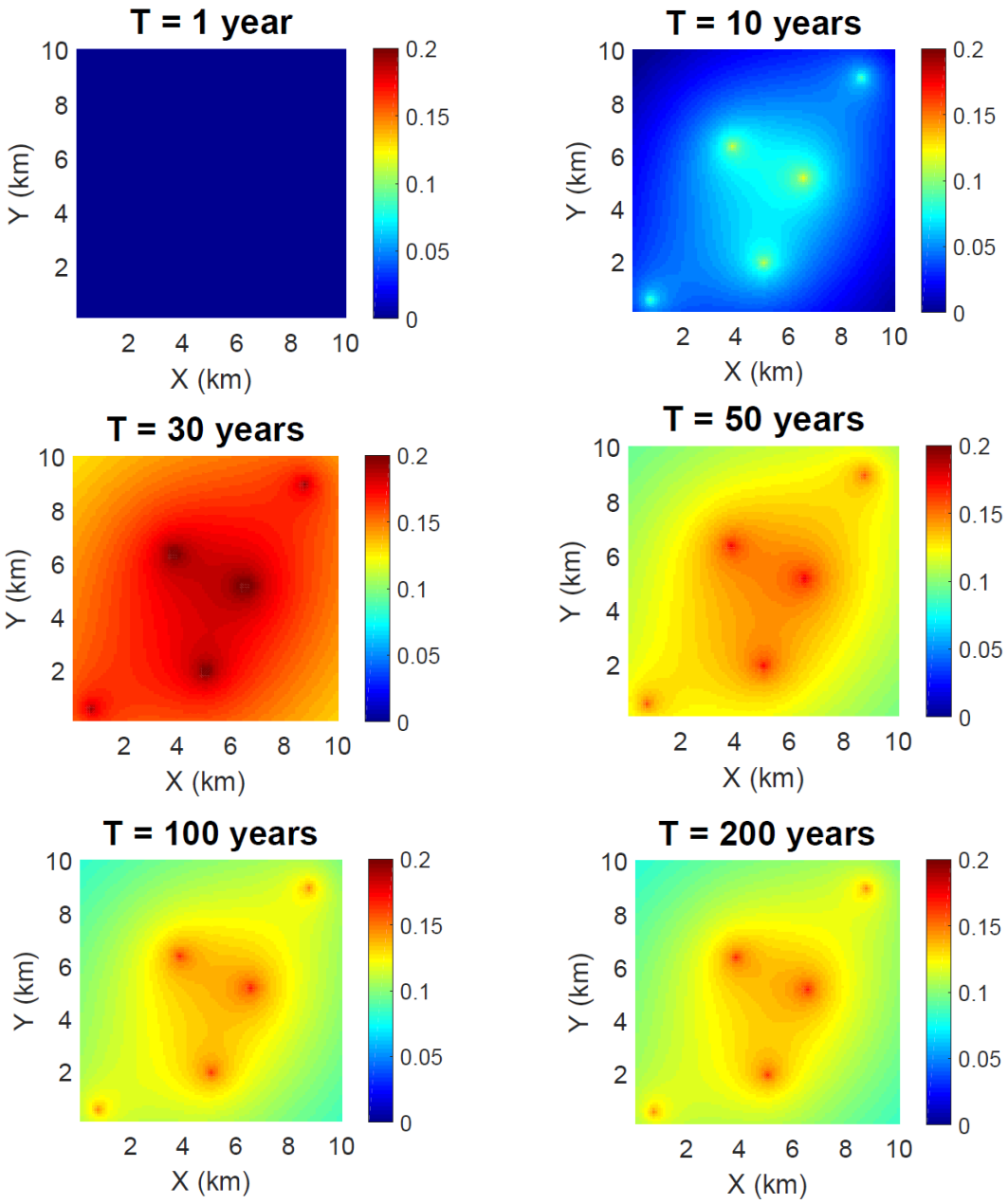

Figure 3-6: Change in pressure response (in MPa) at the top of AZMI for Scenario II (thickness of 90 m) through 200 years of total performance (including 30 years of injection).

The AZMI ROM also calculates the CO_2 saturation distribution in the AZMI over time. However, the saturation calculation is limited by the fact that the input flux to the AZMI ROM is a 1D flux. As mentioned earlier, the AZMI ROM has been developed to be consistent with the IAM development effort of NRAP, which produces vertical 1D flux from the seal ROM, NSealR. This restricts the ability of the AZMI ROM to predict the lateral spread of CO_2 over time. Future work will include the development of a 1D to 2D flux conversion approach that will permit the more accurate prediction of CO_2 saturation in the AZMI. As part of this work, 3D flux data from TOUGH2 numerical simulations were used to generate the saturation profile. Figures 3-7 and 3-8 shows CO_2 saturation distribution at the top of the AZMI layer over time for Scenarios I and II, respectively. In Scenario I, the CO_2 plume in the storage interval tends to migrate out beyond the high permeable zones near the injection well. Since the mobility increases over time due to increase in relative permeability of CO_2, the plume tends to disperse more with time and continues to increase even after the injection stops. In Scenario II, the CO_2 plume in the AZMI is more localized compared to the pressure change and the increase in CO_2 saturation was only seen in the regions very close to the high permeable zones near the injection well. The maximum extent of CO_2 plumes in the AZMI around the high permeable zones near the injection well is shown in the figures 3-7 and 3-8. Since the AZMI thickness is much less in Scenario I compared to that of Scenario II, the mobility of CO_2 near the high permeable zones is much higher in Scenario I and the dispersion rate is quite high. As can be seen from these figures, the maximum extent of the CO_2 plume in Scenario I is 6,350 m compared to that of 3,250 m in case of Scenario II. Considering CO_2 dissolution in brine as part of the model may reduce CO_2 saturation aerial extent, resulting in slower dispersion of the

CO_2 plume.

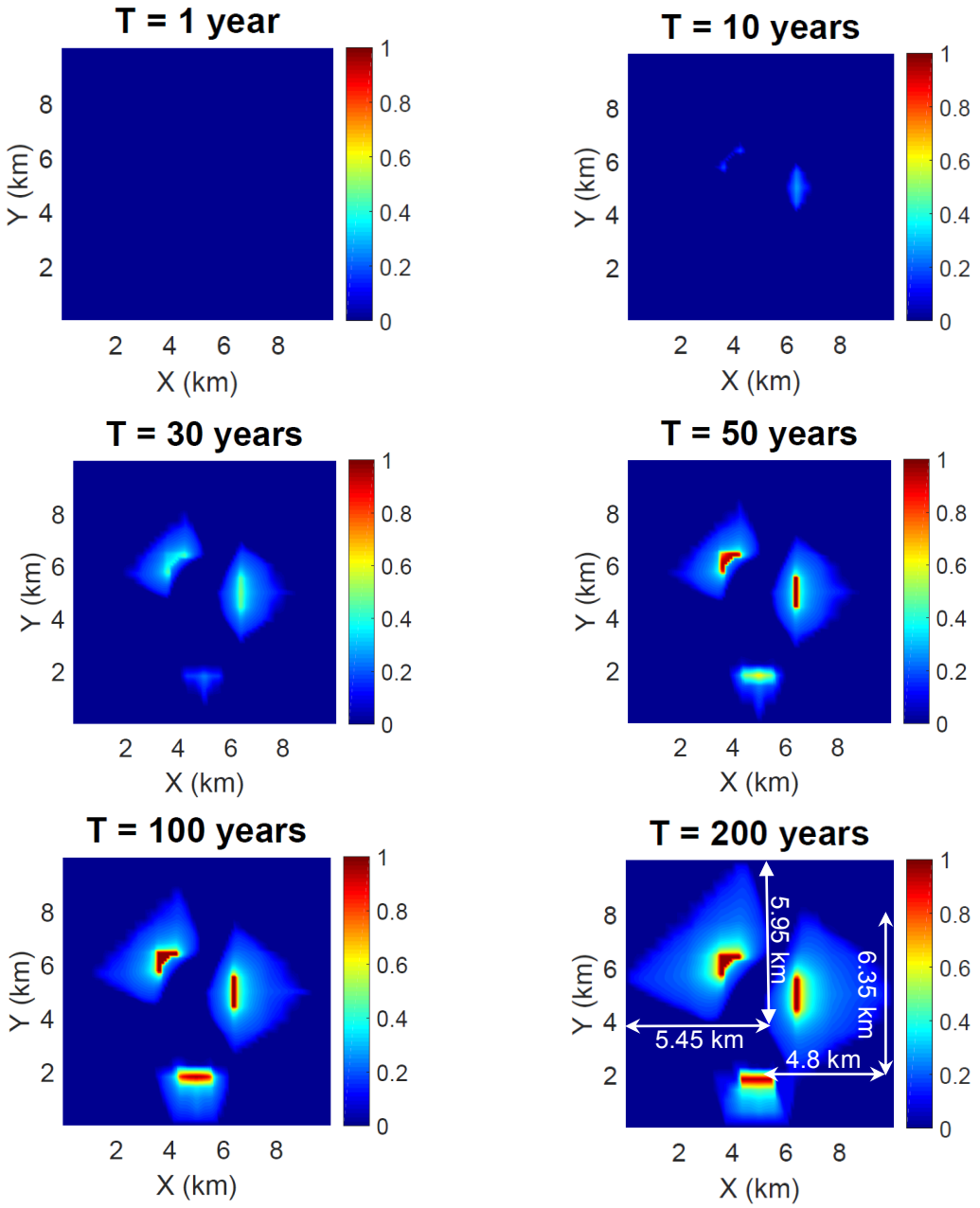

Figure 3-7: Saturation response at the top of AZMI for Scenario I (thickness of 3 m) through 200 years of total performance (including 30 years injection). The spatial extent of gas plume at the end of simulation is also shown.

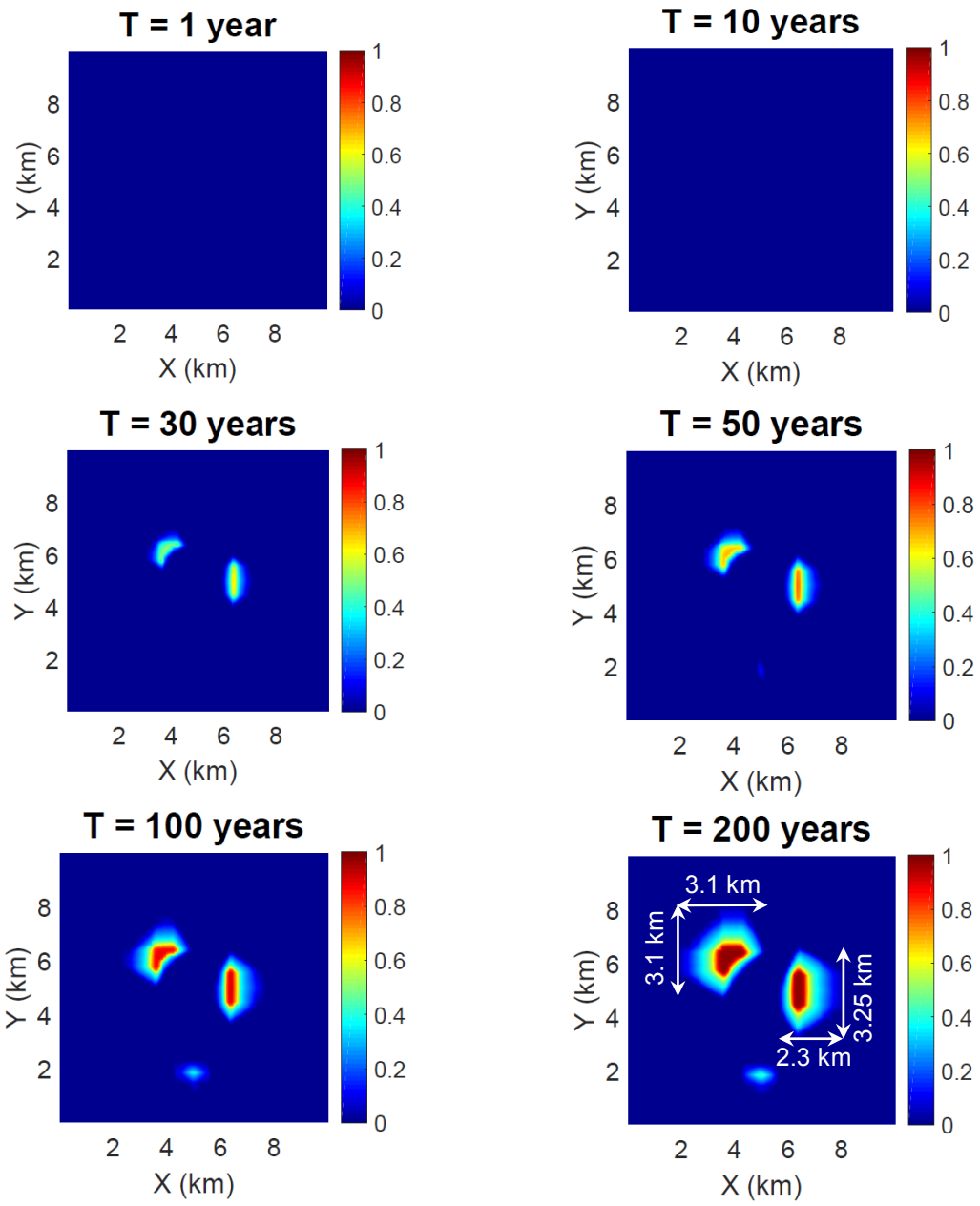

Figure 3-8: Saturation response at the top of AZMI for Scenario II (thickness of 90 m) through 200 years of total performance (including 30 years injection).The spatial extent of gas plume at the end of simulation is also shown.

3.4 MODEL VALIDATION

To verify the computational ability of the AZMI ROM, a comparison of the AZMI ROM pressure change predictions with those of a comparable TOUGH2 model was made. Essentially, this verification effort involved using TOUGH2 flux results from the seal as an input to the AZMI ROM, and then comparing the results of the AZMI ROM with that of TOUGH2 outputs for similar intervals of the storage system for both of the base case scenarios. Figures 3-9 (a) and 3-9 (b) show comparisons of the pressure responses of the AZMI ROM and TOUGH2 simulator at particular locations in the AZMI for Scenarios I and II, respectively. Locations directly above two of the high permeable seal zones (Grid coordinates (38,63) and (50,19)), and the location directly above the injection well (grid coordinate (50,50)) were selected to illustrate the important trends. The spatial difference in the two model predictions is also compared at the end of injection (i.e., 30 years) and at the end of simulation (i.e., 200 years) in Figure 3-10. The absolute pressure deviation is calculated as the absolute difference in the pressure prediction of AZMI ROM to that of the TOUGH2 simulator. Table 3-2 summarizes the simple statistical analysis carried out for the model comparison using mean absolute percentage deviation.

$$Mean\ Absolute\ Percentage\ Deviation = \frac{|\ \Delta P_{AZMI} - \Delta P_{TOUGH2}\ |}{\Delta P_{TOUGH2}} \times 100\% \qquad (3.20)$$

where, ΔP_{AZMI} is the change in pressure predicted by AZMI ROM and, ΔP_{TOUGH2} is the change in pressure predicted by TOUGH2.

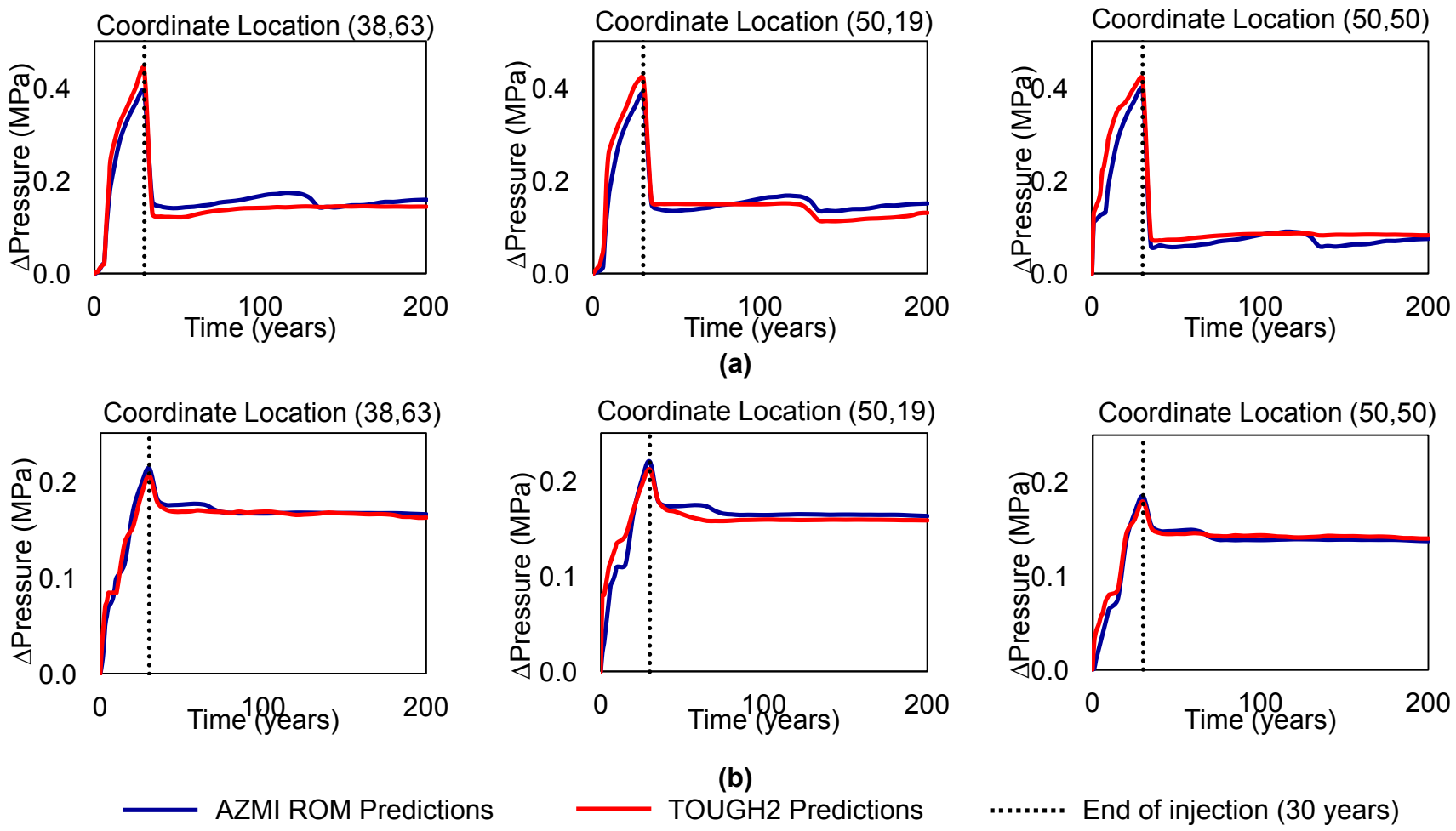

Figure 3-9: Pressure prediction comparison between AZMI ROM and TOUGH2 at three locations: (38, 63), (50, 19) and, (50, 50) at the top of AZMI for (a) Scenario I (thickness of 3 m) and (b) Scenario II (thickness of 90 m) over time. The dashed line represents the time when CO_2 injection ends (t=30 years).

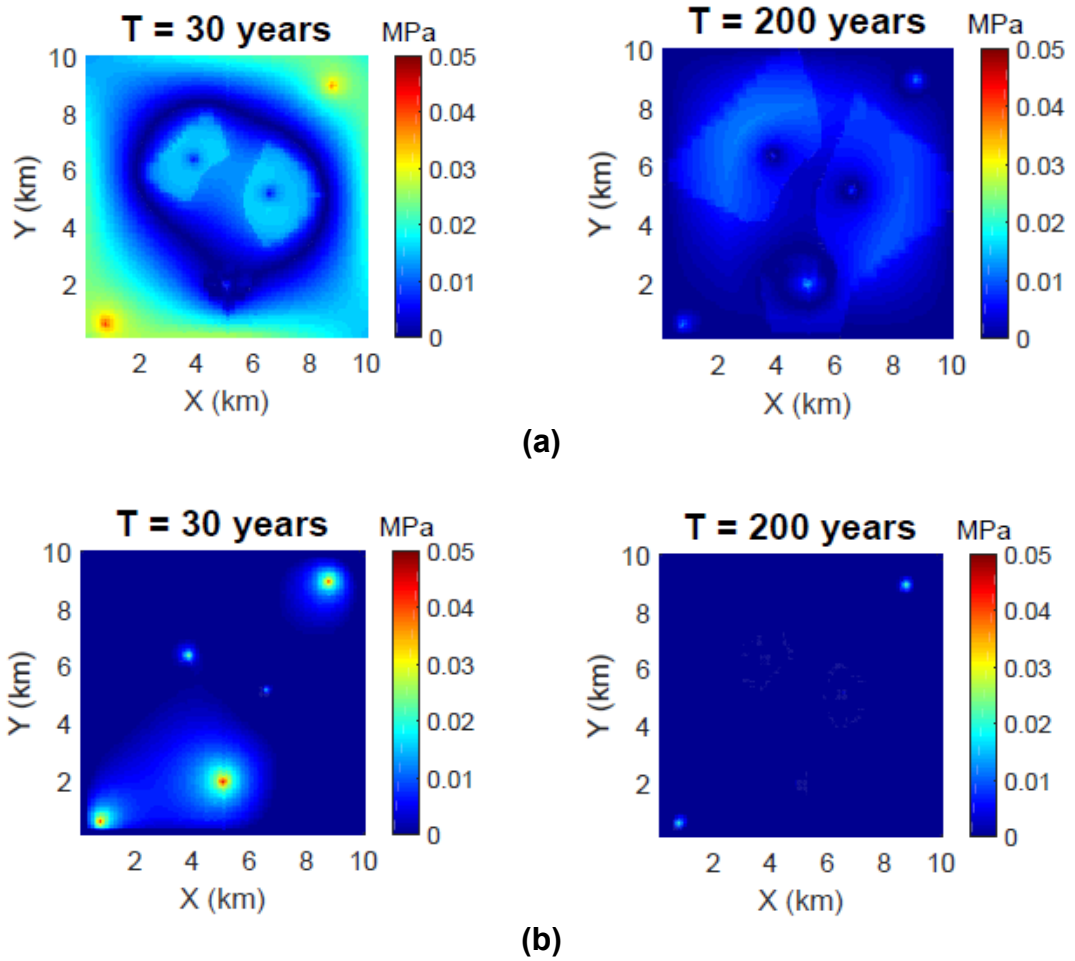

Figure 3-10: Absolute deviation in pressure prediction between AZMI ROM and TOUGH2 simulations at the end of 30 and 200 years for AZMI thickness (a) = 3 m (b) = 90 m.

Table 3-2: Mean absolute percentage deviation of AZMI ROM total pressure predictions from TOUGH2

Time	At the center		At boundary	
(Years)	Scenario I	Scenario II	Scenario I	Scenario II
30	0.75 %	0.80 %	1.2 %	0.71 %
200	0.58 %	0.52 %	0.30 %	0.18 %

** Note: Center is defined by the coordinate (50, 50) and calculations for center is done using average of 400 cells around the center. Boundary calculations are done using average of 400 cells in the outer boundary of the grid system (100 cells each side).*

This analysis shows that the results tend to vary, to some small extent, through the period of injection with TOUGH2 predicting higher pressure compared to that of the AZMI ROM. Once injection stops, the AZMI model seems to provide a better match with that of TOUGH2. During the first 10 years of operation, the pressure is higher in TOUGH2 predictions since the TOUGH2 model captures the 3D flow of the CO_2 in the AZMI, resulting in a resistance to the CO_2 flow from all three directions. As such, in the TOUGH2 model, more cumulative pressure is required by the CO_2 to overcome the resistance to replace the brine in the AZMI, as compared to the AZMI ROM where the CO_2 flow is considered only in one dimension. With the increase in injection time, the CO_2 saturation increases, and so does the relative permeability of CO_2. As a result, a lower pressure is required to overcome the resistance to flow with the increase of CO_2 relative permeability. The deviations in predicted pressure response, as can be seen from Figure 3-10, are greater above the high permeable zones of the seal. Also, it can be seen in Figure 3-9 (a) that pressure starts decreasing at around 130 years from start of injection. This is the time when CO_2 in the AZMI reaches the system boundary. This behavior is only observed in Scenario I, i.e., the 3 m thick AZMI case. There is no pressure decrease observed in Scenario II because CO_2 plume never reaches the system boundary at the top of the 90 m thick AZMI.

Since there have been several model reduction techniques used in the current model development, the minor differences in the models as shown in Table 3-2, where the mean absolute percent deviation ranges from 0.3 to 1.2%, are expected. These results confirm that the AZMI ROM, which is computationally more efficient than TOUGH2, still provides acceptable accuracy

relative to that of the full complexity model. Taking into consideration the fact that discrepancy in the prediction of physical processes can be dominated by uncertainty of subsurface properties (Oladyshkin et al., 2011a), however, suggests that these minor differences may not be overly impactful to the predictive utility of the AZMI ROM. Ultimately, the acceptable degree of deviance from the verifying numerical model will depend on the intended application of this predictive tool, and will incorporate some consideration of the trade-off between that deviance and benefit of computation time. For example, a simulation of 30 years in TOUGH2 takes approximately 8 hours of computational time in a stand-alone machine and that of 200 years of simulation takes around 14 – 15 hours of run-time. On the other hand, the AZMI ROM computation times when coupled with seal ROM, NSealR, for these same scenarios are 15 and 34 seconds, respectively, providing an improvement in computation time by a factor of approximately 2000 times.

Generally, it is expected that the computational efficiency and moderate accuracy of the AZMI ROM, as compared to numerical models, will allow consideration of general trends in AZMI response and development of general insights about the value of AZMI monitoring in the context of full system performance, and related uncertainty. It will likely not, however, have application for evaluation of site-specific geologic storage performance, as the model allows only limited functionality to incorporate spatially varying site characteristics. Chapter 4 will present the results of performing uncertainty quantification and sensitivity analyses of the system during CO_2 injection and subsequent leakage into the AZMI.

3.5 CONCLUSION

This chapter presents a new reduced order model to predict the pressure and saturation response in the Above Zone Monitoring Interval (AZMI). The primary motivation for developing this new model is as a rapid assessment tool to consider the ability to monitor fluid migration into the AZMI in a geologic CO_2 storage setting. This tool can be applied to describe subsurface response to large-scale CO_2 injection, and explore implications of that response for diagnostic purposes of seal integrity, plume disposition and related uncertainties. A flux aggregation approach using a statistical data-clustering algorithm was applied to quantify fluid fluxes of CO_2 and brine into the AZMI. This influx through the primary seal is distributed throughout the AZMI using a multi-phase fluid flow model based on a simplified version of an existing analytical solution developed by Nordbotten et al. (2005) for CO_2 storage. A base case study to describe a credible CO_2 storage scenario was performed using baseline AZMI parameters, and CO_2 and brine flux inputs from the seal TOUGH2 numerical model. The benchmark storage case was also set up in TOUGH2 and fluid migration through the seal predicted. The base case study is used to investigate two scenarios reflecting different AZMI thickness. For both scenarios, comparisons were made between results from the new AZMI ROM and TOUGH2. The AZMI ROM pressure predictions differ from those of TOUGH2 by a maximum of 1.2 % for identical simulation settings. The AZMI ROM tends to under predict in certain cases due to the extensive complexity reduction methodologies that were incorporated into the formulation of the AZMI model. One of the main features of the AZMI ROM is that it is computationally very inexpensive compared to full-scale numerical simulators. In this work, fluid fluxes from TOUGH2 are used

as input to the model. In the future, the model will be coupled with reservoir and seal prediction ROMs in an integrated assessment framework, to permit an assessment of whole system performance.

One limitation of this model is it does not consider the solubility of CO_2 in brine which can lead to inaccurate model predictions. Geomechanical effects are also not considered. Geomechanics can play an important role in pressure predictions above the seal with some of the well-known effects being stresses and strains on overlying formations due to fluid migration; pressure perturbations due to injection of CO_2; and induced faults and fractures in the system leading to local micro-seismic events (Rutqvist, 2012; Varre et al., 2015). On the one hand, pressure build-up in the AZMI can be substantially reduced in case of structural deformation; on the other hand, formation of faults and fractures can lead to more CO_2 and brine migration, which will lead to significant pressure increases above the seal. For these reasons, development of geomechanical reduced order models for future incorporation into the current AZMI ROM is warranted. Nevertheless, the AZMI model presented in this study is able to capture the general trends of numerical reservoir modeling. In presence of site data, other response surface ROMs developed using site-specific numerical realizations can be used to model storage scenarios and those model results then can be used by the AZMI ROM to predict geologic behavior more accurately.

Chapter 4

Probabilistic Assessment of Above Zone Pressure Predictions at a Geologic Carbon Storage Site

The AZMI ROM development involves many conceptual and quantitative uncertainties. Insufficient or lack of information related to geological properties may lead to significant uncertainties in model predictions and can even override the influence of secondary physical processes (Oladyshkin et al., 2011a). Current numerical simulation models inadequately perform stochastic simulation techniques based on brute-force Monte Carlo simulation and related approaches (Maltz and Hitzl, 1979 and Robart and Casella, 2004), because even single deterministic simulations may require high performance parallel computing (Oladyshkin et al., 2013). This makes it favorable to use advanced stochastic tools to model the uncertainties of the complicated processes involved in the modeling of the geologic storage of carbon dioxide. This also holds true for a coupled ROM approach. Application of advanced stochastic tools to predict uncertainties in coupled ROM systems such as the reservoir-caprock-AZMI coupled model used in this study will be computationally efficient over a complex Monte Carlo-like analysis.

In this research, a recently developed data-driven uncertainty quantification approach, called the arbitrary polynomial chaos (aPC) expansion was used. aPC provides a massive stochastic model reduction (Oladyshkin et al., 2011a and Oladyshkin and Nowak, 2012) to analyze the uncertainties in the predictive ability of the AZMI ROM. aPC has certain advantages over more conventional polynomial chaos methods. On one hand it provides more robust convergence (Oladyshkin and Nowak, 2012) in comparison to the classical methods (e.g., Wiener, 1938, Ghanem and Spanos, 1991 and Le Maître and Knio, 2010) once underlying distributions of the modeling parameters are derived from real-world data. On the other hand, arbitrary probability distributions of uncertain parameters can also be used in this method. Another important application of the aPC approach is to rank the influence of model input parameters on the output space. The more complex the system is, the more will be the associated uncertainty of the system models. Uncertainty of any parameter in the modeling procedure propagates through the model to impact the model predictions. Hence, it is important to rank the influence of the model input parameters on the output space. This will provide a better understanding of the system behavior, making the analysis of model uncertainties and sensitivities a very valuable and important task.

Sensitivity analysis is widely used to identify the contribution of uncertainty sources within the modeling process (Oladyshkin and Nowak, 2012) and that in turn helps in improving the understanding of model behavior (Sobol, 2001). A global sensitivity analysis (GSA) was performed on the AZMI model using variance based Sobol sensitivity index parameterization (Sobol, 2001). The purpose of using GSA over a local one is due to the inability of local analysis to

cover the non- linear variation of model responses over the entire range of probability distributions of the input parameters (Ashraf et al, 2013). The aim of the GSA is to quantify the relative importance of each individual input parameter on the AZMI model output prediction and rank them. The aPC-based response surface used in the uncertainty quantification is based on orthonormal polynomials whose properties are well exploited (Oladyshkin et al, 2012). The remainder of this chapter describes a baseline case study of the AZMI model for a CO_2 storage site (§ 4.1), describes the uncertainty quantification methodology and results (§ 4.2), and discusses the implications of the sensitivity analysis on the model predictions (§ 4.3).

4.1 ABOVE ZONE MODEL SETUP

In this modeling effort, the migration of subsurface fluids (here, CO_2 and brine) to the AZMI and the resulting changes in pressure were investigated. The model comprises of three components: reservoir, caprock and the AZMI. The calculations in the reservoir and caprock are necessary to model the pressure changes in the AZMI. This investigation demonstrates the application of above zone pressure modeling using the AZMI ROM by using the Kimberlina CO_2 storage site (California, USA) as an example (Zhou et al., 2011; Birkholzer et al., 2011;Wainwright et al., 2013; Zhang et al., 2016). The reservoir-scale CO_2 migration model developed by Wainwright et al. (2013) is based on a geological study in the Southern San Joaquin Basin, California. The model, which uses geologic and hydrogeologic data obtained from many oil fields in that region, has a domain that extends 72 km in the eastern direction and 92 km in the northern direction (Figure 4-1). The simulation assumes that CO_2 injection is conducted in

the center of the domain into the 400 m thick Vedder formation at a depth of 2750m. The Vedder formation is quite permeable which should allow large industrial scale fluid injectivity. The injection well location is also marked in the Figure 4-1 (b). Since we intend to use the reservoir simulator results in the seal ROM, NSealR (Lindner, 2015), the reservoir area is converted into 100 by 100 grid block system for consistency. The location of the conceptual injection well is at coordinate (34, 46) in that reduced-resolution spatial domain.

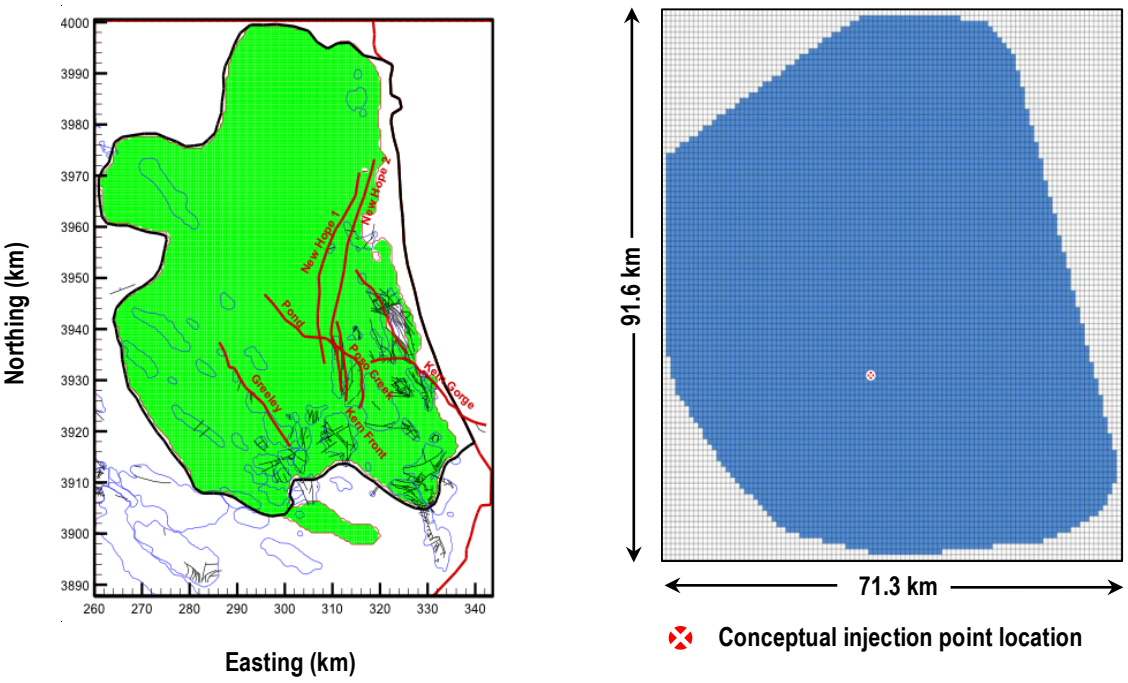

Figure 4-1: Plan view (Wainwright et al., 2013) of (a) the Vedder formation (green area) with faults (red lines), and (b) the model domain (in blue) with numerical grid. In (b), the red point is the location of the conceptual injection well (coordinate (34,46)).

The overlying Temblor–Freeman shale with a thickness of 200 m is considered a suitable caprock for stratigraphic containment of the injected supercritical CO_2. This storage formation site model is used because there is considerable data available in the literature. The modified Kimberlina model of Wainwright et al. (2013) as used by Pawar et al. (2016) was used to simulate the reservoir pressure and saturations. A hypothetical scenario was assumed where 5 million tons of CO_2 is injected per year for a period of 50 years. Figure 4-1 (a) shows the presence of several faults in the reservoir. Fault zone properties are quite uncertain; however, there are qualitative observations that most fault zones are less conductive than the adjacent sandstone formations (Birkholzer et al., 2011). In the reservoir simulations, the potential for leakage of CO_2 and/or brine through permeable faults has been ignored. Also, the potential for fault reactivation is not addressed. Figures 4-2 and 4-3 shows the pressure and saturation at the reservoir-seal interface respectively. The NRAP Seal Barrier ROM, NSealR (Lindner, 2015) was then used to compute the migration of CO_2 and brine through the seal to the overlying AZMI formation through intrinsic permeability and/or the presence of natural/induced fractures in the seal. NSealR uses a two-phase, relative permeability approach with Darcy's law for one-dimension (1-D) flow computations of CO_2 through the horizon in the vertical direction. The reservoir pressure and saturation generated using the Kimberlina model (Wainwright et al., 2013) is used as an input to NSealR to produce CO_2 and brine flux at top of the seal in a 100 by 100 uniform grid format. The CO_2 flux through the 200 m thick Temblor–Freeman shale that was calculated using NSealR is shown in Figure 4-4.

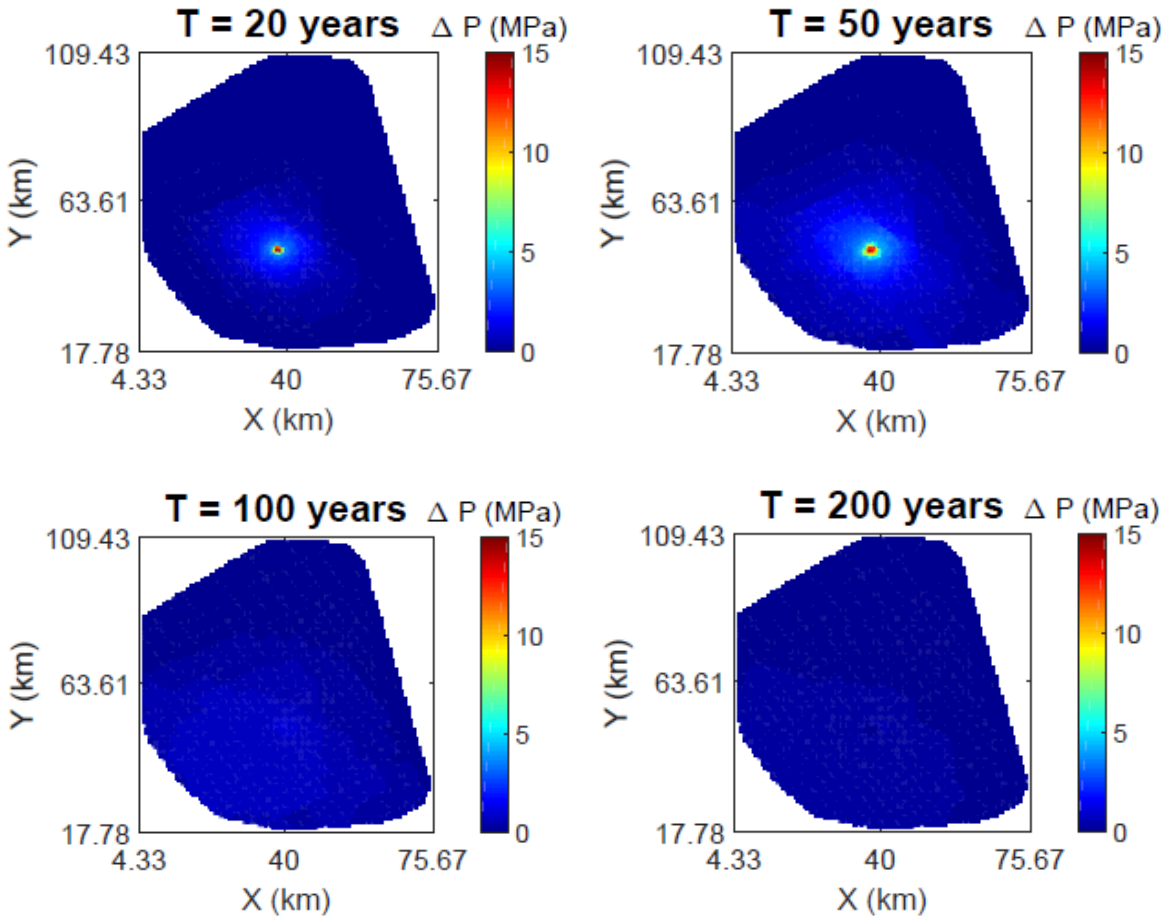

Figure 4-2: Evolution of pressure buildup (in MPa) at the top of the reservoir at 20, 50, 100 and 200 years after the start of CO_2 injection.

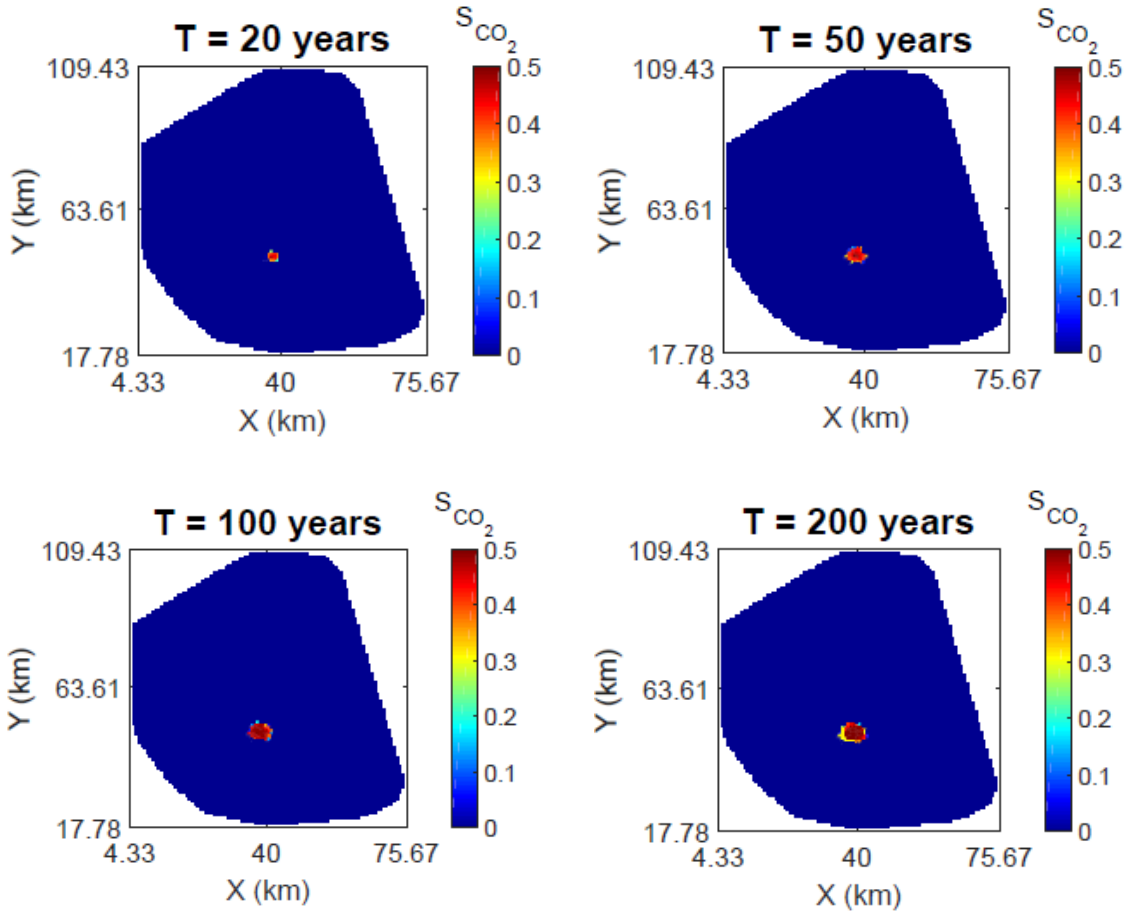

Figure 4-3: Evolution of CO_2 saturation at the top of the reservoir at 20, 50, 100 and 200 years after the start of CO_2 injection.

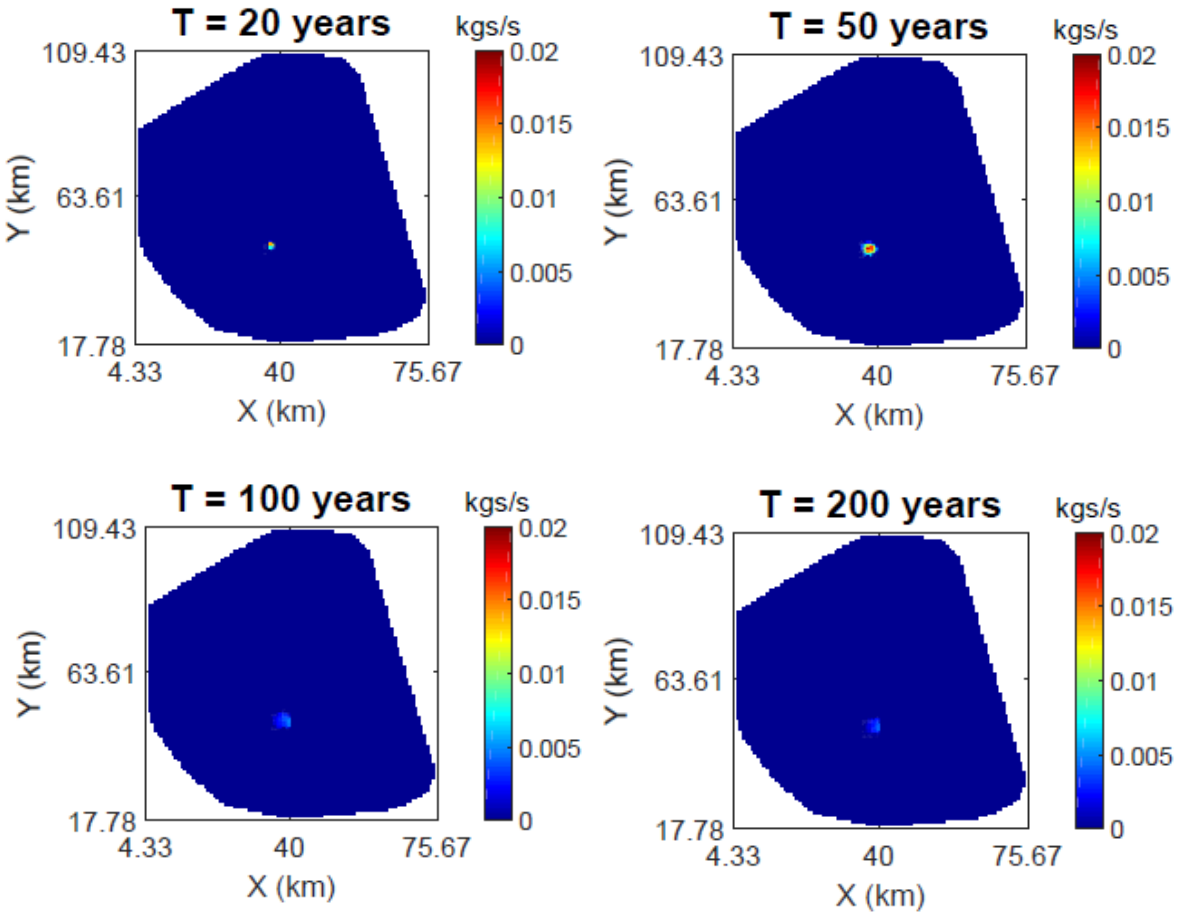

Figure 4-4: CO_2 flux evolution at the top of the caprock at 20, 50, 100 and 200 years after the start of CO_2 injection.

The AZMI ROM used in this investigation to predict above zone pressure changes due to leakage through the primary seal was described in Chapter 3 of this thesis and in Namhata et al. (2016). A hypothetical AZMI system for Kimberlina was defined for the model analysis. This conceptual base case system consists for a 10 m thick AZMI layer overlying the Temblor–Freeman shale of thickness 200 m. The AZMI formation features have been derived from and is assumed to be a part of the existing Olcese sandstone which overlies the Temblor-Freeman shale. It is assumed that the AZMI is initially fully saturated with brine. The reference parameters used for the Kimberlina site in this model are taken from Wainwright et al. (2013) and are shown in Table 4-1.

Figure 4-5 present the changes in pressure response above the AZMI over time generated using flux from the seal for the simulation periods previously discussed. The highest increase in pressure is observed above the injection point at the end of injection (i.e., 50 years), with an observed maximum increase in pressure of 0.185 MPa. The change in pressure gradually decreases away from the injection point location. After CO_2 injection stops, the rate of increase in pressure gradually decreases and normalizes over time by the end of the simulation (i.e., following a post-injection period of 150 years). Figure 4-6 shows the time evolution of pressure change for the base case.

Table 4-1. Reference parameters for Kimberlina model: horizontal permeability (k_h), anisotropy ratio ($k_v/\ k_h$), porosity (Φ), pore compressibility (β_p), van Genuchten parameters ($a,\ m$), Brooks-Corey parameter (γ), bubbling pressure (P_b), residual brine saturation (S_{rb}) and residual CO_2 saturation (S_{rc}).

Parameter	**Reservoir**	**Caprock**	**AZMI**
k_h (mD)	depth dependent*	0.002	0.1
$k_v/\ k_h$	0.2	0.5	0.5
Φ	depth dependent*	0.338	0.32
β_p (10^{-10} Pa^{-1})	4.9	14.5	14.5
a (10^{-5} Pa^{-1})	13	0.42	-
m	0.457	0.457	-
γ	-	-	2
P_b (MPa)	-	0.01	0.02
S_{rb}	0.30	0.45	0.35
S_{rc}	0.25	0.40	0.30

**depth dependent values are taken from Wainwright et al. (2013)*

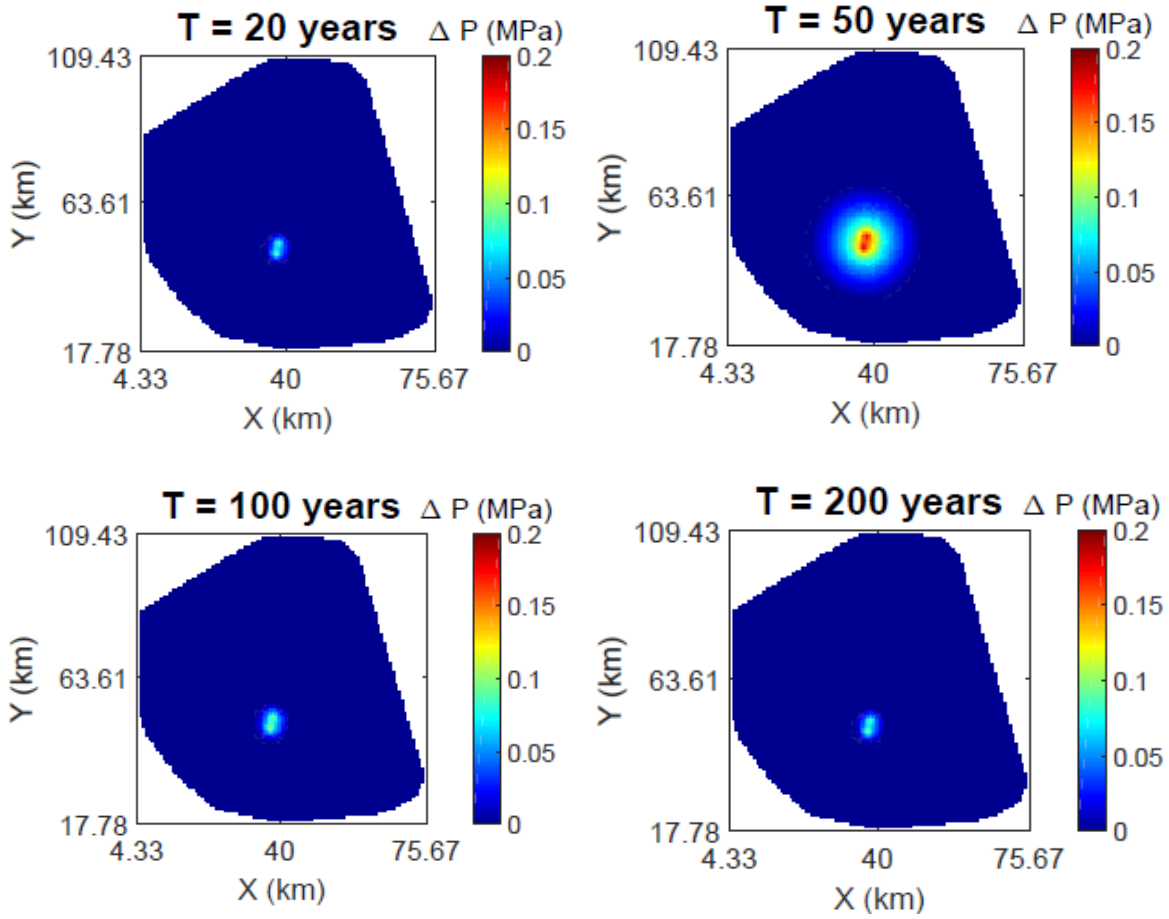

Figure 4-5: Changes in pressure response (in MPa) at the top of the AZMI at 20, 50, 100 and 200 years after the start of CO_2 injection.

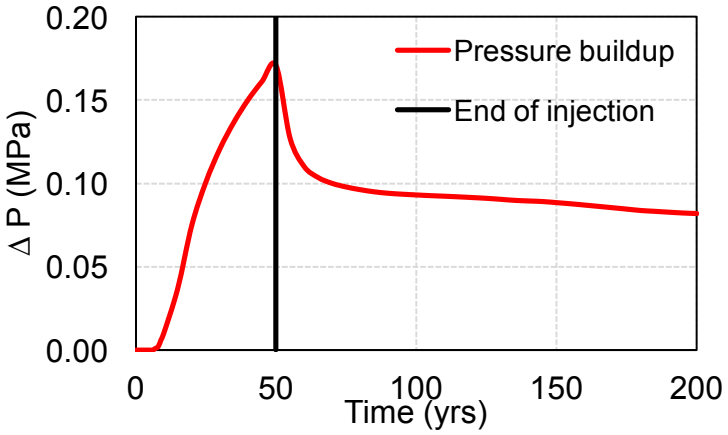

Figure 4-6: Time evolution of pressure buildup (in MPa) at the top of AZMI above the injection well, i.e., coordinate (34,46).

4.2 UNCERTAINTY QUANTIFICATION

Many geologic parameters play crucial roles in governing the CO_2 flow dynamics in the AZMI ROM. Due to lack of information and/or a limited ability to make direct measurements, parameters such as porosity and permeability, to name two, often remain uncertain. These uncertainties can have a substantial effect on the output of the ROM. Thus, a quantitative analysis of the impact of these uncertainties on the predictive capabilities of the model was performed and is presented in this section.

A model-based uncertainty analysis, though efficient, requires statistical data for all of the model parameters, which increases the demand on data availability or results in highly subjective assumptions to deal with missing data (Oladyshkin et al., 2011a). Alternatively, uncertainties can also be quantified using stochastic models based on an approach using data-driven polynomial chaos expansion (PCE) methods. Uncertainties in complex systems can be efficiently and accurately addressed by PCE methods (Eldred and Burkardt, 2009; Li and Zhang, 2007; Xiu and Karniadakis, 2003; Zhang and Sahinidis, 2013). As part of this research, the uncertainty quantification of the AZMI ROM was performed using the arbitrary Polynomial Chaos (aPC) approach from Oladyshkin et al. (2011a) and Oladyshkin and Nowak (2012). In aPC, the statistical moments (e.g.; mean, variance, etc.) are the only source of information required to define the stochastic parameters. Hence, accurate descriptions of the probability density functions (PDF) of the uncertain parameters are not required to perform the analysis.

4.2.1 Arbitrary Polynomial Chaos Expansion

Assuming a physical model,

$$\Omega = f(\omega) \tag{4.1}$$

where,

$\omega = \{\omega_1, ..., \omega_M\}^\top \in \mathbb{R}^M, M \geq 1$ is a vector of uncertain parameters (model inputs); and,

$\Omega = \{\Omega_1, ..., \Omega_N\}^\top \in \mathbb{R}^N, N \geq 1$ is a vector of model outputs of interest.

The model output is a random variable if the parameter vector $\boldsymbol{\omega}$ is uncertain. In this research, the model output function represents above zone pressure buildup.

Polynomial chaos theory has a long history and according to (Wiener, 1938), Ω can be expressed in the following form:

$$\Omega(\boldsymbol{\omega}) = \sum_{i=1}^{M} c_i \psi_i(\boldsymbol{\omega}), \tag{4.2}$$

where, c_i's are coefficients quantifying the dependence of model output on its input and $\psi_i(\boldsymbol{\omega})$ are orthogonal polynomials forming the basis for the input probability space.

Since AZMI ROM is space-time dependent, the model output is written as $\boldsymbol{\Omega}(X, \boldsymbol{\omega})$, where the vector $X = \{x, y, t\}$ consists of two space coordinates and time. Hence, coefficients, c_i is determined for each point in space and time, i.e., $c_i(X)$.

In practice, this PCE is truncated at a finite number of basis functions, ψ_i. The number of the terms M in Eq. (4.2) depends on the total number of input parameters N and the order d of the expansion, i.e., the highest degree of polynomial basis functions is determined according to the following:

$$M = \frac{(N+d)!}{(N!d!)}. \tag{4.3}$$

In this reserach, we choose 3rd order aPC expansion. The choice of an order-three problem is supported by the work of Oladyshkin et al. (2011b) where the authors have shown convergence analysis of aPC-based Sobol analysis concluding that all expansion beyond order 2 can capture the non-linearity of a model. Use of a 3rd order of expansion was chosen since it has the freedom to describe non-monotonic behaviors in comparison to the 2nd order.

For simplicity only one random variable ω_j is considered from the vector $\omega = \{\omega_1, ..., \omega_N\}$ in the following explanation. The basis of degree d for parameter ω_j is defined as $\{P_j^{(0)}, ..., P_j^{(d)}\}$. The polynomial $P_j^{(k)}(\omega_j)$ of degree k in the variable ω_j is defined as:

$$P_j^{(k)}(\omega_j) = \sum_{i=0}^{k} p_{i,j}^{(k)} \omega_j, \quad k = \overline{0,d}, \quad j = \overline{0,N}. \tag{4.4}$$

where,

$p_{i,j}^{(k)}$ are coefficients in $P_j^{(k)}(\omega_j)$.

The coefficients $p_{i,j}^{(k)}$ are constructed in such a way that the polynomials in Eq. (4.4) form an orthogonal basis in arbitrary data distributions. These arbitrary data distributions can be in any discretized, continuous, or discretized continuous form and can be quantified using any generalized statistical format.

The unknown polynomial coefficients $p_{i,j}^{(k)}$ are defined using the following matrix equation (Oladyshkin and Nowak, 2012):

$$\begin{bmatrix} \mu_{0,j} & \mu_{1,j} & .... & \mu_{k,j} \\ \mu_{1,j} & \mu_{2,j} & .... & \mu_{k+1,j} \\ .... & .... & .... & .... \\ \mu_{k-1,j} & \mu_{k,j} & .... & \mu_{2k-1,j} \\ 0 & 0 & .... & 1 \end{bmatrix} \begin{bmatrix} p_{0,j}^{(k)} \\ p_{1,j}^{(k)} \\ .... \\ p_{k-1,j}^{(k)} \\ p_{k,j}^{(k)} \end{bmatrix} = \begin{bmatrix} 0 \\ 0 \\ .... \\ 0 \\ 1 \end{bmatrix}. \tag{4.5}$$

Here $\mu_{i,j}$ are the non-central statistical moments of order i for random variable ω_j. For further analysis the normalized orthogonal basis that have useful properties is employed. This orthonormal basis is obtained as:

$$\hat{P}_j^{(k)}(\omega_j) = \frac{P_j^{(k)}}{||P_j^{(k)}||} \tag{4.6}$$

where, the norm of the polynomial $||\ P_j^{(k)}\ ||$ for space of events Λ (where $\omega_j \in \Lambda$) with probability measure Γ defined as:

$$||P_j^{(k)}||^2 = \int_{\omega_j \in \Lambda} \left[P_j^{(k)}(\xi)\right]^2 d\Gamma(\omega_j)\ . \tag{4.7}$$

Uncertainty analysis using PCE can be typically characterized using two methods: intrusive and non-intrusive. In the present context, non-intrusive

probabilistic collocation method (PCM) (Oladyshkin et al., 2010; Li and Zhang, 2007) is used, since it evaluates the coefficients in model expansion using a small number of model simulations and requires no manipulation using partial differential equation (Zhang and Sahinidis, 2013). The method requires computing model $\boldsymbol{\Omega}$ with M different sets of parameters $\boldsymbol{\omega}$ that are called collocation points. In the current study, the recent version of PCM as described in Oladyshkin et al. (2011a) was used to compute the collocation points.

4.2.2 Statistical Distribution of Input Parameters

The data-driven aPC method only requires information on a finite number of moments, and does not explicitly require the shapes of probability density functions. The arbitrary distributions can be either discrete, continuous, or discretized continuous and can be specified either through a few statistical moments, analytically as PDF/CDF, numerically as a histogram, or theoretically through the even more general format of a probability measure (Oladyshkin et al. 2011a).

In this research, the uncertainty analysis was performed for five input parameters: AZMI permeability (k_{AZMI}), AZMI porosity (Φ_{AZMI}), AZMI thickness (H_{AZMI}), caprock permeability ($k_{caprock}$) and caprock thickness ($H_{caprock}$). Figure 4-7 demonstrates the stochastically generated distributions of the parameters that were used in the analysis. The data distribution pattern was generated based on data available from the US National Petroleum Council Public Database (NPC, 1984 and Kopp et al., 2009).

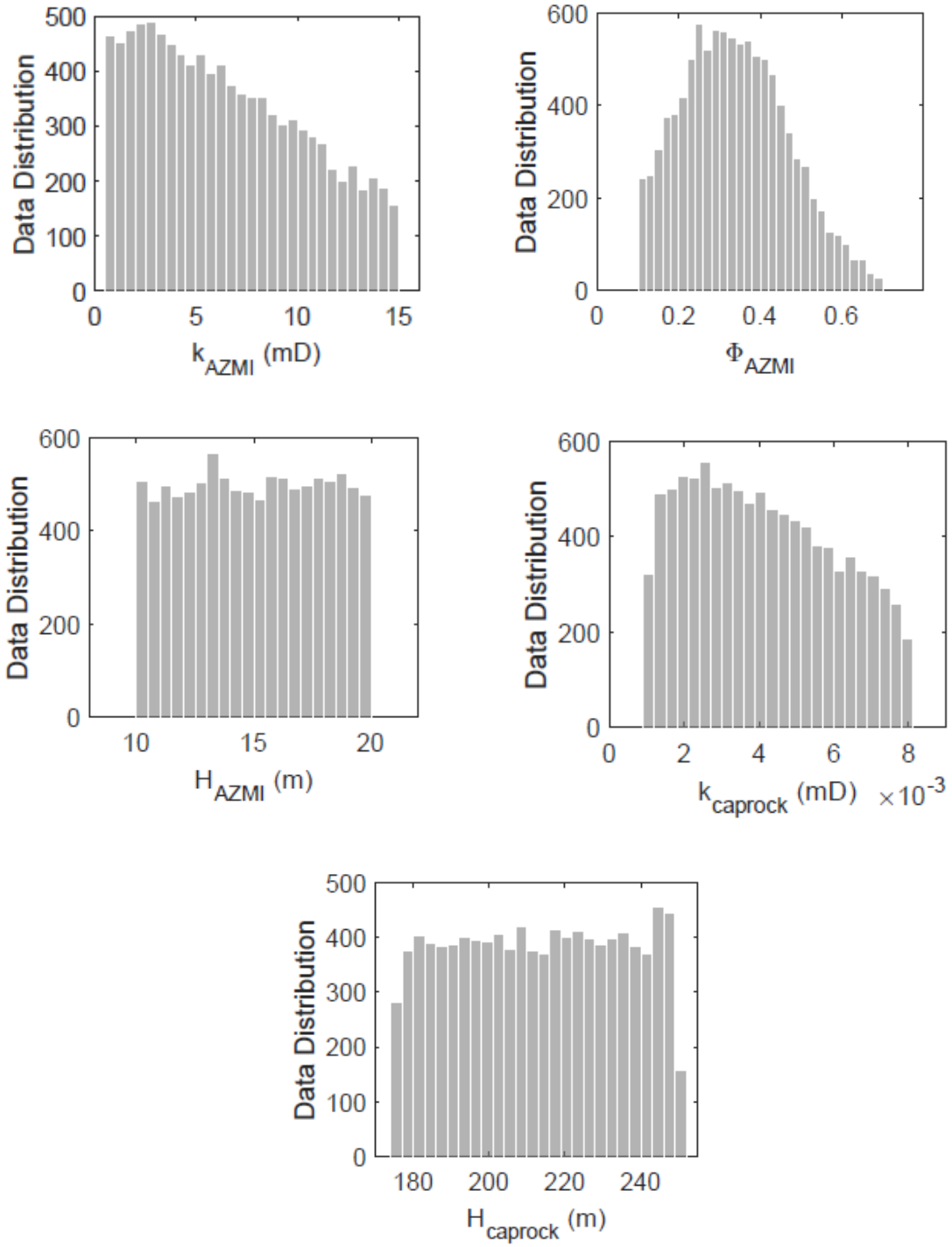

Figure 4-7: Distribution of AZMI permeability (k_{AZMI}), AZMI porosity (Φ_{AZMI}), thickness of AZMI (H_{AZMI}), caprock permeability ($k_{caprock}$) and caprock thickness ($H_{caprock}$) for aPC uncertainty analysis.

4.2.3 AZMI Output Statistics

The model outputs $\Omega(\omega)$ are based directly on the model and the specified distribution of input parameters. The mean value (μ) and standard deviation (σ) of $\Omega(\omega)$ are given by the following analytical relations:

$$\mu(\Omega) = c_1, \qquad \sigma(\Omega) = \sqrt{\sum_{j=2}^{N} c_j^2}, \tag{4.8}$$

Likewise, all other moments of Ω can be obtained analytically, based on expansion coefficients and the moments of input parameters. The uncertainty outputs are space-time dependent, hence they are written $\mu(x, y, t)$ and $\sigma(x, y, t)$. These statistical moments were analyzed for the AZMI ROM for the simulation period of 200 years. Mean and standard deviation of changes in pressure response above the AZMI over time is shown in Figures 4-8 (a) and 4-10 respectively, based on the uncertainty of the five input parameters. A total of 56 ($= (5+3)!/(5! \times 3!)$) detailed simulations (see Eq. (4.3)) were performed o generate the uncertainties in model outputs based on aPC framework. It can be seen from Figure 4-8 (a) that the mean of pressure buildup above the AZMI from the aPC simulations is approximately 0.50 MPa higher than that of the base case scenario. Since the highest pressure buildup above the AZMI occurs right above the injection well location, the variation in pressure change output from the entire set of simulations to that of the calculated mean was examined. The analysis is shown in Figure 4-8 (b) by plotting the range of predictions from the simulations. The probability of detecting a pressure build-up above the injection well was also estimated using a cumulative distribution plot. Figure 4-9 shows the probability

distribution of pressure build-up above the injection point. This result can be used to predict the risk associated with CO_2 leakage into the AZMI. For example, if the system is required to be assessed based on a threshold AZMI pressure, the probability of failure can be calculated based on such results. It can be seen from Figure 4-10 that the areal extent of standard deviation increases as more CO_2 is injected into the system after which it starts to decrease considerably over time. The maximum deviation in pressure change is also above the injection well location. This observation is consistent with the fact that a higher the amount of leakage will result in a higher pressure buildup. Thus it becomes important to understand the geologic properties of the system more accurately. Uncertainties of input parameters can lead to significant deviations in model outputs. Hence, the need for site-specific data is an essential requirement for efficient model predictions. Larger variation in input parameters of a model will lead to large deviations in outputs, which will lead to a failure in the understanding of the storage system and inadequate predictions of the containment risk. The large uncertainties in the AZMI ROM prediction makes it important to analyze the sensitivity of the output space to each individual parameter.

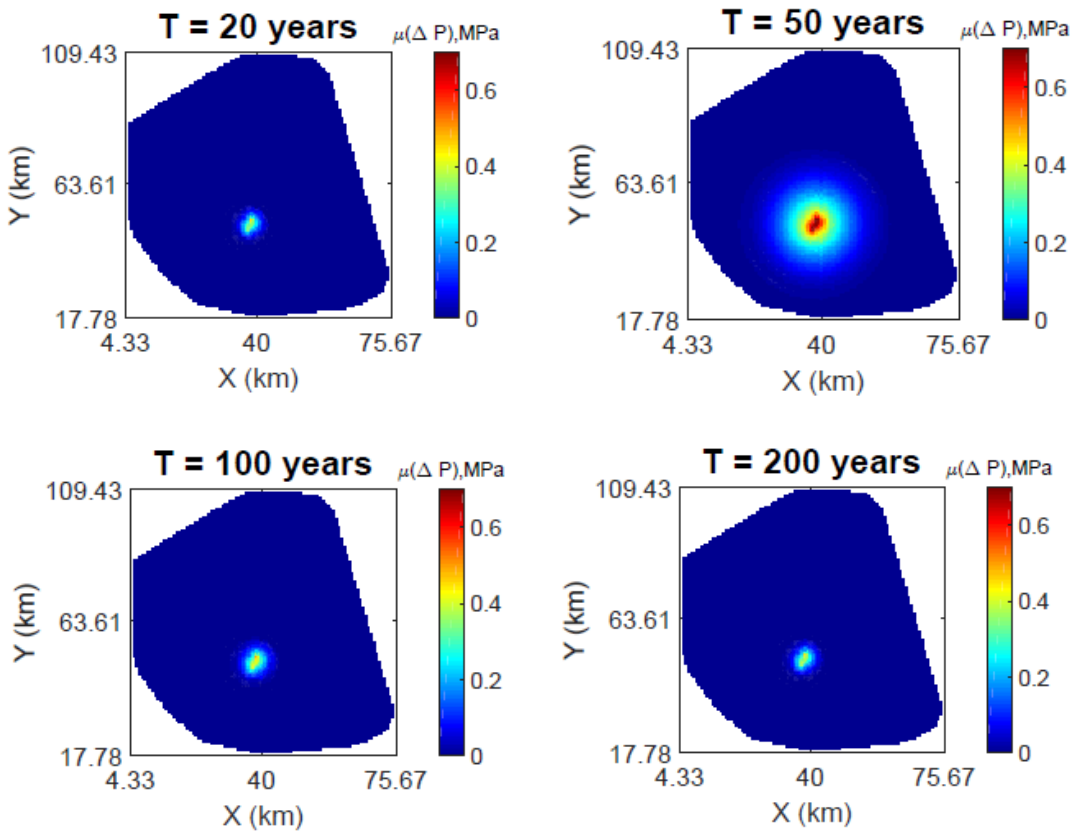

(a)

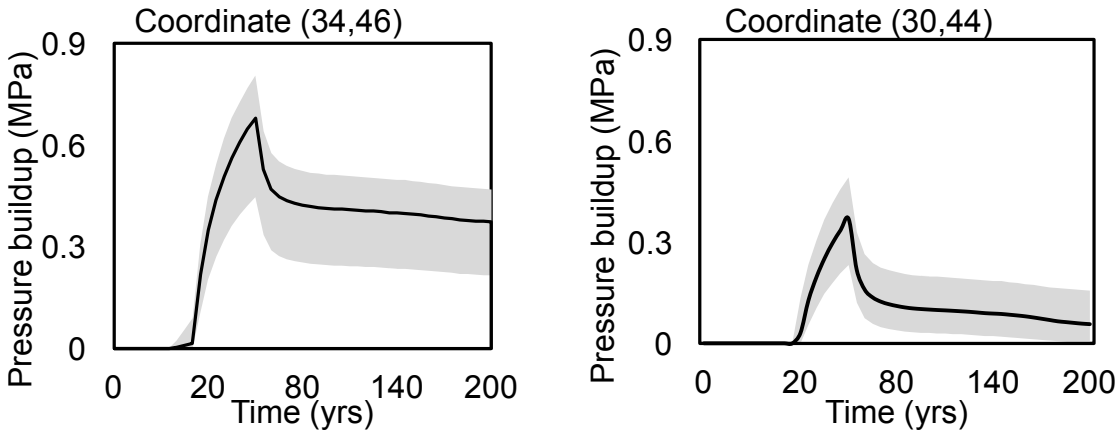

(b)

Figure 4-8: Plots showing (a) mean change in pressure response (in MPa) at the top of AZMI over time, (b) mean pressure change (black line) and range of pressure change from 56 simulations (grey shaded region) above injection point, i.e., coordinate (34,46) and 4 km away from injection well southwards, i.e., coordinate (30,44) over time.

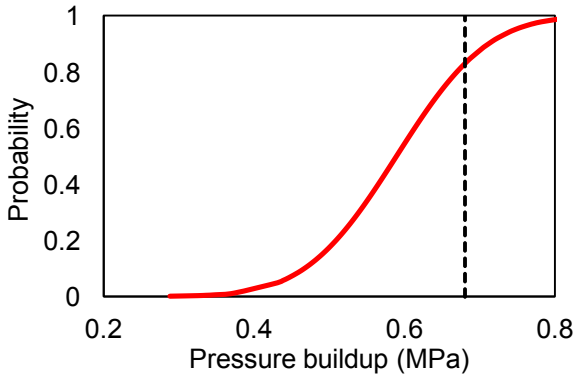

Figure 4-9: Cumulative probability of detection of pressure build-up (shown in red line) at the top of the AZMI above injection point, i.e., coordinate (34,46) at the end of injection. The black dotted line shows the mean of pressure build-up.

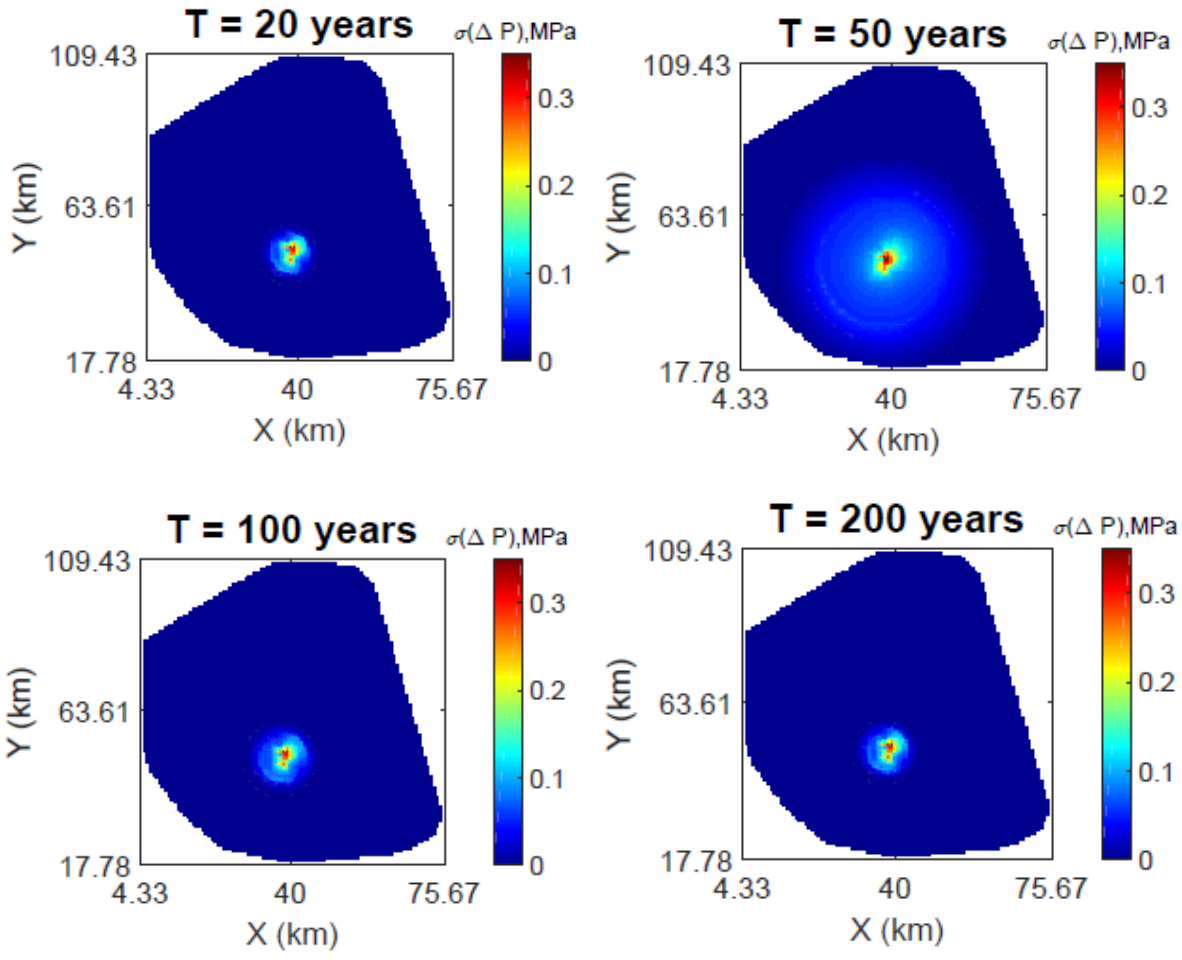

Figure 4-10: Estimation of standard deviation of the change in pressure response (in MPa) prediction by AZMI ROM at the top of AZMI.

4.3 SENSITIVITY ANALYSIS OF MODELING PARAMETERS

Assessment of the relative importance of the input parameters on the AZMI ROM output is required to understand the degree of their individual impact on the model predictions. This assessment is performed using a global sensitivity analysis with Sobol indices that are based on the aPC technique as described in Oladyshkin et al., 2012 and Ashraf et al., 2013. As discussed in these previous works, the global aPC-based sensitivity analysis obtains global sensitivity information at low computational costs.

4.3.1 Sobol Sensitivity Indices

A variance-based sensitivity analysis approach by calculation of Sobol Sensitivity Indices (Sobol, 2001) was used. Studies on the combination of PCE techniques with Sobol indices have been performed in several previous studies (Oladyshkin et al., 2012; Crestaux et al., 2009 and Sudret, 2008). This approach replaces the analyzed system with an approximating function that permits the calculation of numerical and mathematical benefits of a sensitivity analysis (Ashraf et al., 2013). Since the calculation of output variances from statistics of input variables of polynomials is relatively fast, polynomials are used for the approximation. For the AZMI modeling scenario, the solution is approximated by orthogonal polynomials with ascending polynomial degree.

To perform this approach, the system output is broken into components as follows:

$$\Gamma = \Gamma_0 + \sum_i \Gamma_i + \sum_i \sum_{j>i} \Gamma_{ij} + ... \tag{4.9}$$

where, indices i and j shows dependency on two or more variables. If we consider the input vector Θ to have n component θ_i for $i=1,\ldots\ldots,n$, then, $\Gamma_i = f_i(\theta_i)$ and $\Gamma_{ij} = f_{ij}(\theta_i,\theta_j)$, Saltelli et al. (2008) defined the higher order sensitivity index, or Sobol index (Sobol, 1990), representing the significance of variation in output generated from the joint uncertainty in several input variables, i.e., from the interaction of uncertain parameters, as:

$$S_{ij} = \frac{\mathrm{V}[\mathrm{E}(\Gamma|\theta_i,\theta_j) - \mathrm{V}[\mathrm{E}(\Gamma|\theta_i) - \mathrm{V}[\mathrm{E}(\Gamma|\theta_j)]}{\mathrm{V}(\Gamma)} \tag{4.10}$$

where, $\mathrm{V}[\mathrm{E}(\Gamma|\theta_i,\theta_j)$ is the variance of output expectations for a given value of inputs θ_i and θ_j. If all the indices containing a given variable θ_i are added, we get total Sobol index (Ashraf et al., 2013):

$$S_{Ti} = S_i + \sum_{j\neq i} S_{ij} + \sum_{j\neq i} \sum_{k\neq i} S_{ijk} + ... \tag{4.11}$$

The total Sobol index is a sensitivity measure to rank parameters according to their influence on model output. The higher the index, the greater is the effect of the corresponding input parameter on the model output. Sobol indices are calculated analytically (Oladyshkin et al., 2012) from the expansion coefficients of the aPC, shown in Eq. (4.2).

4.3.2 AZMI Sensitivity Analysis

Quantitative sensitivity information for the AZMI ROM is extracted from the polynomial response surface. The calculation of the Sobol indices (Eq. (4.10)) and the total Sobol indices (Eq. (4.11)) were performed for the AZMI modeling scenario. The results are based on the aPC expansion of order three, which was assessed by fifty-six detailed simulations performed for the uncertainty analysis. Model sensitivity analysis is performed for the five previously described input parameters (i.e., AZMI permeability, AZMI porosity, AZMI thickness, caprock permeability and caprock thickness) that have been used to quantify the model uncertainty. The test evaluated the impact of these parameters on the model output – pressure buildup response. The total Sobol sensitivities of input parameters on the AZMI ROM output are summarized in Figure 4-11. The figure presents the sensitivity results above the injection point and a point approximately 4 km south from the injection point at the end of injection period (= 50 years) and at the end of simulation (= 200 years). Table 4-2 represents the ranked 2nd Sobol indices for the five uncertain parameters at the end of injection (= 50 years). The Sobol sensitivity calculation is shown for the 2nd order expansion and not the 3rd. The results are shown as an illustration of how parameter-parameter interaction can play a role in sensitivity calculation.

Figure 4-12 shows the time profile of the total Sobol indices (S_{Ti}) determined using Eq. (4.11), quantifying the contribution of of the individual modeling parameters on the uncertainty of the pressure: (a) above the injection well, i.e. coordinate (34,46) and, (b) 4 km south of the injection well , i.e., coordinate (30,44). The sensitivity is normalized by variance at each time step. It

should be noted that the sum of S_{Ti} of each parameter need not be equal to one, suggesting the presence of parameter-parameter interaction effects (Saltelli, 2008). Form this figure, it can be seen that the AZMI permeability (k_{AZMI}) is clearly the most influential parameter, with a higher total Sobol index corresponding to higher pressure buildup. If the permeability of the AZMI is high, the pressure should easily dissipate, resulting in lower pressure buildup in the AZMI. If the formation has a higher porosity, it means it can store more CO_2 per unit volume of the porous medium. This allows the incoming CO_2 to accumulate in the pore space, causing a pressure change in the area.

When the flow physics changes from injection to a gravity-dominated system, a distinct change can be seen in the sensitivity patterns. During the injection period, H_{AZMI}, $k_{caprock}$ and $H_{caprock}$ are more dominant than k_{AZMI} and Φ_{AZMI}. The reason is that the incoming CO_2 takes time to mobilize and accumulate in the AZMI. Initially the model is largely dominated by the incoming flux through the seal which is dependent on $k_{caprock}$ and $H_{caprock}$ and the pressure buildup is also positively affected by the thickness of the AZMI, H_{AZMI}. Higher permeability of caprock leads to higher CO_2 and brine mobility, which leads to higher pressure buildup in the AZMI from incoming CO_2 and brine. The sensitivity of the pressure output with respect to higher AZMI permeability increases, immediately after stopping the injection.

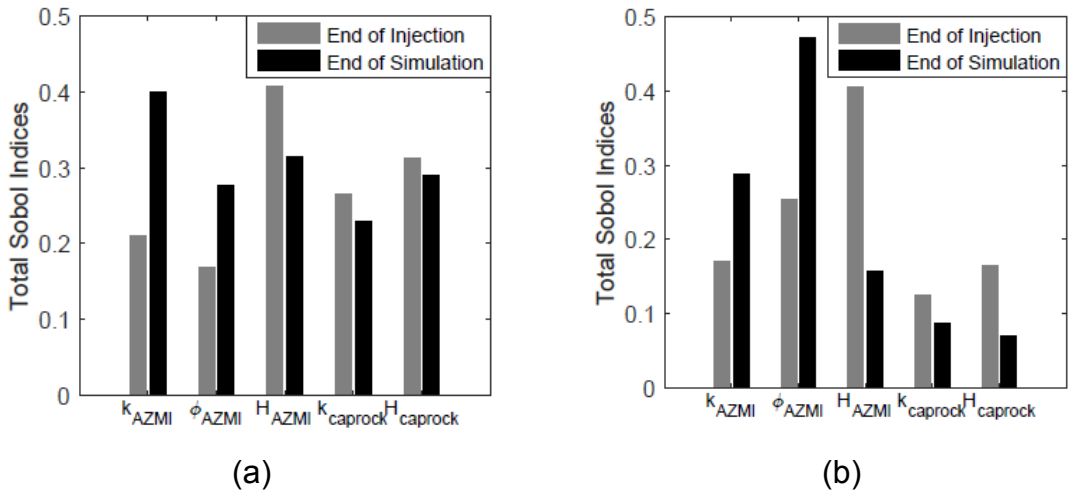

Figure 4-11: Sensitivity of AZMI ROM output for changes in pressure with respect to the uncertain parameters: AZMI permeability (k_{AZMI}), AZMI porosity (Φ_{AZMI}), thickness of AZMI (H_{AZMI}), caprock permeability ($k_{caprock}$) and caprock thickness ($H_{caprock}$) at: (a) above the injection well, i.e. coordinate (34,46) and, (b) 4 km south of the injection well, i.e., coordinate (30,44).

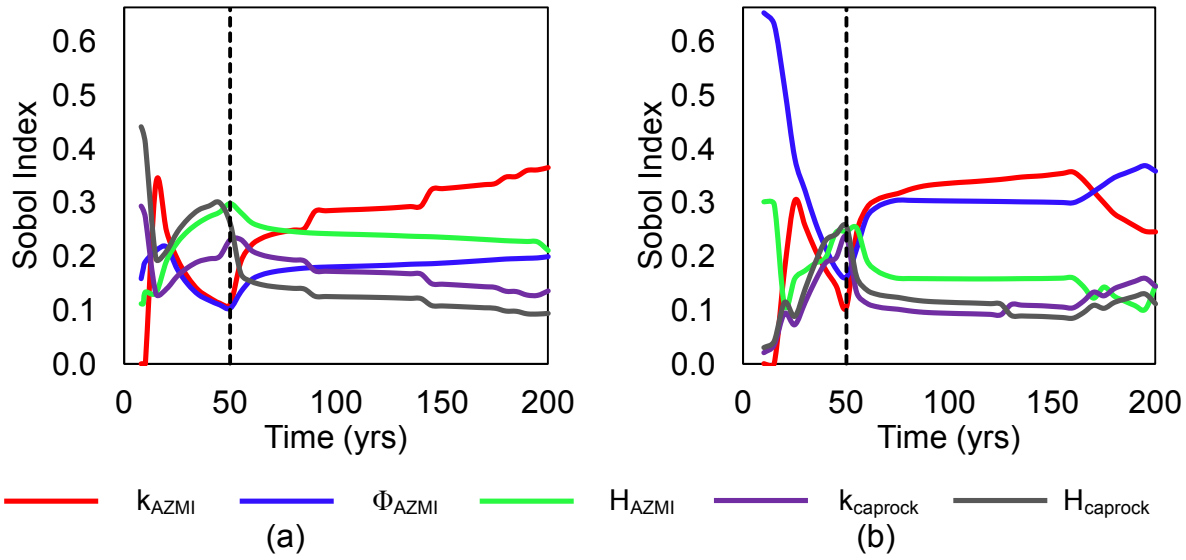

Figure 4-12: Sobol sensitivity results for AZMI ROM outputs over time at (a) above the injection well, i.e. coordinate (34,46) and, (b) 4 km south of the injection well , i.e., coordinate (30,44).

Table 4-2: Second-order Sobol indices for five parameters: [1] AZMI permeability (k_{AZMI}), [2] AZMI porosity (Φ_{AZMI}), [3] thickness of AZMI (H_{AZMI}), [4] caprock permeability ($k_{caprock}$) and [5] caprock thickness ($H_{caprock}$) at coordinates above the injection well, i.e. coordinate (34,46) and, 4 km south of the injection well , i.e., coordinate (30,44) at the end of injection (= 50 years).

Sobol index	Value at (34,46)	Rank at (34,46)	Value at (30,44)	Rank at (30,44)
S_1	0.215	4	0.285	2
S_2	0.171	5	0.467	1
S_3	0.397	1	0.165	3
S_4	0.268	3	0.081	6
S_5	0.303	2	0.073	7
S_{1-2}	0.042	8	0.102	4
S_{1-3}	0.055	7	0.037	8
S_{1-4}	0.003	10	0.003	11
S_{1-5}	0.001	14	0.002	13
S_{2-3}	0.017	9	0.085	5
S_{2-4}	0.001	13	0.004	10
S_{2-5}	0.001	15	0.003	12
S_{3-4}	0.002	11	0.001	14
S_{3-5}	0.001	12	0.001	15
S_{4-5}	0.073	6	0.006	9

4.4 CONCLUSION

This chapter presents the application of reduced order models (ROMs) to predict the pressure response in the Above Zone Monitoring Interval (AZMI) and flux response above the caprock using the hypothetical Kimberlina CO_2 storage site (California, USA) as an illustrative base case. A data-driven arbitrary polynomial chaos expansion (aPC) method for uncertainty and sensitivity analysis of above zone pressure predictions is presented and discussed. The data-driven approach provides a response surface based on a global orthonormal polynomial basis for arbitrary distributions. The method does not require extensive statistical knowledge for the data analysis. Thus, the aPC approach provides the ability to model complex systems with unknown probability distribution functions, when only data sets of limited size or prior knowledge are available. These results demonstrate the application and feasibility of using aPC-based methods to analyze realistic CO_2 injection scenarios. Using the base case Kimberlina storage scenario, five uncertain parameters with assumed uncertainty distributions were used to compute the mean of the above zone pressure buildup and the associated deviations in prediction related to the model uncertainties. The results show large uncertainties in the above zone pressure prediction, making it important to analyze the role of each individual parameter on the output space. Also, they emphasize the need for site-specific data for efficient model predictions. The above zone pressure sensitivity to different geological parameters was also evaluated and quantified using Sobol indices. These results show that the most influential parameter for the pressure buildup responses is the permeability of the AZMI layer. The other parameters are less important but have almost equal influence on the predictions with different trends over time.

Since the uncertainties of the input variables are hypothetical and are provided solely for demonstration purposes, the implications of this study are limited to the probabilistic assumptions made in this research, which would have to be reviewed and adjusted when applying the methodology to an actual CO_2 storage system.

Chapter 5

Bayesian Design of an Above Zone Pressure Monitoring System

Injecting large volumes of CO_2 into the subsurface may cause significant increases in pressure over large spatial domains that could cause unwanted fluid migration or induce seismic activity and potentially adversely affect nearby resources (e.g., groundwater resources) (Birkholzer and Zhou, 2009; Pruess, 2004). To protect the environment and public health, a comprehensive understanding of how risks evolve through time should be developed for geologic storage (GS) projects. Monitoring at CO_2 storage sites can help to identify and resolve the onset, location, and volume of potential fluid migration from the storage reservoir in a systematic, efficient, and timely manner. The monitoring of pressure changes, as an indication of leakage, represents one approach to provide this information (Jung et al., 2013; Sun and Nicot, 2012). Due to cost concerns and logistical constraints, it is important to design monitoring networks efficiently, i.e., using the fewest number of new and/or pre-existing wells to obtain the information that is necessary for decision making.

There is great deal of literature on the general concept of environmental monitoring network design and optimization. Previous studies have focused on

groundwater quality compliance monitoring (Loaiciga, 1989; Loaiciga et al., 1992; Meyer et al., 1994; Reed and Minsker, 2004), early warning systems for water distribution network contamination (Berry et al., 2006; Krause et al., 2008; Xu et al., 2010), contaminant source identification (Dhar and Datta, 2007; Mahar and Datta, 1997; Sun et al., 2006), and experimental-based monitoring framework design (Bayer et al., 2010; Singh and Minsker, 2008; Ucinski and Patan, 2007). However, there have been very few studies focusing on the optimization of monitoring systems for the geologic storage of carbon dioxide. Most notable are the efforts of Yang et al. (2011), which evaluated detectability of CO_2 leakage flux in the near surface environment for different monitoring network densities and parameter ranges; Sun et al. (2013) which proposed a new pressure-based monitoring network ; Azzolina et al. (2014), which demonstrated a pressure-monitoring approach for improving the ability to detect smaller leaks in a more timely manner; Wang and Small (2014), which characterized the CO_2 leakage level in an idealized storage site through an assessment of the integrity of caprock inferred from injection zone pressure measurements; and Yonkofski et al. (2016), which presented robust site specific monitoring designs using existing data generated from physics-based simulations of CO_2 leakage. Pressure monitoring in AZMI has been proposed for early detection of leakage (Hovorka et al., 2013) because of the fast traveling speed of pressure perturbations and the proximity of the AZMI to storage formations (Nordbotten et al., 2004). However, unlike the storage formations, the AZMI will be subjected to less pressure disturbance during injection activities, which will require a monitoring network capable of detecting these smaller signals as well as interpreting potential anomalous pressure signals. From an operations perspective, deep pressure monitoring wells are costly to drill and maintain—drilling and instrumentation costs can easily

exceed $ 1 million per well, which is in addition to annual maintenance and operation costs (U.S. Environmental Protection Agency, 2010). Thus, there is strong incentive to optimize the design of pressure-based monitoring networks (Sun et al., 2013).

This chapter focuses on the diffusive flux of CO_2 and brine through the primary caprock and the monitoring of the resulting pressure changes in the AZMI. The primary aim of this work is to characterize the time required to interpret AZMI pressure outcomes and associated leakage scenarios through a probabilistic assessment of the integrity and permeability of the caprock and the amount of CO_2 injected into the reservoir. Four different fractured seal scenarios were designed for the primary caprock based on literature data. These scenarios represent caprock permeability from almost impermeable to highly permeable cases. The probability distributions of pressure build-up in the AZMI for each of these scenarios were modeled, with the modeled pressure fields assumed to be observed with measurement errors. These distributions serve as the likelihood function for a Bayesian classification model, in which the posterior probabilities are computed for each of the four caprock fracture scenarios. The influence of the thickness of the caprock and the CO_2 injection rate on the modeled pressure build-up and the subsequent performance of the Bayesian classification procedure were also evaluated. The entire modeling scheme used to complete this effort is based on the workflow shown in Figure 5-1.

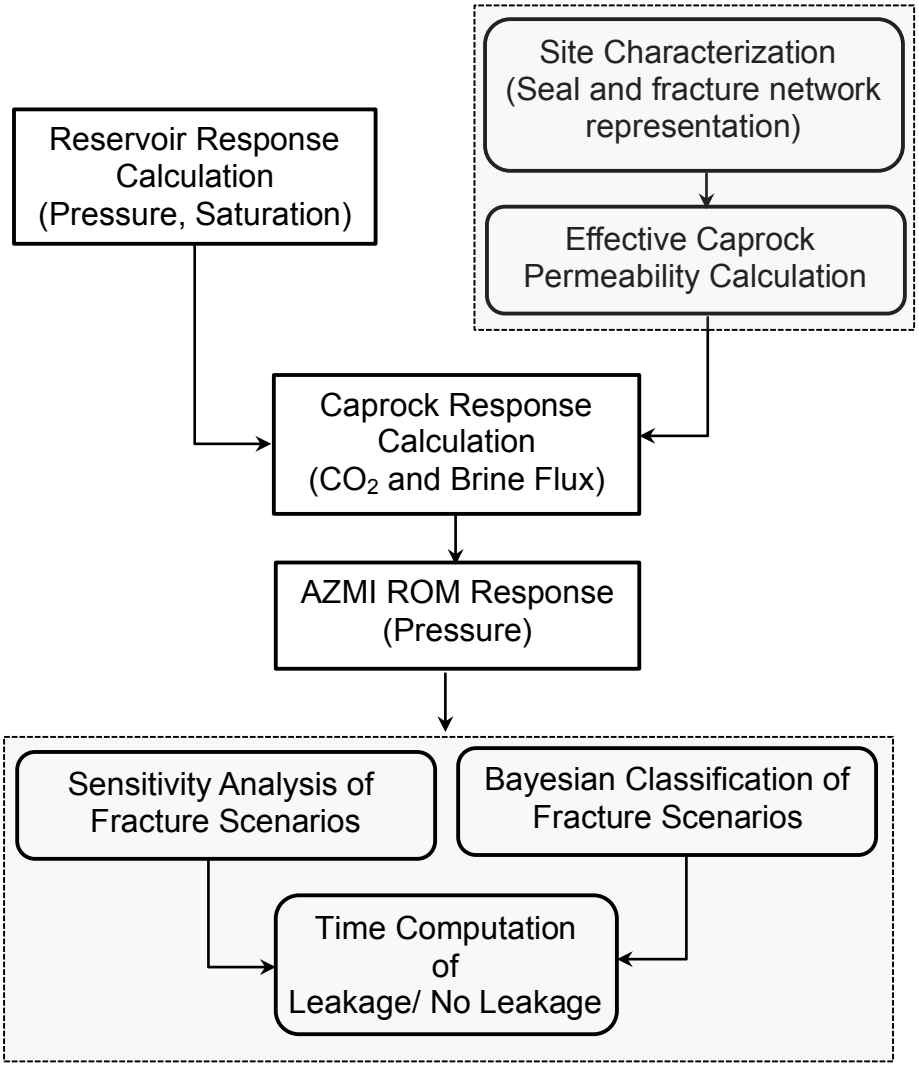

Figure 5-1: Schematic framework of Bayesian design for above zone pressure monitoring. The components developed in this study are in rounded rectangular box and the components in rectangular boxes are either developed earlier in this thesis or taken from other studies.

5.1 MODEL SETUP

The CO_2 storage system is modeled as a three-layer system with two aquifers separated by a sealing caprock of thickness 50 m (Figure 5-2 (a)). The

lower aquifer is the storage reservoir where CO_2 is being injected at a base case rate of 1 MT per year for a period of 30 years. The base case thickness of the reservoir is assumed to be 100 m. The top of the reservoir is located at a depth of 1000 m. The areal extent of the subsurface storage system is defined to be 10 km $\times$ 10 km. The reservoir features used in this study were previously summarized in Table 3-1. Reservoir simulations (Figure 5-3) were conducted using TOUGH2. CO_2 and brine flux from the seal were simulated for a period of 30 years of injection and 170 years of post-injection using NSealR. The above zone thickness used in this study is 50 m. It was assumed that the AZMI layer has a porosity of 0.1 and a permeability of 10.5 mD. The residual CO_2 and brine saturations were set at 0.01 and 0.02 respectively and the bubbling pressure was set to equal 0.01 MPa. The reference CO_2 and brine viscosities and the CO_2 and brine density corresponding to the AZMI were calculated from the lookup tables as described in § 3.1.6 (Appendix B, Section B-1). Three base case monitoring wells at 900 m depth were also considered. The locations of the monitoring wells are shown in Figure 5-2 (b). The locations were chosen to be representative of a possible spatial layout, primarily for demonstration purposes.

The sealing caprock was modeled for four different fractured network scenarios: (I) fractured network with low aperture; (II) randomly distributed clusters of fractures with high aperture; (III) fractured network zone with high aperture near the injection well and; (IV) densely fractured network with high aperture. These four scenarios were assumed to be representative of the range of possible storage seal scenarios with an impermeable seal layer with almost no leakage possible represented by scenario (I); permeable and high risk storage scenarios represented by scenarios (III) and (IV); and high integrity seal with low

leakage risk chances being represented by scenario (II). § 5.2 describes each of these scenarios.

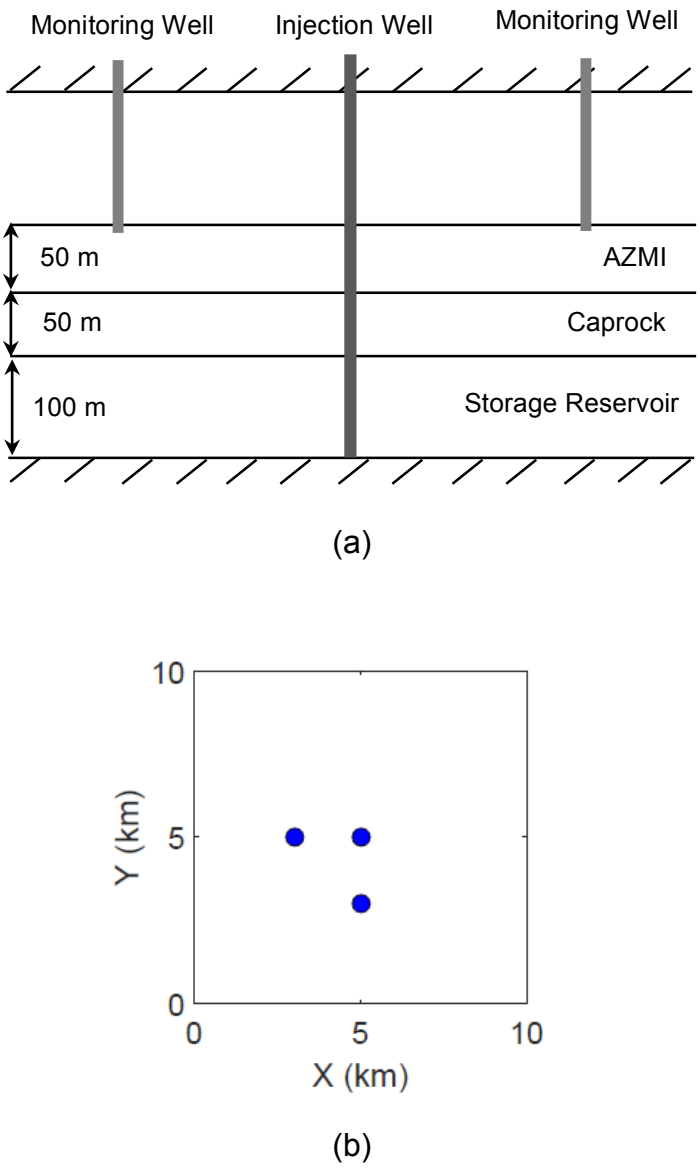

Figure 5-2: (a) Schematic diagram of the simplified geological model used for the base case study; (b) Top view of the spatial locations of base case monitoring wells.

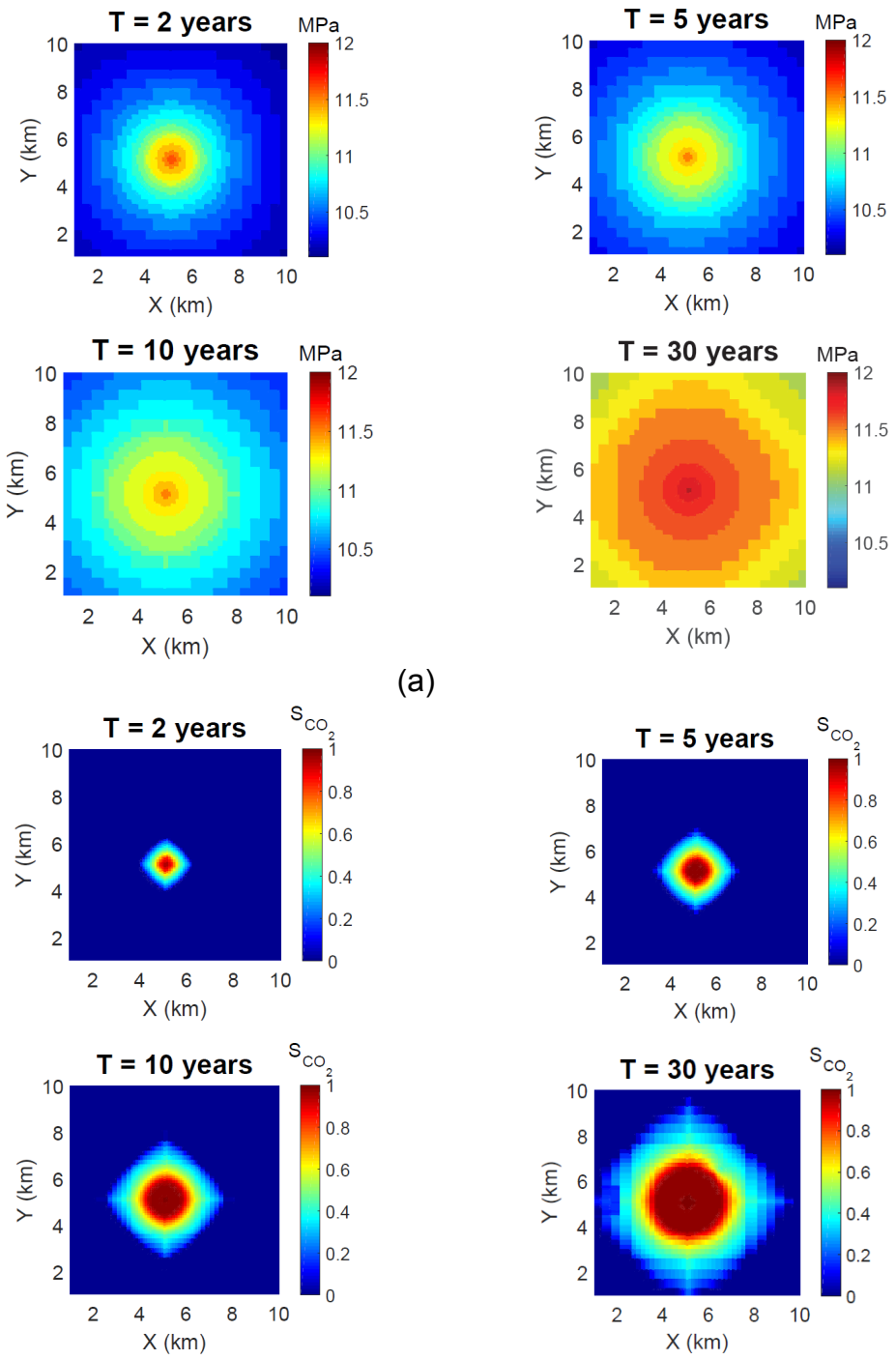

Figure 5-3: Evolution of (a) pressure (in MPa) and, (b) CO_2 saturation at the top of the injection reservoir at 2, 5, 10 and 30 years after the start of CO_2 injection.

5.2 FRACTURED SEAL SCENARIOS

Quantitative assessment of storage system performance suggests that safe, effective long-term containment is highly probable in cases where there is an intact low-permeability seal to prevent vertical fluid migration. To date, however, little consideration has been given to scenarios in which the primary sealing layer contains regions of fracturing or faulting that effectively represent heterogeneities in seal permeability. In this model, the sealing caprock was considered to be 50 m thick. In order to add heterogeneity to the analysis, a characteristics of a semi-stochastic fracture network were simulated using FRACGEN (McKoy et al., 2006). This software is specifically designed for modeling fracture networks and fractured reservoirs. The fracture network used in this model was based on the stochastic allocation of fractures' length, position, orientation and density in space. Model details are provided in Appendix C.

For demonstration purpose, four representative heterogeneous fractured seal types were defined and used for the model analysis as represented graphically in Figure 5-4. Fracture modeling details used in each of these scenarios can be found in Table 5-1. The four seal scenarios generated for this work are expected to be representative of fractured seal scenarios ranging from an almost impermeable caprock layer (good storage seal case) to a highly permeable caprock (worst storage seal case). These scenarios are intended to illustrate how alternative seal fracture properties can be defined, simulated, and used to induce a leakage and fluid migration pattern from the injection zone, through the caprock and into the AZMI. Since the NSealR model uses seal permeability as an input, a parallel plate model for fractures was used to compute the effective

permeability of the fractured networks. The detailed calculations are presented in § 5.3.

5.3 EFFECTIVE CAPROCK PERMEABILITY

Defining the aperture and the permeability of a fracture separately seems counterintuitive, since these parameters are considered to be mutually dependent, and directly related if the fractures are rectangular slits. Parallel plate theory (Snow, 1964; Sarkar, 2004) was used to compute fracture permeability in this research, where flow through a fracture is compared to flow between parallel plates. The relation between the total discharge and the pressure gradient for flow through a smooth rectangular slit is given by (Sarkar, 2004; van der Most, 2008):

$$Q = \frac{2}{3}\left(\frac{d}{2}\right)^3 \frac{w}{\mu}\nabla P \tag{5.1}$$

where, Q is the total discharge, d the distance between the two plates, w the width of the plate, μ the viscosity of the fluid and ∇P is the pressure gradient. This can be rewritten as:

$$Q = \frac{d^2}{12}(w \cdot d)\frac{\nabla P}{\mu} \tag{5.2}$$

According to Darcy's law for flow through porous media:

$$Q = k \cdot A\frac{\nabla P}{\mu} \tag{5.3}$$

where, k is the permeability of the sample and A the cross-sectional area

available for flow. When a fracture is considered as a rectangular slit, this area can also be written as:

$$A = w \cdot d \tag{5.4}$$

From equations (5.2), (5.3) and (5.4), the effective permeability of a fracture can be described as:

$$k_f = \frac{d^2}{12} \tag{5.5}$$

And, the relationship for effective block permeability therefore becomes:

$$k_{b,f} \quad \sum_{i=1}^{n} \frac{d_i \cdot k_{f,i}}{w} \tag{5.6}$$

where, $k_{b,f}$ is the block permeability, assuming the fractures run across the block parallel to the direction of flow, i is the number of the respective fracture and n is the number of fractures in the block, parallel to the flow direction. Figure 5-5 shows the effective permeability plot for all the four fractured scenarios. The calculated permeabilities were then used to compute flow through the seal using NSealR. As this study focuses on the above zone pressure build up due to associated diffusive CO_2 leakage through the primary caprock, the four different fractured captured scenarios were assumed to serve as a surrogate to the pressure build up (Table 5-2).

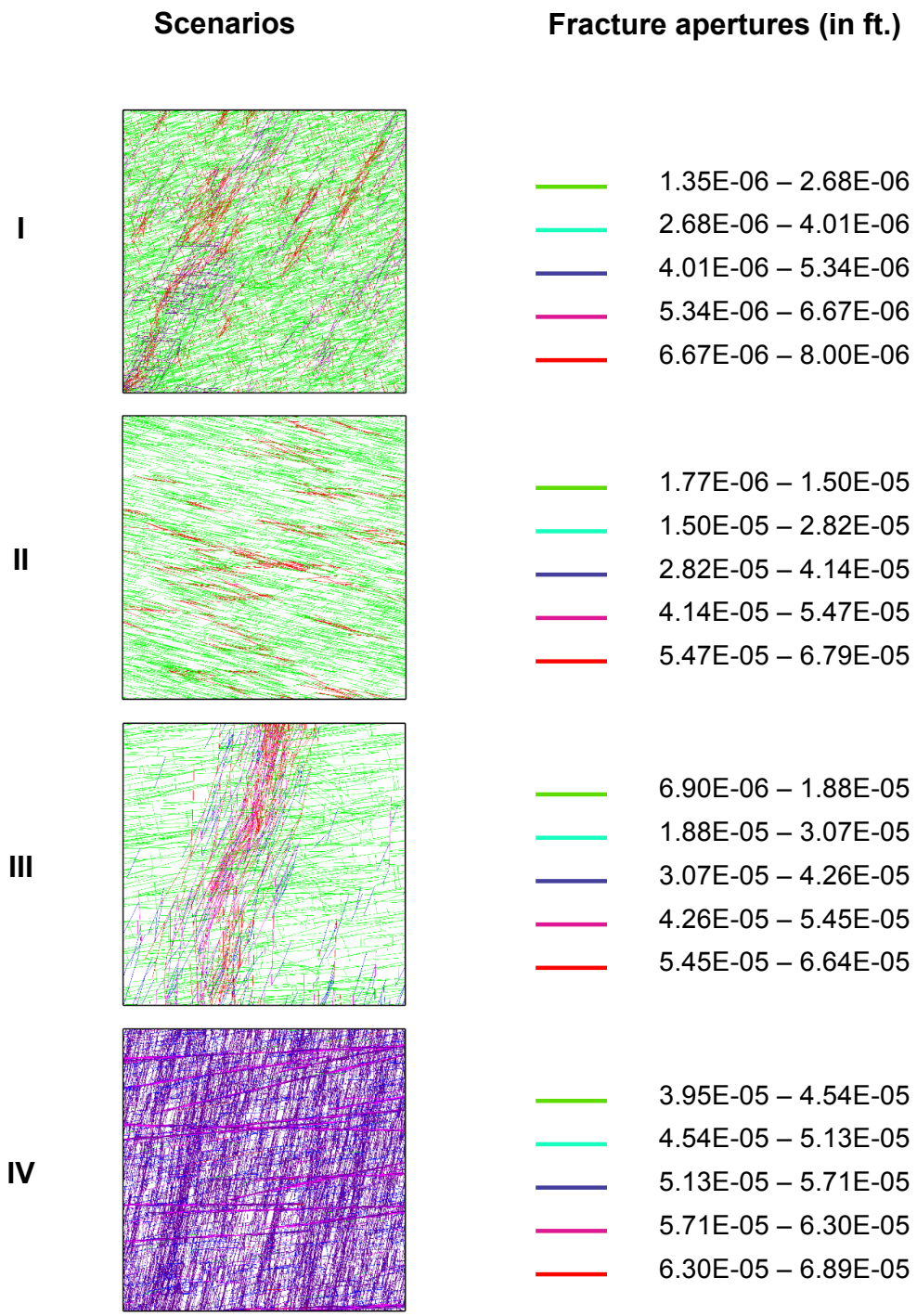

Figure 5-4: Graphical representation of fractured seal scenarios: (I) fractured network with low aperture; (II) densely fractured network with high aperture; (III) randomly distributed clusters of fractures with high apertures and; (IV) fractured network zone with high aperture above injection well.

Table 5-1: Distribution of parameters used in creating fractured network scenarios

Scenario	Fracture Set	Mean (S.D.) of fracture orientation	Mean (S.D.) of cluster orientation	Min./ Mean and Max./ Dev. fracture length (Distribution)	Min./ Mean and Max./ Dev. cluster length (Distribution)	Mean (S.D.) of fracture aperture	Density of fracture center points	Mean of intra-cluster fracture spacing	Mean (S.D.) of intra-cluster fracture density	Density of cluster center points
I	1	32 (14)	–	1000/ 5000 (2)	–	0.0000065 (0.0000003)	0.00000016	–	–	–
	2	95 (6)	32 (3)	1500/ 5500 (2)	2000/ 12000 (0)	0.000005 (0)		650	0.0000004 (0)	0.000000004
	3	32 (12)	–	500/ 3000 (2)	–	0.0000045 (0)	0.00000030	–	–	–
	4	360 (15)	32 (3)	800/ 2800 (2)	3000/ 10000 (0)	0.000008 (0)	–	250	0.0000018 (0)	0.000000016
	5	360 (10)	32 (3)	500/ 3000 (0)	3000/ 10000 (0)	0.00000175 (0)	–	250	0.0000011 (0)	0.000000016
	6	95 (6)	–	1000/ 5000 (0)	–	0.0000015 (0)	0.0000002	–	–	–
	7	71 (6)	–	500/ 2000 (0)	–	0.00000135 (0)	0.000007	–	–	–
	8	162 (7)	–	100/ 800 (0)	–	0.000008 (0)	0.000003	–	–	–
II	1	102.7 (4.28)	0 (0)	2711/ 1161.6 (2)	8750/ 3750 (2)	0.0000066 (0.0000016)	–	714.7	0.00000007 (0)	0.00000058
	2	68.3 (10.4)	0 (0)	555/ 230 (2)	6250/ 4000 (2)	0.0000045 (0.0000011)	–	5815.5	0.00000003 (0)	0.00000011
	3	103 (10)	0 (0)	2500/ 1000 (2)	10000/ 5000 (2)	0.000060 (0.0000025)	–	50	0.00000373 (0)	0.00000003
	4	360 (0)	–	335.5/ 135 (3)	–	0.0000039 (0.000001)	0.00000075	–	–	–
	5	0.7 (12.8)	–	318/ 625 (2)	–	0.0000019 (0.0000005)	0.00000391	–	–	–

Scenario	Fracture Set	Mean (S.D.) of fracture orientation	Mean (S.D.) of cluster orientation	Min./ Mean and Max./ Dev. fracture length (Distribution)	Min./ Mean and Max./ Dev. cluster length (Distribution)	Mean (S.D.) of fracture aperture	Density of fracture center points	Mean of intra-cluster fracture spacing	Mean (S.D.) of intra-cluster fracture density	Density of cluster center points
III	**1**	360 (6)	0 (0)	4000/ 10000 (0)	10000/ 22000 (0)	0.0000539 (0.000001)	–	2400	0.0000001 (0)	0.000000002
	2	20 (8)	–	2000/ 4000 (0)	–	0.00002 (0.000001)	0.0000002	–	–	–
	3	83 (6)	0 (0)	8000/ 19000 (0)	11000/ 26000 (0)	0.000001 (0)	–	1000	0.00000012 (0)	0.000000001
	4	124 (6)	0 (0)	8000/ 19000 (0)	11000/ 26000 (0)	0.000009 (0)	–	1000	0.0000001 (0)	0.000000001
	5	360 (8)	12 (5)	800/ 3100 (0)	4000/ 20000 (1)	0.00006 (0.00000205)	–	600	0.0000006 (0)	0.000000006
	6	83 (8.4)	–	4882/ 2140 (2)	–	0.0000069 (0)	0.000000663	–	–	–
	7	172 (9.2)	–	800/ 1500 (0)	–	0.000008 (0)	0.0000003	–	–	–
IV	**1**	80.4 (8.6)	–	3845.2/1647.6 (2)	–	0.0000524 (0.000006)	0.00000095	–	–	–
	2	360 (4)	83.9 (4)	3845.2/1647.6 (2)	48816/21402 (2)	0.0000576 (0.000004)	–	27	0.00001342 (0)	0.000000007
	3	172 (9.2)	–	450.7/370.2 (2)	–	0.0000498 (0.000002)	0.00000332	–	–	–
	4	12.1 (7)	0 (0)	436.3/ 4000 (1)	20000/ 60000 (0)	0.0000562 (0)	–	6.2	0.00001907 (0)	0.000000197
	5	124 (15)	–	48816/ 21402 (2)	–	0.00005 (0)	0.000000005	–	–	–

Fracture and Cluster orientation logic: *0: Uniform; 1: Exponential; 2: Lognormal; 3: Fracture Intersection Frequency Control option*

The empty cells represents that the particular fracture set doesn't form any cluster

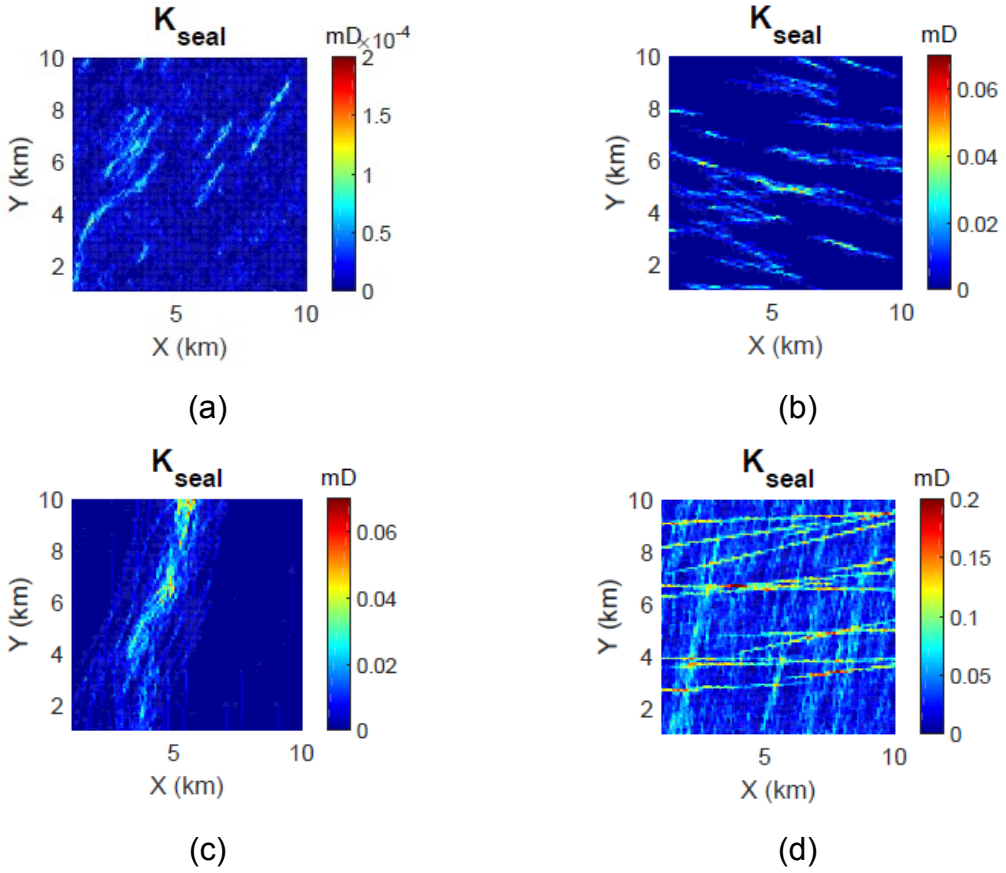

Figure 5-5: Calculated effective permeability (in mD) for base case model with four caprock fracture scenarios: (a) Scenario I, (b) Scenario II, (c) Scenario III and, (d) Scenario IV.

5.4 AZMI ROM RESULTS

The AZMI ROM (Namhata et al., 2016) was used to calculate the above zone pressure build up for each of the caprock scenarios. Figure 5-6 presents the changes in pressure responses in the AZMI over time using flux from the seal for each of the fracture scenarios for the simulation periods previously discussed.

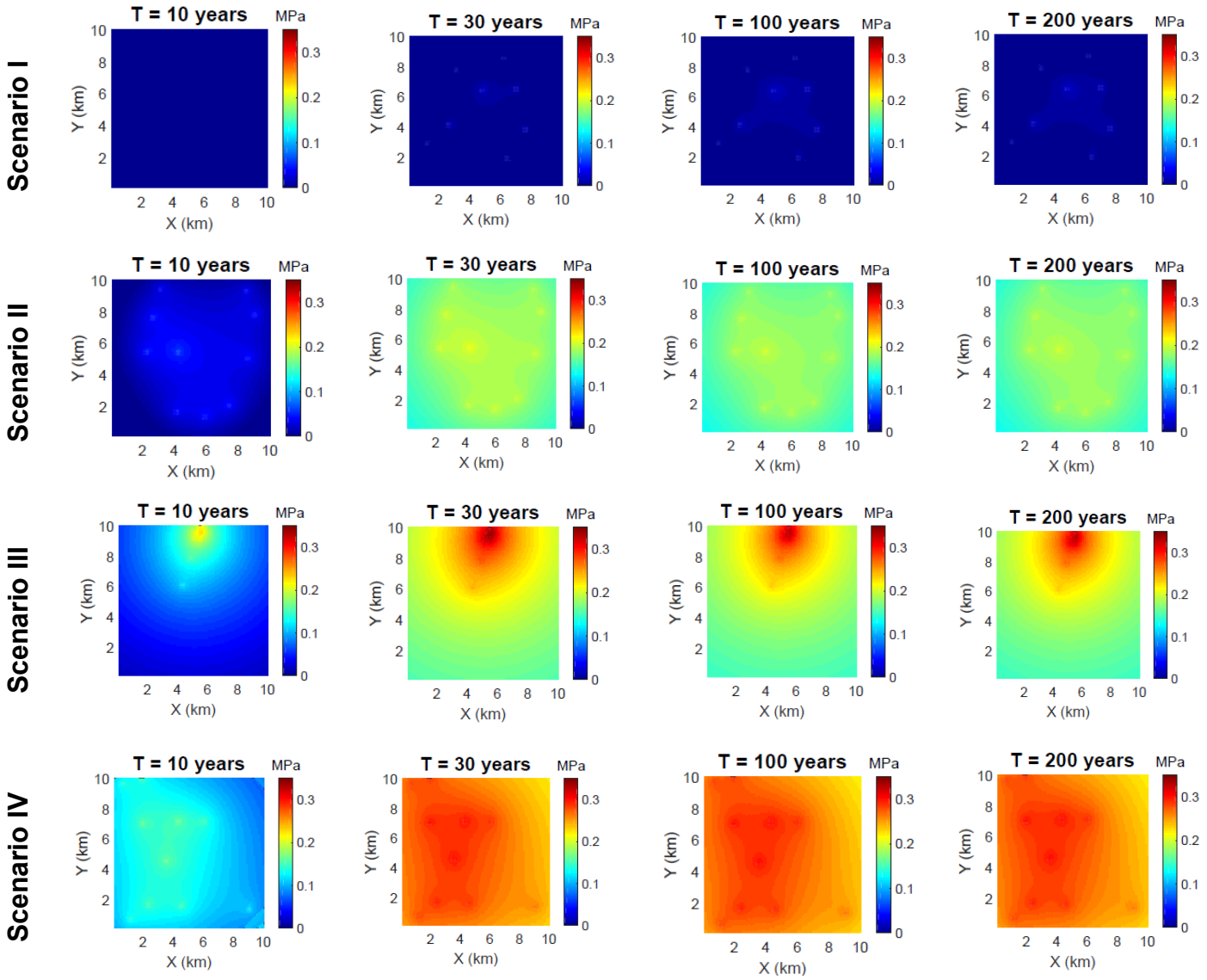

Figure 5-6: Change in pressure response (in MPa) at the top of AZMI through 200 years from the start of injection for the base case model with four caprock fractured scenarios.

5.5 BAYESIAN CLASSIFICATION METHODOLOGY

An expert's belief regarding the relative probability that each caprock fracture scenario is present at a site can be combined with observed pressure monitoring and modeling results using Bayesian classification theory. The belief of the expert is assumed to be a prior distribution of the presence of each of the four scenarios at a CO_2 storage site. In the Bayesian classification methodology, the posterior distribution is then derived by combining the prior distribution and the monitored pressure at the three monitoring locations. If there is no information on the prior distribution, the results will totally depend on the monitored (or modeled) pressure outputs. In this case, the posterior probability of a fracture scenario is proportional to the likelihood function for the modeled pressure outputs (time and location dependent), given each fracture scenario.

To characterize the performance of the classification procedure, simulated leakage – pressure outcomes are generated for each scenario and translated into an assumed sequence of AZMI pressure measurements. The likelihood function for the above zone pressure measurements using AZMI ROM has two components: first, the uncertainty in the true value of the above zone pressure that results from uncertainties in caprock fracture properties; and second, the uncertainty that might be associated with the modeling error. The first uncertainty was captured by 100 discrete FRACGEN simulation results. The latter was captured by assuming log normal measurement error function that maps simulated modeling results to pressure values that are assumed to be measured. To determine the ability to infer the true caprock fracture scenario

type at the site, multiple realizations for each fracture scenario were simluated, assuming they are measured with error, and the Bayesian rule was used to infer the probability that each scenario is present. Good performance occurs when the procedure predicts high probability for the scenario used to simulate the leakage – pressure realizations (and low probability for the others).

5.5.1 Mean Pressure Buildup

As shown in Figure 5-2 (b), three above zone monitoring wells were assigned for our base case analysis. The number and location of the monitoring wells chosen in this study are illustrative. The regions closer to the injection well are expected to see higher pressure build up, making them an obvious choice for monitoring. The three locations chosen are in regions right above or near the injection well. In this analysis, the above zone pressure build up due to CO_2 injection in the storage reservoir was calculated for each of the fractured seal scenarios (Figure 5-6). The pressure build-up at the three monitoring locations was then calculated for each scenario and at each time step. The mean of the monitored pressure build up for those three wells was then used for the analysis. The purpose of choosing the mean pressure build up ($\Delta P_{simulated}$) over individual monitoring point analysis is the ability of the mean pressure build up to capture the spatial variability in output predictions over individual analysis. The range of the mean pressure build up from the 100 simulations for each scenario is shown in Figure 5-7.

5.5.2 Inferring Fracture Scenario

Assuming no knowledge about the seal, an equal prior probability (= 0.25) was assigned for each of the four fracture scenarios (Table 5-2). The mean above zone pressure build up in the three monitoring wells ($\Delta P_{simulated}$) was chosen to be the variable for analysis of the fracture seal scenarios. The expected effective permeability of the caprock for each of the fracture scenarios are shown in Table 5-2. The greater the effective permeability of the seal, the greater will be the pressure build up in the AZMI resulting in higher $\Delta P_{simulated}$. For the cases considered and simulated in this research, the $\Delta P_{simulated}$ ranges from 0 to 0.325 MPa. Since measurement errors were considered, the observed values tend to extend beyond this range. For simplicity in statistical analysis (mainly for lognormal analysis), a minimum threshold value of 0.001 MPa was added to the $\Delta P_{simulated}$.

Table 5-2: Different fracture scenarios with their expected effective permeability and leakage behavior.

Caprock scenario	Expected effective permeability	Expected CO_2 leakage magnitude	Assumed prior probability
I	Low	Negligible	0.25
II	Very Low	Moderate	0.25
III	High	High	0.25
IV	Very High	Very High	0.25

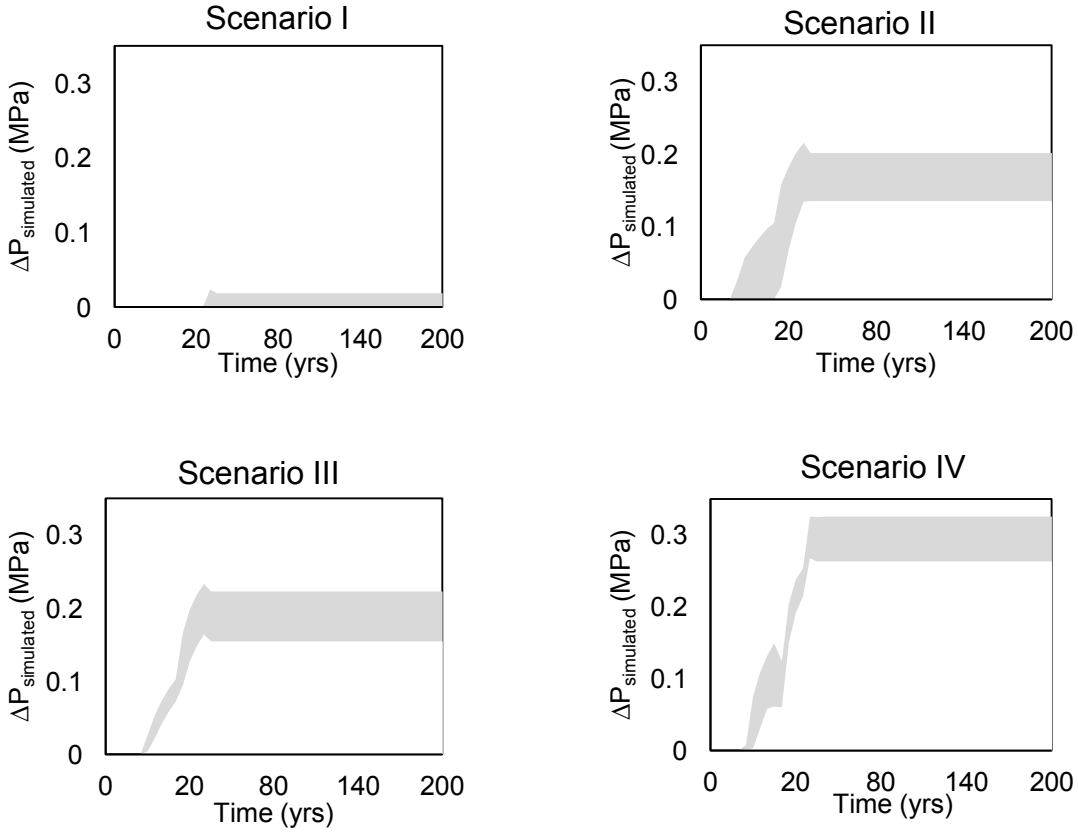

Figure 5-7: Range of mean of pressure build up at three designated monitoring well locations for all caprock fracture scenarios over time.

The likelihood of observing $\Delta P_{simulated}$ given each caprock fracture scenario, $f(\Delta P_{simulated} | Scenario\ j)$, where j is the scenario number, was estimated. This was initiated with the generation of 100 realizations of each caprock fracture scenario incorporating the values shown in Table 5-1, and the computation of $\Delta P_{simulated}$. Secondly, the effects of measurement errors were simulated by assuming that the above zone pressure build ups ($\Delta P_{measured}$) are log-normally distributed about the model simulation values:

$$\Delta P_{measured} \sim \text{lognormal}\ (a,b) \tag{5.7}$$

where,

$$a = \log(\Delta P_{simulated})$$

$$b = [\log(c.v.^2 + 1)]^{1/2}$$

The median $\Delta P_{simulated}$ values were calculated from each FRACGEN simulation for the respective lognormal distributions of $\Delta P_{measured}$ (specifying the parameters a representing the logarithm of the median of the respective measurements). The second parameter b represents the standard deviation of the logarithm of $\Delta P_{measured}$. These second parameters are specified by the coefficients of variation $(c.v.)$ of $\Delta P_{measured}$.

Thus, the lognormal distribution of $\Delta P_{measured}$ was computed using the simulation results of $\Delta P_{simulated}|i$ for each simulation i and at each time step t and the assumed measurement error (coefficient of variation here) for each $\Delta P_{simulated}$ measurement (determined by b). The pdf of the lognormal distribution serves as the likelihood function for the pressure observations given the simulation result:

$$f(\Delta P_{measured}(t) \mid a_i, b) = \log\left(\frac{1}{\Delta P_{measured}(t) \times a_i \times \sqrt{2\pi}} \exp\left\{ \frac{-(\log(\Delta P_{measured}(t)) - a_i)^2}{2b^2} \right\} \right) \quad (5.8)$$

The overall log-likelihood of a given fracture scenario is given by the sum of individual log-likelihoods from all 100 simulations for each case:

$$\text{log-likelihood (Scenario } j(t)) = \sum_{i=1}^{100} f(\Delta P_{measured}(t) \mid a_i, b) \quad (5.9)$$

and, thus, the overall likelihood will be given by:

$$\text{likelihood (Scenario } j(t)) = E[\text{Scenario } j(t)] = \exp\left[\sum_{i=1}^{100} f(\Delta P_{measured}(t) \mid a_i, b) \right] \quad (5.10)$$

Using Bayes theorem, the prior distribution of caprock fracture scenario and the likelihood function were combined to calculate the posterior distribution of each caprock fracture scenario given by:

$$\pi(\text{scenario } j(t) \mid \Delta P_{measured}(t)) = \frac{E[\Delta P_{measured}(t) \mid \text{Scenario } j] \times \text{Prob}[\text{Scenario } j]}{\sum_{i=1}^{4} E[\Delta P_{measured}(t) \mid \text{Scenario } i] \times \text{Prob}[\text{Scenario } i]} \quad (5.11)$$

5.5.3 Time to Detect Leakage

The primary aim of this work is to compute the time required to interpret the above zone pressure outcomes and the associated leakage scenarios. The time to detect leakage or no leakage were calculated using the posterior probabilities given each of the four scenarios. Two different time values were computed: (a) the time to no leakage assurance given there is no leakage ($T_{no\ leak}$) and, (b) time to leakage confirmation given there is a leakage (T_{leak}). For simplicity, it was assumed that the fracture scenario I is a no leakage scenario. $T_{no\ leak}$ provides an assessment of the system behavior by calculating the time required to understand that there is no leakage from the caprock assuming that the caprock is of scenario I type i.e., almost impermeable caprock. T_{leak} provides an estimate of how long is it going to take to understand that there is leakage from the caprock assuming that the caprock is of scenario types II, III and IV. Mathematically,

$$T_{\text{no leak}} = t \text{ when } \pi(\text{Scenario I}(t) \mid \Delta P_{measured}(t)) \geq 0.9 \mid \text{Scenario I}(t)) \quad (5.12)$$

and,

$$T_{\text{leak}} = t \text{ when } \pi(\text{Scenario I}(t) \mid \Delta P_{measured}(t)) < 0.9 \mid \text{Scenario } j(t)) : j \neq 1 \quad (5.13)$$

5.5.4 Influence of Input Parameters

Along with the uncertainties in fracture properties represented in Table 5-1, there can be other uncertainties associated with a CO_2 storage system that can have an impact on the above zone pressure monitoring. To illustrate the sensitivity of model predictions to variations in selected modeling parameters, changes in CO_2 injection rate and thickness of the primary caprock were made to compute their effect on simulation results and the probability of inferring caprock fracture scenarios. The base case model was set up for a caprock of thickness 50 m and an injection rate of 1 MT/ year for 30 years; changes to the base case and simulation results were also generated for 10 m and 100 m thick caprock and injection rates of 10 MT/ year and 50 MT/ year.

5.6 RESULTS

The base case model was set up for each of the four caprock fracture scenarios. The above zone pressure buildup was then calculated using the AZMI ROM. For posterior analysis, the mean pressure buildup from three monitoring well locations, as described previously, were used. Figure 5-8 shows the posterior probability of each of the caprock fracture scenario as a function of time from the start of injection. The posteriors are calculated for all the fracture scenarios given a particular fracture scenario. This provides an understanding of the probability of a leakage/ pressure change given any particular scenario. Since the fracture scenarios are just a representation of probable caprock types with different leakage potential, the results can be interpreted as a simple representation of

what the monitoring pattern will be for similar scenarios.

In Figure 5-8, the posterior distribution of each scenario given one of the four scenarios is presented. All the plots extend through 35 years from start of injection. Since the main aim of this work is to identify the time required to distinguish above zone pressure outcomes and the associated leakage scenarios, it was concluded from all the simulations that the maximum associated time is less than 35 years. It can be seen from the scenario I plot that the posterior probability of scenario I given scenario I reaches 0.90 at 5 years from the start of injection. This is expected because the posterior is expected to reach a higher value for a particular scenario given the same scenario. A similar trend is expected for the other scenarios too but they vary in magnitude and the time required to reach a statistically significant posterior probability. In each of the plots, there is no change in posterior probability from the prior values (= 0.25) in the first 3 years since there is no flow of CO_2 in the initial years to the AZMI, resulting in no pressure buildup. Scenario I, being distinctively different from the rest of the scenarios, has a very distinct posterior pattern. Since this scenario represents a negligible leakage case, an increase in the posterior of other scenarios, especially Scenarios III and IV, is not observed. Since Scenario II is a low leakage case and there will be no/ very little migration of fluids, only a slight increase in its posterior is initially observed.

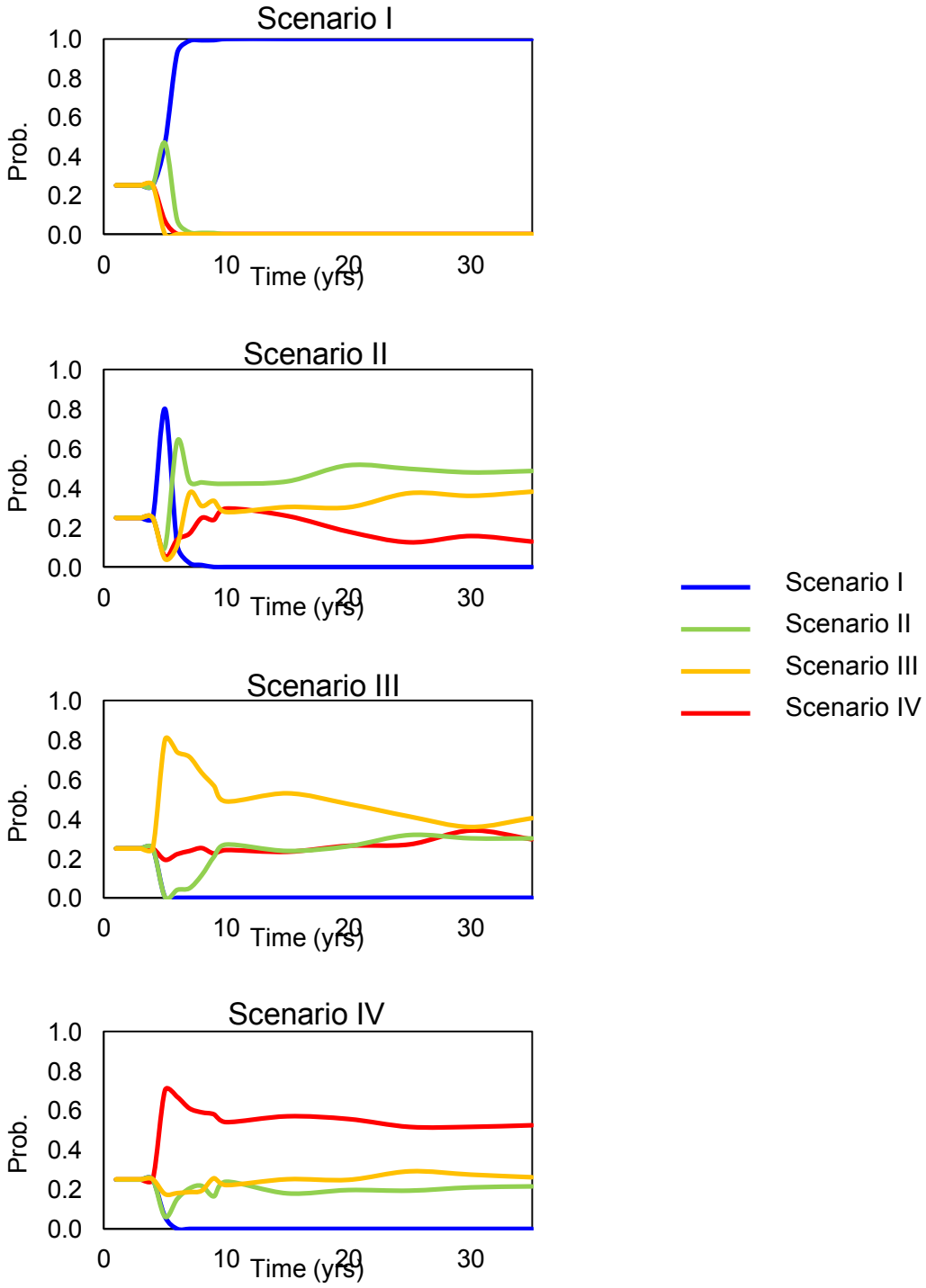

Figure 5-8: Posterior probabilities inferred for four different caprock fracture scenarios given a true value for a particular scenario (mentioned on top of the plots) until 35 years from the start of injection. Base case caprock thickness of 50 m and base case injection rate of 1 MT/yr.

For posterior probability plots of Scenarios III and IV given Scenarios III and IV respectively, there is an increasing trend as these scenarios are representative of high leakage cases with almost no effect from that of Scenario I and substantially less impact as compared to Scenario II. Given Scenario III, an increase in posterior probability of Scenarios II and IV can be seen at a later stage of injection since both these scenarios also have increasing pressure buildup over time. But the posteriors are not able to by-pass the posterior of Scenario III. In the case of Scenario II, which is representative of low permeability caprock with potential of low to moderate amount of CO_2 leakage, higher probability of scenario I compared to scenario II itself can be seen in the first 5 years. The reason being in its initial years, there is no leakage of CO_2 in Scenario II similar to that of Scenario I. As such, the posterior distribution tends to be similar in these cases.

As discussed in § 5.5.4, a sensitivity analysis was conducted to determine the effect of changing caprock thickness (from the base case 50 m) and the injection rate (from the base case 1 MT/ year) on model inferences as follows:

(a) Caprock thickness of 10 m and 100 m

(b) Injection rate of 0.25 MT/ year and 5 MT/ year.

Figures 5-9 and 5-10 shows the posterior distribution over time for caprock thickness 10 m and 100 m, respectively, keeping all the other simulation values the same as the base case simulation. Figures 5-11 and 5-12 shows the posterior distribution over time for injection rate of 0.25 MT/ year and 5 MT/ year

respectively for 30 years. From Figures 5-9 and 5-10 it can be seen that the general characteristic trend of the posteriors are similar to that in figure 5-8. With a decrease in caprock thickness to 10 m (Figure 5-9), there will be more leakage of CO_2 in the AZMI compared to that of 50 m.

This distinctive feature is captured for posteriors given Scenario II plot, where the time to predict confidently that the change in pressure is due to Scenario II is increased from the base case. For Scenarios III and IV, which are in general high leakage scenarios, the pattern is similar to that of the base case. When the caprock thickness is increased to 100 m (Figure 5-10), it is expected that lower CO_2 will leak into the AZMI compared to that of the base case. In this case too, the Scenario II is not able to distinguish itself from that of Scenario I as fast as rest of the scenarios. Comparing the curves in Figures 5-9 and 5-10 to that of 5-11 suggests that changing of caprock thickness has very little effect on the magnitude of predicted probabilities. This is not the case when we change the injection rates. Lowering of injection rates results in lower or similar statistical ability to infer the caprock fracture scenario compared to that of the base case while increasing the injection rate (Figure 5-11) yields an increase in the statistical ability for inferring the caprock fracture scenario. This is as expected since increasing the injection rate increases the likelihood of CO_2 leakage as well as increases in the above zone pressures, yielding more likely detection of caprock fracture scenarios.

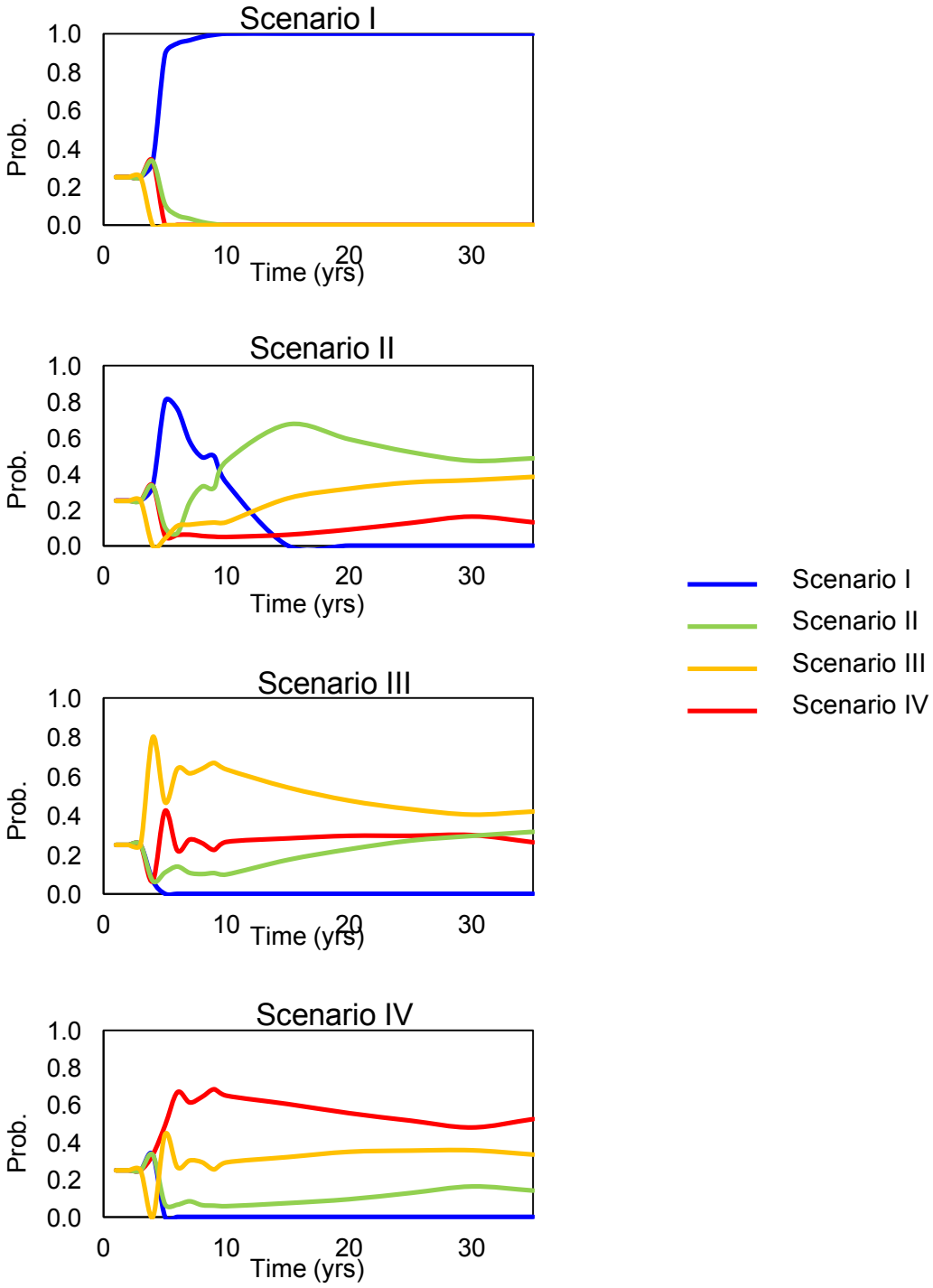

Figure 5-9: Posterior probabilities inferred for four different caprock fracture scenarios given a true value for a particular scenario (mentioned on top of the plots) until 35 years from the start of injection. Low caprock thickness case of 10 m and base case injection rate of 1 MT/yr.

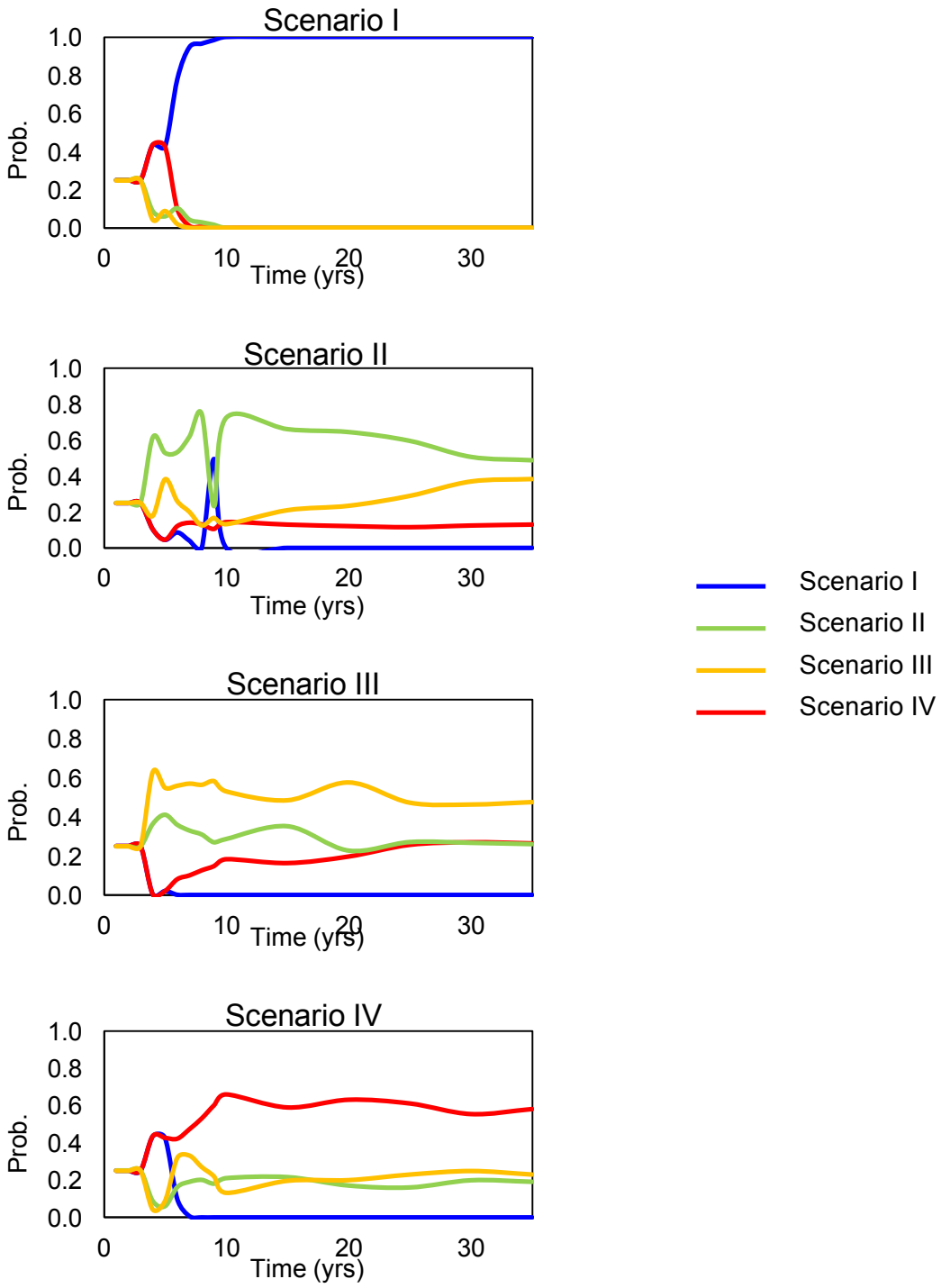

Figure 5-10: Posterior probabilities inferred for four different caprock fracture scenarios given a true value for a particular scenario (mentioned on top of the plots) until 35 years from the start of injection. High caprock thickness case of 100 m and base case injection rate of 1 MT/yr.

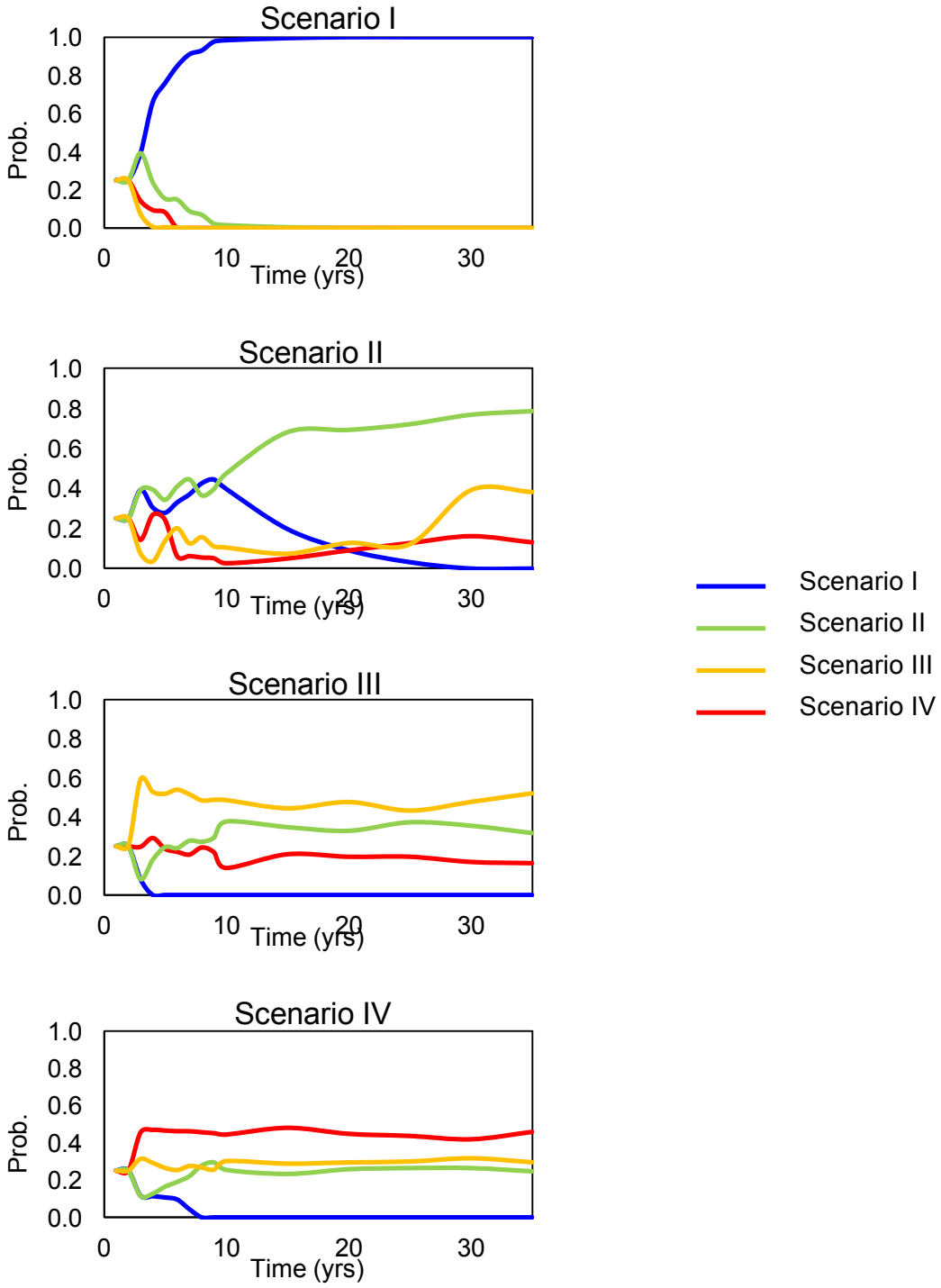

Figure 5-11: Posterior probabilities inferred for four different caprock fracture scenarios given a true value for a particular scenario (mentioned on top of the plots) until 35 years from the start of injection. Base case caprock thickness of 50 m and low case injection rate of 0.25 MT/yr.

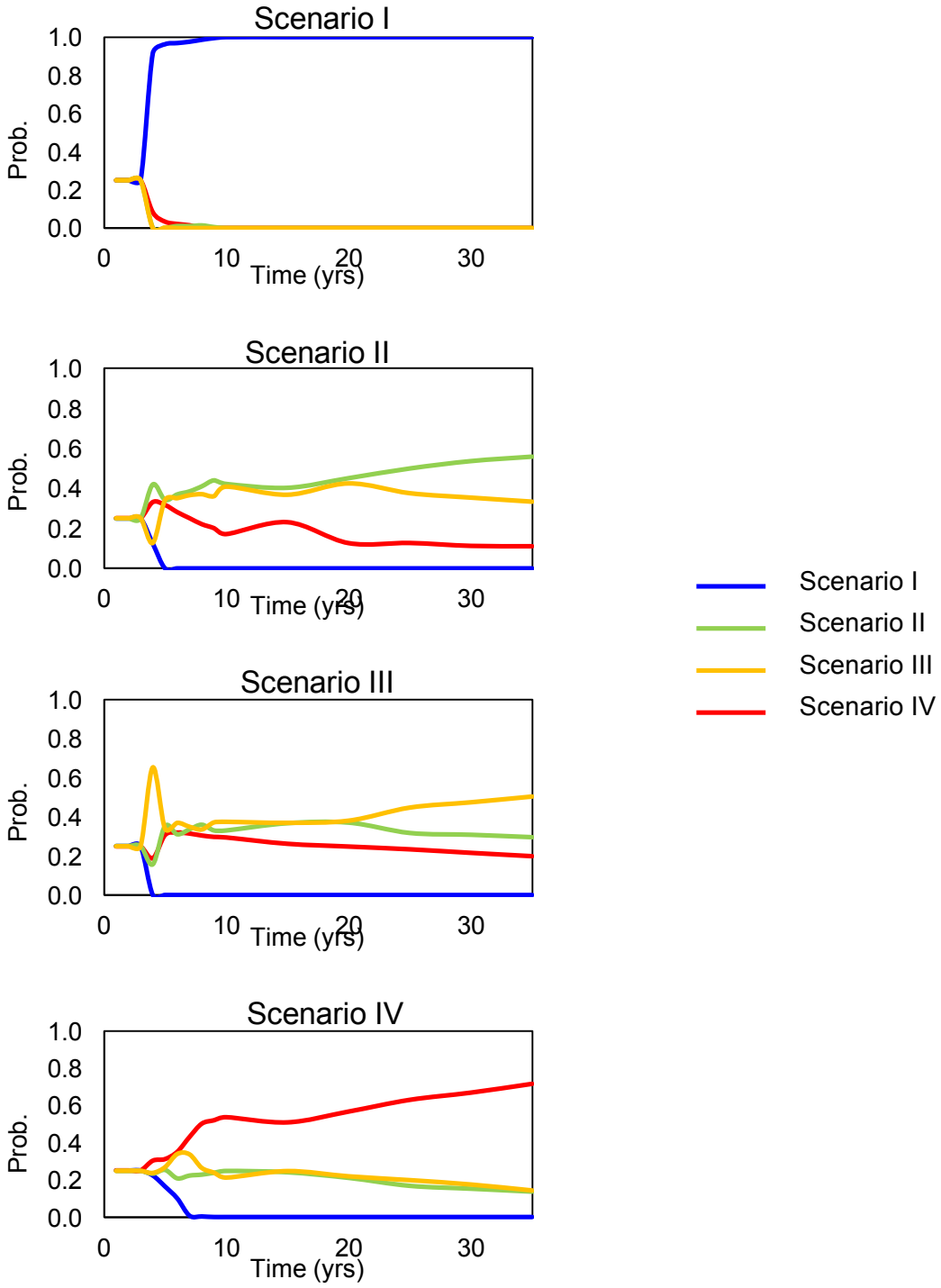

Figure 5-12: Posterior probabilities inferred for four different caprock fracture scenarios given a true value for a particular scenario (mentioned on top of the plots) until 35 years from the start of injection. Base case caprock thickness of 50 m and high case injection rate of 5 MT/yr.

With regards to $T_{no\ leak}$ and T_{leak}, the respective times for the base case and the four other scenarios are presented in Tables 5-3 and 5-4. The time to no leak assurance in Table 5-3 helps in understanding the minimum time required to confidently say that there is no significant monitorable pressure change in the AZMI. The higher the caprock thickness and lower the injection rate, more will be the time required to reach a no leak assurance conclusion since low leakage is expected in such a situation. For an opposite scenario, with low caprock thickness and high injection rate, the time to no leak assurance will be much less. The time to leakage confirmation shown in Table 5-4 provides the time at which it is determined that there will most probably be a leakage in the system based on the AZMI pressure data. The most time taken to understand that there is a leakage in the system is shown in Scenario II when the caprock thickness is low and the injection rate is low and medium. This is the case since there is expected to be very little or no leakage as part of this scenario. As such, ittakes more time to reach a statistically significant point where there is a chance that leakage has occurred. In contrast, in Scenario III, where the fractured zones are above the injection well and below the monitoring wells, high leakage rates are expected for almost all of the scenarios. Thus the time to leakage confirmation is much lower in this case. For Scenario IV, where the caprock is highly fractured throughout the space, a higher distribution of flux, and in turn higher pressure in the AZMI, are expected; the ability to detect a leak is also higher for this scenario. This can be seen from Table 5-4, where the average time to detect a leak is 6 years.

Table 5-3: Time to no leakage assurance given there is no leakage ($T_{no\ leak}$)

Scenario	Seal Thickness	Injection Rate	Time to no leak assurance, Prob [Scenario 1 $\geq$ 0.9|Scenario 1]
I	Low	Low	7
		Medium	6
		High	4
	Medium	Low	8
		Medium	6
		High	3
	High	Low	10
		Medium	7
		High	5

Table 5-4: Time to leakage confirmation given there is a leakage (T_{leak})

Scenario	Seal Thickness	Injection Rate	Time to leakage confirmation, Prob [Scenario 1 < 0.1|Scenario j] where j ≠ 1
II	Low	Low	20
		Medium	15
		High	5
	Medium	Low	10
		Medium	7
		High	4
	High	Low	9
		Medium	7
		High	4
III	Low	Low	3
		Medium	4
		High	4
	Medium	Low	3
		Medium	5
		High	4
	High	Low	3
		Medium	4
		High	3
IV	Low	Low	6
		Medium	5
		High	7
	Medium	Low	6
		Medium	5
		High	8
	High	Low	8
		Medium	6
		High	8

5.7 CONCLUSION

In this study, the characteristics of a semi-stochastic fracture network are simulated using FRACGEN (McKoy et al., 2006). For demonstration purposes, four representative heterogeneous fractured seal types are generated using FRACGEN which range from an almost impermeable caprock layer (good storage seal case) to a highly permeable caprock layer (worst storage seal case). Existing reduced order models (ROMs) are used to predict the pressure response in the Above Zone Monitoring Interval (AZMI) and flux response above the caprock using a hypothetical base case CO_2 storage problem. The probability distributions of pressure build-up in the AZMI was modeled for each of the four caprock fracture scenarios. The modeled pressure fields were assumed to be observed with measurement errors. A Bayesian classification methodology was then developed where the pressure distributions were used as likelihood functions to compute posterior probabilities for each scenario. The Bayesian model was primarily used to calculate two parameters: (1) the probability to infer a given fracture scenario and (2) the time required to distinguish above zone pressure outcomes and the associated leakage scenarios. The results indicate that in an ideal storage case, where the caprock is very thick and almost impermeable, the time taken to infer that there will be no fluid migration to the AZMI is very short. If the storage scenario is not ideal for CO_2 injection, i.e., the thickness of the seal is low and it is highly fractured with high permeability, then the time to infer a leakage is also short. The injection rate and the thickness of the caprock both influence the predicted caprock fracture scenario and the detection power of the above zone pressure monitoring. Reduction in uncertainties of caprock

geology, especially more knowledge of fracture network properties through site characterization, can lead to higher confidence in the predicted caprock fracture scenario and also improve the statistical detection power of a leakage through the caprock. Above zone pressure monitoring, combined with other monitoring techniques such as groundwater quality monitoring, seismic monitoring, surface deformation monitoring and any other applicable monitoring techniques can be used to effectively predict CO_2 leakage rates from the reservoir in a timely manner and with higher confidence.

Chapter 6

Expected Contributions and Broader Impact

At the conclusion of this research, I will have contributed significant knowledge related to the modeling of geologic carbon storage. While the context of this work primarily relates to environmental risk assessment of CO_2 storage, the conceptual models and tools developed in this study can also be applied to the subsurface processes encountered during shale gas development or desalination waste-brine management. Moreover, the AZMI and IAM modeling framework can also be replicated for the coincidental storage of CO_2 that occurs at enhanced oil recovery sites, as well.

To be more specific, achieving the individual objectives of this Ph.D. research will contribute to the improved understanding of subsurface fluid migration and environmental risks associated with the geologic storage of CO_2. The AZMI ROM for fluid migration and pressure characterization above the primary seal provides a site-specific linkage of leaks from the storage reservoir with key environmental receptors such as groundwater resources. This ROM will also assist in the investigation of using AZMI pressure signals as part of a deep subsurface monitoring network for the early detection of unexpected leakage through from the storage reservoir. Currently, this linkage between the storage

reservoir and receptors of interest is hard-wired as a direct link for all storage systems. This simplifying assumption will likely result in poor predictions (both under- and over-estimates) of the actual risk at a storage site.

The quantification of the uncertainty of the pressure predictions of the AZMI model reflects the uncertainties of the input geological properties and other storage system parameters. By quantifying the uncertainty of the model outputs and understanding the sensitivity of the model outputs to the individual input parameters, the ability to properly interpret the model outputs has been improved and future site characterization efforts can be streamlined to focus on those parameters which have the most impact on the storage system performance. Finally, the AZMI ROM also provides information for the Bayesian design of an AZMI pressure monitoring network. Deep subsurface, pressure-based monitoring is a key monitoring, mitigation and verification technology for many geologic carbon storage sites because of its early detection capability. The time required to distinguish above zone pressure outcomes for anticipated leakage scenarios will not only provide more accurate real-time predictions of the associated risks of a storage system but will also reduce the capital and operating costs of the long-term monitoring of the subsurface that is required for the early detection of leaks from geologic storage systems.

Bibliography

Ashraf, M.; Oladyshkin, S.; Nowak, W. (2013) Geological storage of CO_2: Global sensitivity analysis and risk assessment using arbitrary polynomial chaos expansion, *International Journal of Greenhouse Gas Control*, 19, 704-719.

Azzolina, N. A., Small, M. J., Nakles, D. V., & Bromhal, G. S. (2014). Effectiveness of subsurface pressure monitoring for brine leakage detection in an uncertain CO_2 sequestration system. *Stochastic Environmental Research and Risk Assessment*, 28(4), 895-909.

Bachu, S. (2008) CO_2 storage in geological media: Role, means, status and barriers to deployment, *Progress in Energy and Combustion Science*, 34, 254-273.

Bacon, DH, Keating EH, Dai, Z, Harp DH, Pawar, RJ. (2014) Reduced Order Model for the Impacts of Carbon Dioxide and Brine Leakage into an Unconfined, Oxidizing Carbonate Aquifer, Generation 3.0. *PNNL-23297*

Bayer, P., de Paly, M., Bürger, C.M. (2010) Optimization of high-reliability-based hydrological design problems by robust automatic sampling of critical model realizations. *Water Resour. Res.* 46, W05504.

Berry, J.; Hart, W.E.; Phillips, C.A.; Uber, J.G.; Watson, J.P. (2006) Sensor placement in municipal water networks with temporal integer programming models. *J. Water Resour. Plan. Manag.* 132, 218–224.

Bielinski, A., 2007. Numerical simulation of CO_2 sequestration in geological formations. *Ph.D. Dissertation, Universität Stuttgart, Germany.* Available at: http://elib.uni-stuttgart.de/opus/volltexte/2007/2953/

Birkholzer, J.T.; Zhou, Q. (2009) Basin-scale hydrogeologic impacts of CO_2 storage: capacity and regulatory implications. *Int. J. Greenh. Gas Con.* 3, 745–756.

Birkholzer, J.T.; Zhou, Q.; Cortis, A.; Finsterle, S. (2011). A sensitivity study on regional pressure buildup from large-scale CO_2 storage projects. *Energy Procedia* 4, 4371–4378.

Bromhal, G.S., Birkholzer, J., Mohaghegh, S.D., Sahinidis, N., Wainwright, H.,

Zhang, Y., Amini, S., Gholami, V., Zhang, Y., Shahkarami, A., (2014). Evaluation of rapid performance reservoir models for quantitative risk assessment. *Energy Proc.* 63, 3425–3431.

Brooks, R. H.; Corey, A. T. (1966) Properties of Porous Media Affecting Fluid Flow. Journal of the Irrigation and Drainage Division, *Proceedings of the American Society of Civil Engineers*, 92 (IR 2), 61–88.

Bryant, S. L., Lakshminarasimhan, S. and Pope, G. A., (2008). Buoyancy-dominated multiphase flow and its effect on geological sequestration of CO_2. *SPE Journal*, 13(04), 447-454.

Carroll, S. A.; Mansoor, K.; Sun, Y. (2014) Second-Generation Reduced-Order Model for Calculating Groundwater Impacts as a Function of pH, Total Dissolved Solids, and Trace Metal Concentration, NRAP-TRS-III-002-2014, *NRAP Technical Report Series*; U.S. Department of Energy, National Energy Technology Laboratory: Morgantown, WV.

Chalbaud, C.; Robin M.; Lombard J.-M.; Bertin H.; Egermann P. (2010) Brine/ CO_2 Interfacial Properties and Effects on CO_2 Storage in Deep Saline Aquifers. *Oil and Gas Science and Technology*, 65: 541-555.

Cihan A, Birkholzer JT, Zhou Q (2012) Pressure buildup and brine migration during CO_2 storage in multilayered aquifers. *Ground Water.* doi:10.1111/j.1745-6584.2012.00972.x

Crestaux, T.; Le Maitre, O.; Martinez, J.-M. (2009) Polynomial chaos expansion for sensitivity analysis, *Reliability Engineering and System Safety*, 94(7), 1161–1172.

Dhar, A., Datta, B. (2007) Multi objective design of dynamic monitoring networks for detection of groundwater pollution. *J. Water Resour. Plan. Manag.* 133, 329–338.

Eldred, E. S.; Burkardt, J. (2009) Comparison of non-intrusive polynomial chaos and stochastic collocation methods for uncertainty quantification. *47th AIAA Aerospace Sciences Meeting including the New Horizons Forum and Aerospace Exposition*, Orlando, FL, January 5—8, AIAA paper 2009-0976.

Ghanem, R., Spanos, P. (1993) A stochastic galerkin expansion for nonlinear random vibration analysis. *Probabilist Eng Mech*; 8:255–64

Heath, J. E., McKenna, S. A., Dewers, T. A., Roach, J. D., & Kobos, P. H., (2014). Multiwell CO_2 Injectivity: Impact of Boundary Conditions and Brine Extraction on Geologic CO_2 Storage Efficiency and Pressure Buildup. *Environmental Science & Technology*, 48(2), 1067-1074.

Hovorka, S.D., Meckel, T.A., Trevi˜no, R.H., (2013) Monitoring a large-volume injection at Cranfield, Mississippi—project design and recommendations. *Int. J. Greenhouse Gas Control*.

Huerta, N. J.; Vasylkivska, V. S. Well Leakage Analysis Tool (WLAT) User's Manual; NRAP-TRS-III-XXX-2015; *NRAP Technical Report Series*; U.S. Department of Energy, National Energy Technology Laboratory: Morgantown, WV, 2015.

IEA (International Energy Agency). (2008) CO_2 capture and storage: a key carbon abatement option. *IEA/OECD: Paris.*

IEA (2013) Technology Roadmap: Carbon Capture and Storage. *IEA/ OECD: Paris.*

IPCC (Intergovernmental panel on climate change) (2005) IPCC Special Report on Carbon Dioxide Capture and Storage. Prepared by Working Group III of the Intergovernmental Panel on Climate Change [Metz, B., O. Davidson, H. C. de Coninck, M. Loos, and L. A. Meyer (eds.)]. *Cambridge University Press*, Cambridge, United Kingdom and New York, NY, USA, 442 pp.

IPCC (2013) Climate change 2013: The physical science basis. Fourth assessment report, *IPCC Secretariat, Geneva, Switzerland.*

Jiang, Xi. (2011) A review of physical modelling and numerical simulation of long-term geological storage of CO_2. *Applied Energy*, 88, 3557-3566.

Jung, Y.; Zhou, Q.; Birkholzer, J.T. (2013). Early detection of brine and CO_2 leakage through abandoned wells using pressure and surface-deformation monitoring data: concept and demonstration. *Adv. Water Resources.*

Kopp, A., Class, H., Helmig, R. (2009) Investigations on CO_2 storage capacity in saline aquifers. Part 1: dimensional analysis of flow processes and reservoir characteristics. *Int J Greenhouse Gas Control*; 3:263–76

Krevor, S., Pini, R., Zuo, L., & Benson, S. M. (2012). Relative permeability and trapping of CO_2 and water in sandstone rocks at reservoir conditions.

Water Resources Research, 48(2).

Krause, A., Leskovec, J., Guestrin, C., VanBriesen, J., Faloutsos, C. (2008) Efficient sensor placement optimization for securing large water distribution networks. *J. Water Resour. Plan. Manag.* 134, 516–526.

Le Maî tre, O., Knio, O. (2010). Spectral Methods for Uncertainty Quantification: With Applications to Computational Fluid Dynamics. *Springer, New York.*

Li, H.; Zhang, D. (2007) Probabilistic collocation method for flow in porous media: Comparisons with other stochastic methods. *Water Resour. Res.*,43, 44−56.

Lindner, E. (2015) NSealR—A Brief User's Guide for Gen3; NRAP-TRS-III-0XX-2015; *NRAP Technical Report Series*; U.S. Department of Energy, National Energy Technology Laboratory: Morgantown, WV; p 118.

Loaiciga, H.A. (1989) An optimization approach for groundwater quality monitoring network design. *Water Resour. Res.* 25, 1771–1782.

Loaiciga, H.A.; Charbeneau, R.J.; Everett, L.G.; Fogg, G.E.; Hobbs, B.F.; Rouhani, S. (1992) Review of ground-water quality monitoring network design. *J. Hydraul. Eng.* 118,11–37.

Lucier, A., Zoback, M., Gupta, N., Ramakrishnan, T. S. (2006). Geomechanical aspects of CO_2 sequestration in a deep saline reservoir in the Ohio River Valley region. *Environmental Geosciences*, 13(2), 85-103.

Luckner, L.; van Genuchten, M. Th.; Nielsen, D. R. (1989) A consistent set of parametric models for the two-phase flow of immiscible fluids in the subsurface. *Water Resources Research*, 25, 2187–2193.

MacQueen, J. B. (1967) Some Methods for classification and Analysis of Multivariate Observations. Proceedings of 5th Berkeley Symposium on Mathematical Statistics and Probability. *University of California Press.* pp. 281–297.

Mahar, P.S., Datta, B. (1997) Optimal monitoring network and ground-water-pollution source identification. *J. Water Resour. Plan.* Manag. 123, 199–207.

Maltz, F. H.; Hitzl, D. L. (1979) Variance reduction in Monte Carlo computations using multi-dimensional hermite polynomial. *J Comput*

Phys; 2:345–76.

McKoy et al. (2006) FRACGEN User's Guide; U.S. Department of Energy, *National Energy Technology Laboratory*: Morgantown, WV.

Meng,Q., Jiang, X. (2014) Numerical analyses of the solubility trapping of CO_2 storage in geological formations. *Applied Energy*, 130, 581-591.

Meyer, P.D.; Valocchi, A.J.; Eheart, J.W. (1994) Monitoring network design to provide initial detection of groundwater contamination. *Water Resour. Res.* 30, 2647–2659.

Namhata, A.; Zhang, L.; Dilmore, R.M.; Oladyshkin, S.; Nakles, D.V. (2016) Modeling pressure changes due to migration of fluids into the Above Zone Monitoring Interval of a Geologic Carbon Storage Site, *Applied Energy*, *Submitted*.

NETL (National Energy Technology Laboratory) (2011) National Risk Assessment Partnership (NRAP) Project Summary, http://www.netl.doe.gov/publications/factsheets/rd/R%26D179.pdf, 15/01/2014

NETL (2014a) "National Risk Assessment Partnership (NRAP) - FY14 Project Management Plan", Field Work Proposal Number: NRAP_FY14, *National Energy Technology Laboratory*, Office of Research and Development, March 31 (Revision 1).

NETL (2014b) "National Risk Assessment Partnership and Regional Carbon Sequestration Partnerships – Opportunities for Collaboration", Draft Report, *National Energy Technology Laboratory*, Office of Research and Development, February 28.

Nicot JP, Oldenburg CM, Bryant SL, Hovorka SD et al (2009) Pressure perturbations from geologic carbon sequestration: area of review boundaries and borehole leakage driving forces. *Energy Procedia* 1(1):47–54

Nielsen, L. C.; Bourg, I. C.; Sposito, G. (2012) Predicting CO_2-water interfacial Tension Under Pressure and Temperature Conditions of Geologic CO_2 storage. *Geochimica et Cosmochimica Acta*, 81, 28-38.

Nordbotten J, Celia M, Bachu S (2004) Analytical solutions for leakage rates through abandoned wells. *Water Resources Research*, 40

Nordbotten, J.M., Celia, M.A., Bachu, S. (2005) Injection and storage of CO_2 in deep saline aquifers: analytical solution for CO_2 plume evolution during injection. *Transp. Porous Media,* 58, 339–360.

Nordbotten, J. M.; Celia, M. A. (2006) Similarity solutions for fluid injection into confined aquifers. *J. Fluid Mech.*, 561, 307–327.

NPC (National Petroleum Council), (1984). U.S. National Petroleum Council Public Database. http://www.npc.org.

Oladyshkin S, Class H, Helmig R, Nowak W.. (2010) Highly efficient tool for probabilistic risk assessment of ccs joint with injection design, Computational Methods in Water Resources (CMWR), XVIII *International Conference on Water Resources*, Barcelona, Spain.

Oladyshkin S., Class H., Helmig R. and Nowak W. (2011a) A concept for data-driven uncertainty quantification and its application to carbon dioxide storage in geological formations. *Advances in Water Resources*, 34: 1508–1518.

Oladyshkin, S.; Class, H.; Helmig, R.; Nowak, W. (2011b), An integrative approach to robust design and probabilistic risk assessment for storage in geological formations. *Comput. Geosci.* 15, 565—577.

Oladyshkin S.; de Barros, F. P. J.; Nowak W. (2012), Global sensitivity analysis: a flexible and efficient framework with an example from stochastic hydrogeology. *Advances in Water Resources*, 37, 10-22.

Oladyshkin, S., Nowak, W., (2012). Date-driven uncertainty quantification using the arbitrary polynomial chaos expansion. *Reliab. Eng. Syst. Saf.* 106, 179–190.

Oladyshkin, S., Schröder, P., Class, H., Nowak, W. (2013). Chaos Expansion based Bootstrap Filter to Calibrate CO_2 Injection Models. *Energy Procedia*, 40, 398-407

Oldenburg, C.M., Pruess, K. and Benson, S.M., (2001). Process Modeling of CO_2 Injection into Natural Gas Reservoirs for Carbon Sequestration and Enhanced Gas Recovery. *Energy & Fuels*, Vol. 15, No. 2, pp. 293-298.

Pawar, R.; Bromhal, G.; Dilmore, R.; Foxall, B.; Jones, E.; Oldenburg, C.; Stauffer, P.; Unwin, S.; Guthrie, G. (2013) Quantification of Risk Profiles for Atmosphere and Groundwater, NRAP-TRS-III-003-2013, *NRAP*

Technical Report Series, US Department of Energy, National Energy Technology Laboratory, Morgantown, WV, January 25.

Pawar, R; Bromhal, G.; Chu, S.; Dilmore, R.M.; Oldenburgh, C. M.; Stauffer, P. H.; Zhang, Y.; Guthrie, G.D. (2016) The National Risk Assessment Partnership's integrated assessment model for carbon storage: A tool to support decision making amidst uncertainty, International Journal of Greenhouse Gas Control. 52, 175-189.

Pruess, K., (2004). Numerical simulation of CO_2 leakage from a geologic disposal reservoir, including transitions from super-to subcritical conditions, and boiling of liquid CO_2. *SPE Journal*, 9(02), 237-248.

Pruess K (2005) ECO2N: a TOUGH2 fluid property module for mixtures of water, NaCl, and CO_2. Report LBNL-57952. *Lawrence Berkeley National Laboratory*, Berkeley

Pruess, K. (2008). On CO_2 fluid flow and heat transfer behavior in the subsurface, following leakage from a geologic storage reservoir. *Environmental Geology*, 54(8), 1677-1686.

Pruess, K., & Nordbotten, J., (2011). Numerical simulation studies of the long-term evolution of a CO_2 plume in a saline aquifer with a sloping caprock. *Transport in porous media*, 90(1), 135-151.

Pruess, K., Oldenburg, C., Moridis, G., (2012). TOUGH2 User's Guide, Version 2. *Lawrence Berkeley National Laboratory.*

Raza, Y. (2009), Uncertainty analysis of capacity estimates and leakage potential for geologic storage of carbon dioxide in saline aquifers. (M.S. Thesis), *Massachusetts Institute of Technology.*

Reed, P.M.; Minsker, B.S. (2004) Striking the balance: long-term groundwater monitoring design for conflicting objectives. *J. Water Resour. Plan. Manag.* 130, 140–149.

Robert, C. P.; Casella, G. (2004) Monte Carlo methods. *New York: Springer.*

Saltelli, A.; Ratto, M.; Andres, T. (2008), Global Sensitivity Analysis: The Primer, *John Wiley & Sons.*

Rohmer, J., & Seyedi, D. M. (2010). Coupled large scale hydromechanical modelling for caprock failure risk assessment of CO_2 storage in deep saline aquifers. *Oil & Gas Science and Technology*–Revue de l'Institut Français

du Pétrole, 65(3), 503-517.

Rutqvist, J., (2012). The geomechanics of CO_2 storage in deep sedimentary formations. *Geotechnical and Geological Engineering*, 30(3), 525-551.

Saadatpoor, E., Bryant, S. L., Sepehrnoori, K. (2010). New trapping mechanism in carbon sequestration. *Transport in porous media*, 82(1), 3-17.

Sarkar, S., Toksöz, M. N., Burns, D.R. (2004), Fluid Flow Modeling in Fractures, Dept. of Earth, Atmospheric and Planetary Sciences, *Massachusetts Institute of Technology*, Cambridge, MA.

Singh, A., Minsker, B.S. (2008) Uncertainty-based multi objective optimization of groundwater remediation design. *Water Resour. Res.* 44, W02404.

Snow, D.T. (1964), A parallel plate model of fractured permeable media, *Ph.D. Thesis, University of California, Berkeley*, USA.

Sobol, I.M. (1990), On sensitivity estimation for nonlinear mathematical models, *Mathem. Mod.* 2 (1), 112–118.

Sobol, I. (2001), Global sensitivity indices for nonlinear mathematical models and their Monte Carlo estimates, *Math. and Compu. in Sims.*, 55, 271–280.

Soeder D.J.; Sharma, S.; Pekney, N.; Hopkinson, L.; Dilmore, R.; Kutchko, B.; Stewart, K.C.; Hakala, A.; Capo, R. (2014) An approach for assessing engineering risk from shale gas wells in the United States, *International Journal of Coal Geology*, 126:4-19.

Sudret, B. (2008), Global sensitivity analysis using polynomial chaos expansions, *Reliability Engineering and System Safety*, 93(7), 964–979.

Sun, A.Y., Painter, S.L., Wittmeyer, G.W. (2006) A robust approach for iterative contaminant source location and release history recovery. *J. Contam. Hydrol.* 88,181–196.

Sun, A.Y.; Nicot, J.P. (2012) Inversion of pressure anomaly data for detecting leakage at geologic carbon sequestration sites. *Adv. Water Resour.*, 20–29.

Sun, A.Y., Nicot, J.-P., Zhang, X. (2013) Optimal design of pressure-based leakage detection monitoring networks for geologic carbon sequestration repositories. *Int. J. Greenh. Gas Control* 19, 251–261.

Szulczewski, M.; Juanes, R. (2009), A simple but rigorous model for calculating CO_2 storage capacity in deep saline aquifers at the basin scale, *Energy Procedia*,Volume 1, Issue 1, GHGT9 Procedia, Pages 3307-3314.

Ucinski, D., Patan, M. (2007) D-optimal design of a monitoring network for parameter estimation of distributed systems. *J. Global Optimiz.* 39, 291–322.

U.S. DOE (2009) Best practices for: monitoring, verification, and accounting of CO_2 stored in deep geologic formations. *US Department of Energy*, DOE/NETL-311/081508

U.S. Environmental Protection Agency, (2010) Geologic CO_2 Sequestration Technology and Cost Analysis. *EPA, Washington, DC.*

Van der Most, M.A. (2008) The analysis of directional permeability of fractured reservoirs: A case study from the Tata area, Morocco, M.S. Thesis, Delft University of Technology.

Varre, S. B., Siriwardane, H. J., Gondle, R. K., Bromhal, G. S., Chandrasekar, V., & Sams, N., (2015). Influence of geochemical processes on the geomechanical response of the overburden due to CO_2 storage in saline aquifers. *International Journal of Greenhouse Gas Control*, 42, 138-156.

Vilarrasa, V., Carrera, J., Bolster, D., & Dentz, M., (2013). Semianalytical solution for CO_2 plume shape and pressure evolution during CO_2 injection in deep saline formations. *Transport in porous media*, 97(1), 43-65.

Wainwright, H.M., Finsterle, S., Zhou, Q., Birkholzer, J.T., (2013). Modeling the performance of large-scale CO_2 storage systems: a comparison of different sensitivity analysis methods. *Int. J. Greenh. Gas Control* 17, 189–205.

Wang, Z.; Small, M.J. (2014) A Bayesian approach to CO_2 leakage detection at saline sequestration sites using pressure measurements. *International Journal of Greenhouse Gas Control*. 30, 188-196.

Wang, Z., & Small, M. J. (2015). Statistical performance of CO_2 leakage detection using seismic travel time measurements. *Greenhouse Gases: Science and Technology.*

Wiener N. (1938), The homogeneous chaos. *Am J Math*, 60: 897–936.

Xiu, D.; Karniadakis, G. E. (2003), Modeling uncertainty in flow simulations via generalized polynomial chaos. *J. Comput. Phys.* 187, 137—167.

Xu, T., Apps, J. A. and Pruess, K., (2004). Numerical simulation of CO_2 disposal by mineral trapping in deep aquifers. *Applied geochemistry*, 19(6), 917-936.

Xu, J., Johnson, M.P., Fischbeck, P.S., Small, M.J., VanBriesen, J.M. (2010) Robust placement of sensors in dynamic water distribution systems. *Eur. J. Oper. Res.* 202,707–716.

Yang, Y.M., Small, M.J., Ogretim, E.O., Gray, D.D., Bromhal, G.S., Strazisar, B.R., Wells, A.W. (2011) Probabilistic design of a near-surface CO_2 leak detection system. *Environ. Sci. Technol.* 45, 6380–6387.

Yonkofski, C.M.R; Gastelum, J.A.; Porter, E.A.; Rodriguez, L.R.; Bacon, D.H.; Brown, C.F. (2016) An optimization approach to design monitoring schemes for CO_2 leakage detection, International Journal of Greenhouse Gas Control, 47, 233-239, http://dx.doi.org/10.1016/j.ijggc.2016.01.040.

Zhang, L., Dilmore, R., Bromhal, G. (2016). Effect of boundary openness, reservoir size and effective permeability of CO_2 on pressure and CO_2 saturation predictions by numerical simulation under geologic carbon sequestration conditions. *Greenhouse Gases: Science & Technology.* In press. DOI: 10.1002/ghg.1586.

Zhang, Y.; Liu, Y.; Pau, G.; Oladyshkin, S.; Finsterle, S. (2016) Evaluation of multiple reduced-order models to enhance confidence in global sensitivity analysis. *Int. J. Greenh. Gas Control* 49, 217-226.

Zhang, Y.; Pau, G. Reduced-Order Model Development for CO_2 Storage in Brine Reservoirs; NRAP-TRS-III-005-2012; *NRAP Technical Report Series*; U.S. Department of Energy, National Energy Technology Laboratory: Morgantown, WV, (2012); p 20.

Zhang, Y.; Sahinidis, N.V. (2013), Uncertainty Quantification in CO_2 Sequestration Using Surrogate Models from Polynomial Chaos Expansion, *Industrial & Engineering Chemistry Research*, 52(9).

Zhou, Q., Birkholzer, J. T., Mehnert, E., Lin, Y. F., & Zhang, K. (2010). Modeling basin - and plume - scale processes of CO_2 storage for full - scale deployment. *Ground water*, 48(4), 494-514.

Zhou, Q., Birkholzer, J.T., Wagoner, J.L. (2011). Modeling the potential impact of geologic carbon sequestration in the southern San Joaquin basin, California. *The Ninth Annual Carbon Capture & Sequestration Conference*, Pittsburgh, PA.

Appendices

Contents

Appendix A

Supporting Information for Chapter 2

A.1 Storage Reservoir Reduced Order Models (ROMs)

Lawrence Berkley National Laboratory (LBNL) has developed the first reservoir ROM, in the form of look-up tables. It is based on TOUGH-2 simulations of a naturally faulted sandstone reservoir with mild to moderate complexity (Kimberlina, CA) (Wainright, 2012). The look-up tables were generated by using the numerical model to perform multiple simulations of large-scale CO_2 injection for 50 years at a rate of 5 million tons/year. Each of the simulation runs was performed for 200 years including 150 years of post-injection relaxation. In total, 300 simulation runs were performed to capture the effect of variability in three reservoir parameters, i.e., porosity and permeability of target reservoir and permeability of caprock. Sensitivity analysis on these parameters was used to further reduce the 300 runs to 54 representative runs that captured the effect of variability in the reservoir parameters. The time and space-dependent reservoir pressure and saturation results for these 54 runs were incorporated into look-up tables for use by the IAM. This was followed by a second generation ROM, also in the form of a look-up table, which was based on the same reservoir and injection scenario but which included a 950 year post-injection period.

NRAP has also been focused on the development of second-generation reservoir ROMs using surrogate reservoir (oil field reservoir and saline formation) models and polynomial chaos expansion (oil field reservoir).

A.1.1 Oil Field and Depleted Gas Field Formation Reservoir ROM using Grid-Based Surrogate Reservoir Model (SRM)

The SRM model was developed using a neural network approach that employs machine-learning techniques to train, calibrate and validate a data driven model that is capable of replicating the results of fluid flow through porous media in a simulation grid cell. The model is trained to reproduce pressure and saturation changes within a simulation grid cell as a function of reservoir characteristics, imposed physics and operational constraints throughout the field. This ROM has been developed and applied to the depleted gas fields of the Otway site in Australia as well as the SACROC oil field in Texas. In both cases, the SRM results were compared to the results of commercial reservoir simulators (e.g., Schlumberger's Eclipse simulator or the Computer Modeling Group reservoir simulation software, IMEX and CMOST), which had been history-matched using actual site monitoring data. Figure A-1 shows the comparison of SRM results to that of a simulator.

A.1.2 Oil Field Reservoir ROM - Polynomial Chaos Expansion (PCE)

The PCE modeling approach uses a Mixed Integer Programming (MIP) based, best subset selection method to iteratively build PCE models for

predicting subsurface conditions (e.g., pressure, CO_2 saturation) during geologic CO_2 storage. This particular PCE method is able to capture synergistic effects between low- and high-order polynomial terms, thus providing high accuracy and computational efficiency. The technique has been used to conduct simulations of a two-dimensional benchmark problem as well as the SACROC oil field in Texas. In both cases, output variables from a numerical simulator (i.e., Schlumberger's Eclipse simulator) have been approximated as polynomial functions of uncertain parameters (Zhang and Sahinidis, 2012). Figure A-2 shows the comparison of PCE reservoir simulator results to that of a TOUGH-2 simulator.

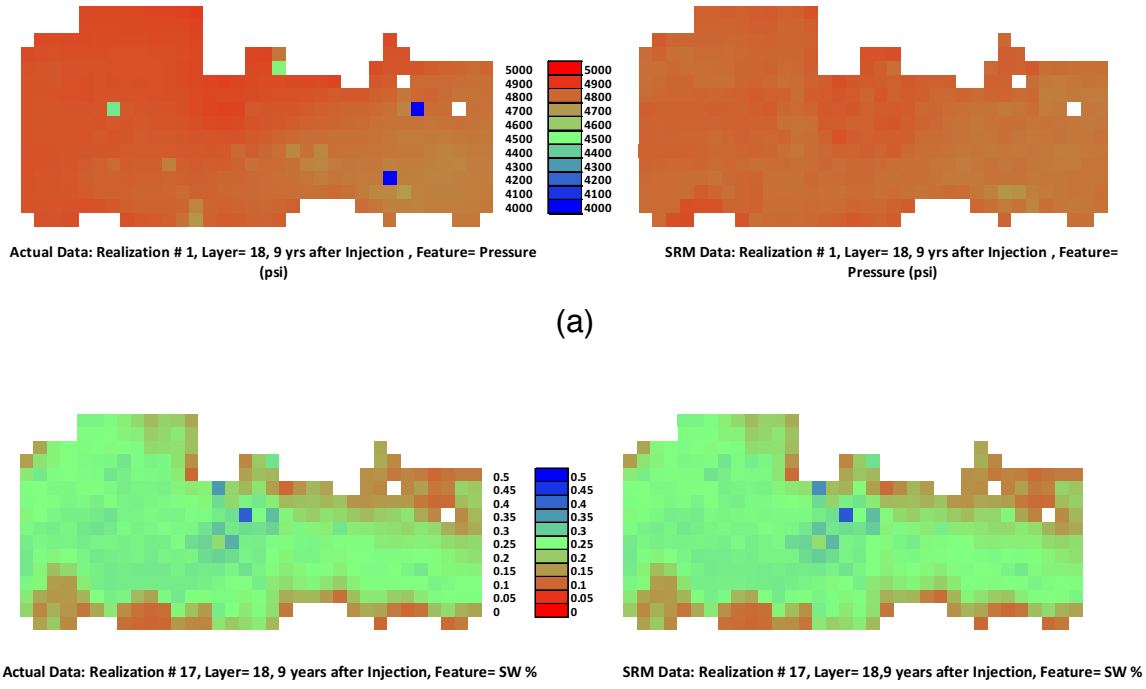

Figure A-1: Comparison between the results of simulation model (left) and SRM (right) for (a) pressure distribution (b) water saturation, 9 years after injection (Shahkarami et al., 2014).

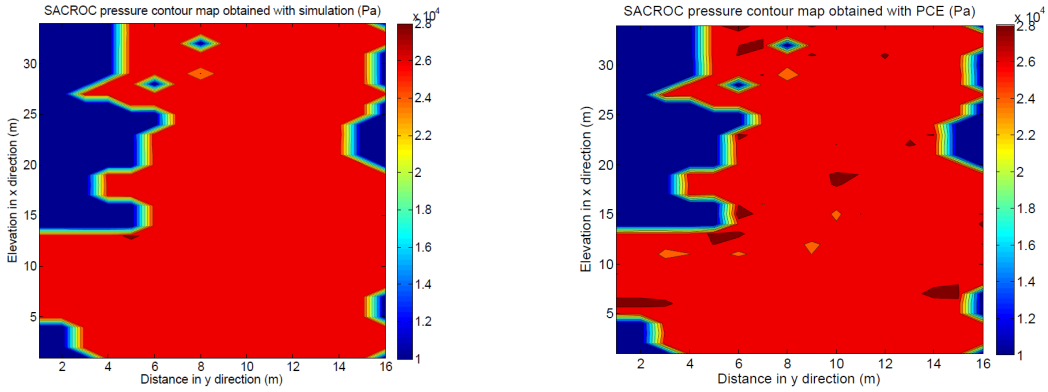

(a)

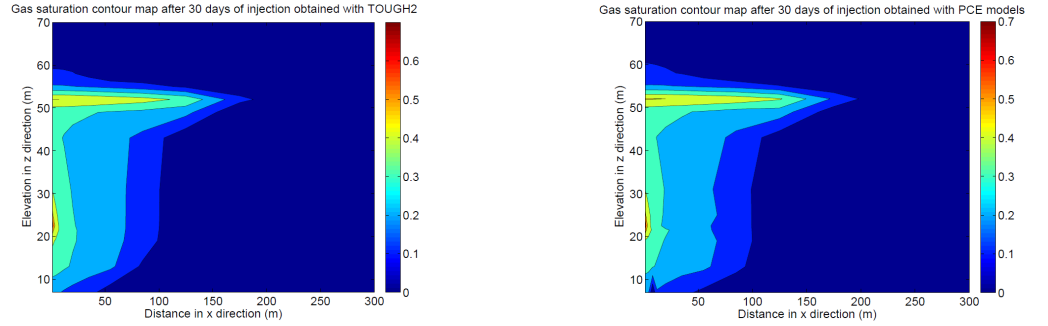

(b)

Figure A-2: Comparison between the results of TOUGH-2 (left) and PCE (right) for (a) pressure distribution (b) CO_2 saturation.

A.2 Wellbore ROMs

The models in the WLAT tool are built based on two approaches:

a. Full-physics simulations are performed over a range of expected parameter space with the results compiled into ROMs to be sampled based on given input conditions and,

b. Physical models, based on a first principles approach, are simplified based on assumptions, mathematical tools, and empirical observations to create computationally efficient reduced-physics models.

The WLAT uses four different ROMs from the literature, developed within and outside the NRAP framework (Huerta and Vasylkivska, 2015):

i. **Cemented Wellbore Model:** This model was developed by running many full-physics simulations over a range of key parameters at Los Alamos National Laboratory (LANL), as part of NRAP. The results are constructed into ROMs to be sampled based on input conditions. These ROMs estimate the multiphase flow of CO_2 and brine along a cemented wellbore. The model can treat leakage to a thief zone, aquifer, or to the atmosphere.

ii. **Multi-segmented Wellbore Model**: This model is an adaptation of the models developed at Princeton University. Reduced-physics models were used to treat the leakage of CO_2 and brine along wells with multiple thief zones. This model provides a useful validation case for the Cemented Wellbore Model.

iii. **Open Wellbore Model**: This model, developed at Lawrence Berkeley National Laboratory (LBNL) as part of NRAP, is a reduced-physics model based on the drift-flux approach. This model treats the leakage of CO_2 up an open wellbore or up open (i.e., uncemented) casing/tubing.

iv. **Brine Leakage Model**: This reduced-physics model was developed based on simple reactive transport theory and is tuned with experimental observations at the National Energy Technology Laboratory (NETL), as part of NRAP. This model estimates the leakage of brine considering the effects that geochemical alteration (e.g., dissolution and precipitation) may have on the leak-path permeability.

A.3 NSealR ROM

The NSealR code has been developed to simulate the flow through a thin seal formation during CO_2 storage as part of a larger analysis effort, all defined within the CO_2-PENS (Predicting Engineered Natural Systems) (Stauffer et al., 2009) integrated system analysis code to evaluate storage risk. CO_2-PENS incorporates a number of distinct components for CO_2 generation, transport, and injection into a geologic reservoir, including the potential migration out of target reservoir and impact to resources such as shallow groundwater aquifers to simulate the behavior of the entire system at the site (reservoir to receptor). To simulate the storage of CO_2 during and after injection, distinct sub-models are linked to describe the geologic storage site, including models of the reservoir, injection wells, the overlying aquifers, and potential leakage pathways from the reservoir such as existing wellbores and faults.

As such, the NSealR is conceptually a middleman for the CO_2-PENS model, taking the output from the reservoir model (in the form of CO_2 saturation and pressures at the base of the seal horizon) and providing input to the

overlying aquifer models in the form of CO_2 and brine mass flux at the top of the seal horizon. The structure of NSealR is relatively simplistic in concept and divides the major operations into three tasks. The basic computation tasks/models of NSealR are: (1) define the permeability of each cell; (2) define the thickness of each cell; and (3) compute fluid flow.

Appendix B

Supporting Information for Chapter 3

B.1 Fluid Properties

These fluid property variations with depth have been incorporated in the present version of AZMI ROM. Depending on the depth of the AZMI formation defined by the user; the code calculates the fluid properties based on look-up tables. The property data in the look-up tables were taken from multiple sources (Lemmon et al., 2010; Wagner and Pruss, 2002; Huber et al., 2009; Span and Wagner, 1996; Fenghour et al., 1998). The fluid density and viscosity were generated using NSealR ROM, which relies upon recent equation-of-state publications on pure water, saline solutions, and CO_2 over a range of 0.10 to 60 MPa, 0 to 180 ^{o} C, and 0 to 80,000 ppm salinity. A multi-model predictive system solubility calculator (Wang et al., 2013) was used to compute the solubility of CO_2 in brine. Using bilinear interpolation of the available datasets, the fluid properties were calculated for defined storage scenarios.

The variability of the various fluid properties with temperature, pressure, and/or salinity is shown in Figures B-1 to B-4 for scenarios above the CO_2 critical point (7.38 MPa at 31.1 ° C).

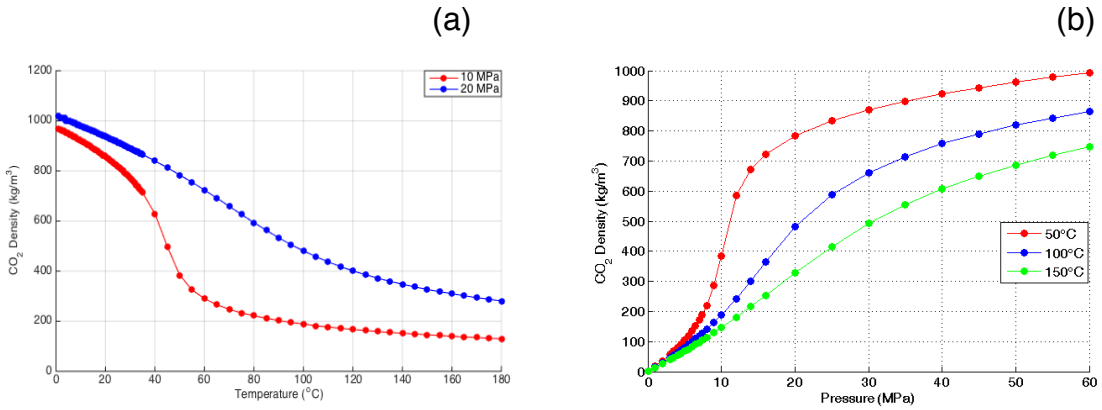

Figure B-1: CO_2 density as a function of: (a) temperature and, (b) pressure

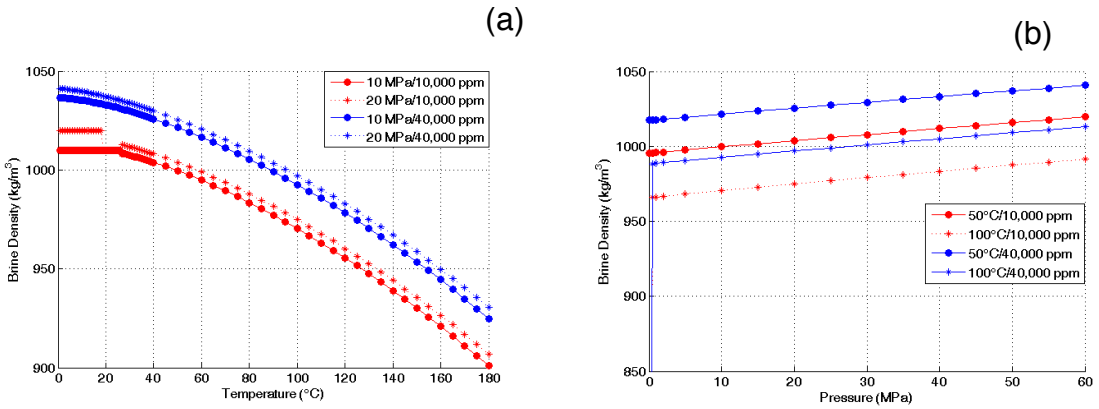

Figure B-2: Brine density as a function of: (a) temperature at different pressures and salt concentrations and, (b) pressure at different temperatures and salt concentrations.

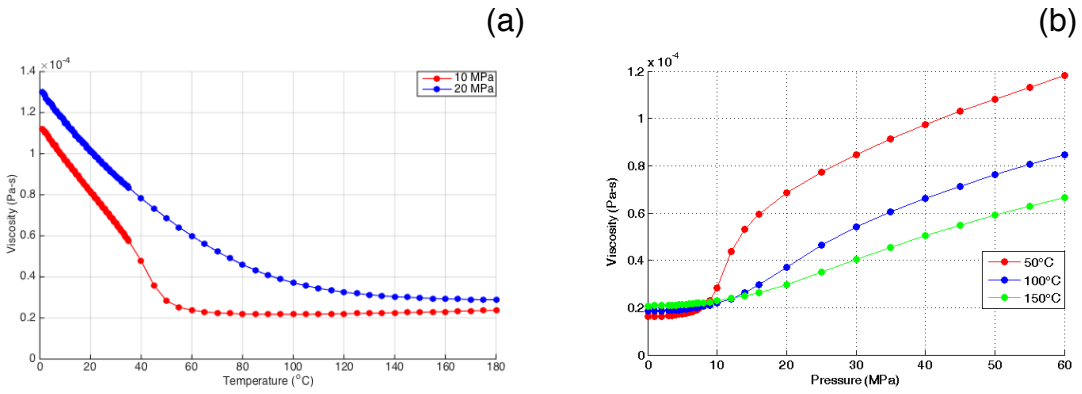

Figure B-3: CO_2 viscosity as a function of: (a) temperature at different pressures and, (b) pressure at different temperatures.

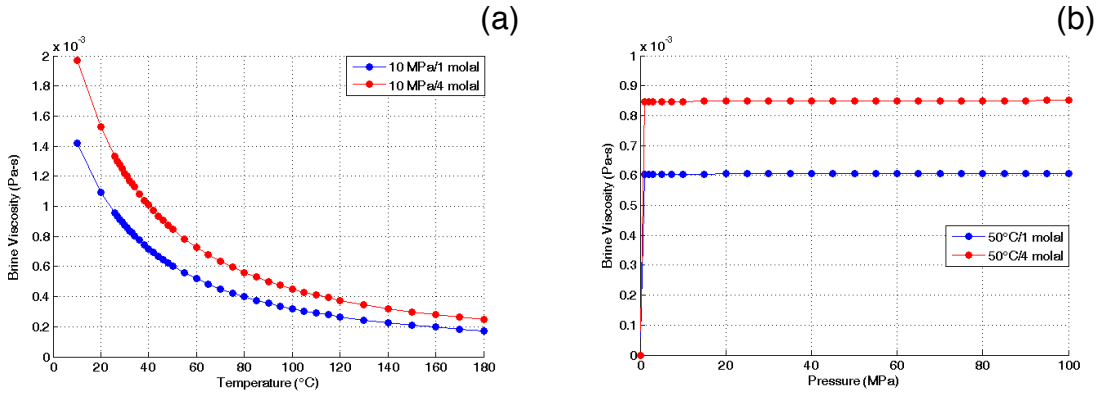

Figure B-4: Brine viscosity as a function of (a) temperature at different pressures and salt concentrations and, (b) pressure at different temperatures and salt concentrations.

B.2 TOUGH2 Model Setup

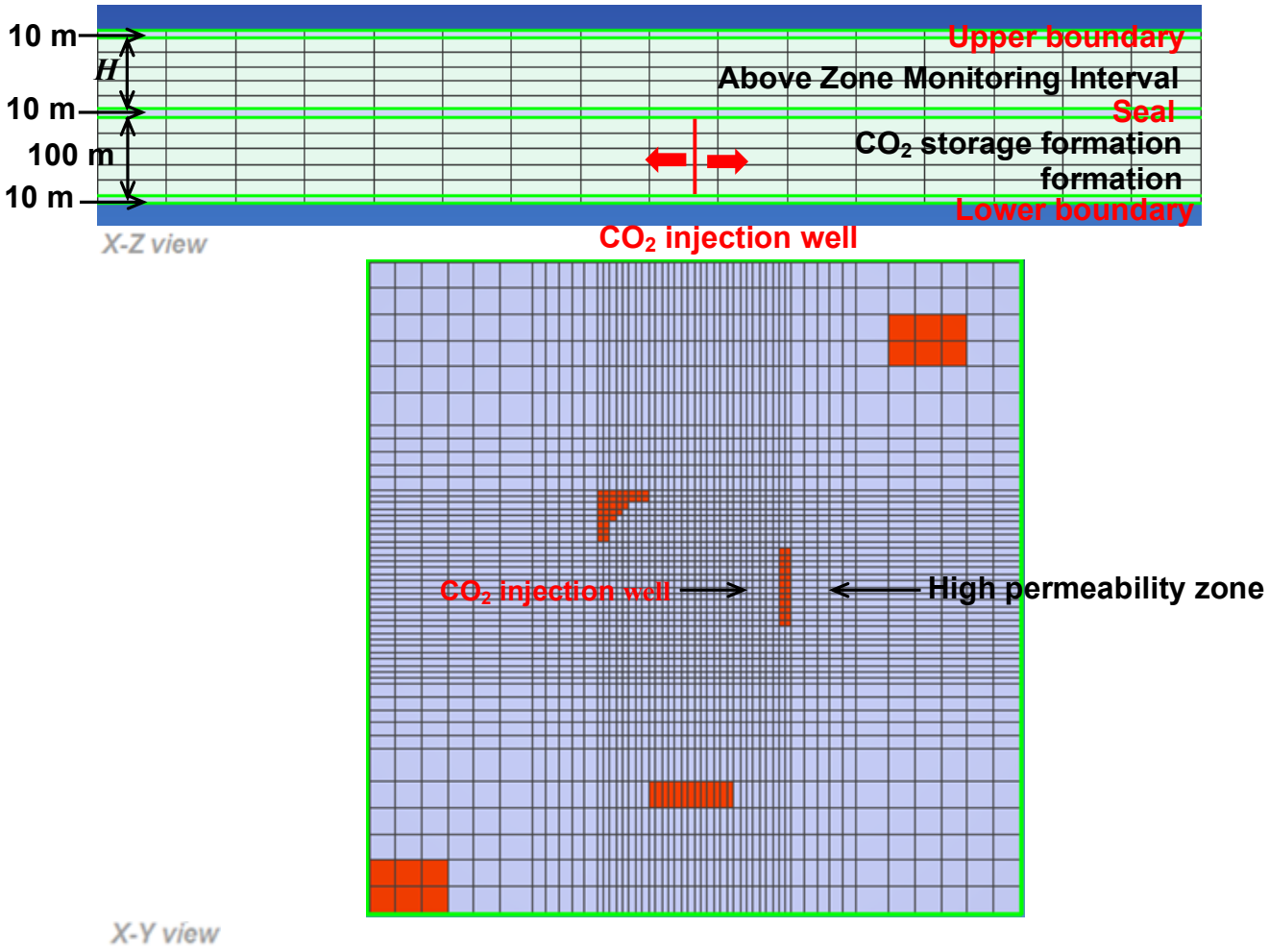

Figure B-5: Configuration of the 3-D TOUGH2 Model. The X-Y view shows small grid blocks in the central region surrounding the CO_2 injection well. The thickness of the CO_2 storage formation is 100 m. The thickness of the AZMI (H) is 3 m for Scenario I, and H is 90 m for Scenario II.

Appendix C

Supporting Information for Chapter 5

C.1 FRACGEN

The models described in this study for generating the fracture networks are implemented by FRACGEN (McKoy et al., 2006). FRACGEN generates fractures or clusters centered within a generation region, but it presents only the network generated within an unbiased "flow region," which is the rectangular area in which flow can be modeled (McKoy and Sams, 2007). FRACGEN requires input file containing parameters and statistics for fracture attributes (length, position, orientation and density in space). Most of the input describes fracture network attributes of individual sets and may be classified as either fixed variables, statistics, or percent. Table C-1 presents some generalized equations for calculating a few useful common statistics.

Table C-1: Equations for Calculating Common Statistics

Gaussian Distribution	$\chi = (\sum_{i=1}^{n} x_i)/n$ $s_x = ((\sum_{i=1}^{n} (x_i - \chi)^2) / (n-1))^{1/2}$
Exponential Distribution	$\chi = (\sum_{i=1}^{n} x_i)/n$ $s_x = (\sum_{i=1}^{n} x_i)/n$
Lognormal Distribution	$\chi = \exp(U + 0.5 s_u^2)$ $s_x = (\chi^2 (\exp(s_u^2) - 1))^{1/2}$ $U = (\sum_{i=1}^{n} \ln(x_i))/n$ $s_u^2 = (\sum_{i=1}^{n} (\ln(x_i) - U)^2/(n-1)$
Uniform Distribution	$\chi = n/q$
Poisson Distribution	$\chi = n/q$ $s_x = (\sum_{i=1}^{q} (x_i - n/q)^2 / (q-1))^{1/2}$
Fracture Center-Point Density	$D_i = \lambda_i / (b_i l_i \cos(\phi_i)) = \Lambda_i / (b_i l_i)$ $b_i = \int_{\theta min}^{\theta max} \cos(\theta)\ p(\theta) d\theta,$ ϕ_i = angle between pole to fracture set and scanline sample, θ = fracture orientation. Λ_i = the average number of fractures encountered per unit length of sample line that is oriented normal to the fracture set.
Cluster Center-Point Density	$D_{ci} = \lambda_{ci} / (b_i l_{ci} \cos(\phi_i)) = \Lambda_{ci} / (b_i l_{ci})$ l_{ci} = cluster length Λ_{ci} = the average number of clusters encountered per unit length of sample line that is oriented normal to the fracture set.
Degree of Clustering	$\zeta = 100\%(1 - n/qs^2) / (1 - n/qs^2_{max})$ n = number of fractures of set i q = number of segments in sample line s^2 = variance in number of fractures per segment s^2_{max} = variance if all fractures fall into one segment

Appendix References

Fenghour, A.; Wakeham, W. A.; Vesovic, V. (1998) The Viscosity of Carbon Dioxide. *Journal of Physical and Chemical Reference Data*, 27, 31–44.

Huber, M. L.; Perkins, R. A.; Laesecke, A.; Friend, D. G.; Sengers, J. V.; Assael, M. J.; Metaxa, I. M.; Vogel, E.; Mares, R.; Miyagawa, K. (2009) New International Formulation for the viscosity of H_2O. *Journal Physical and Chemical Reference Data*, 38, 101–125.

Huerta, N. J.; Vasylkivska, V. S. Well Leakage Analysis Tool (WLAT) User's Manual; NRAP-TRS-III-XXX-2015; *NRAP Technical Report Series*; U.S. Department of Energy, National Energy Technology Laboratory: Morgantown, WV, 2015.

Lemmon, E. W.; Huber, M. L.; McLinden, M. O. (2010) NIST Standard Reference Database 23: Reference Fluid Thermodynamic and Transport Properties-REFPROP, Version 9.0; Standard Reference Data Program; U.S. Department of Commerce, *National Institute of Standards and Technology*: Gaithersburg, MD.

McKoy et al. (2006) FRACGEN User's Guide; U.S. Department of Energy, *National Energy Technology Laboratory*: Morgantown, WV.

McKoy, M.L., Sams, W.N. (2007), Tight gas reservoir simulation: Modeling discrete irregular strata-bound fracture network flow, including dynamic recharge from the matrix. United States. UNT Digital Library. http://digital.library.unt.edu/ark:/67531/metadc690581/, Accessed July 18, 2016.

Shahkarami, A.; Mohaghegh, S.D.; Gholami, V.; Haghighat, A.; Moreno, D. (2014) Modeling pressure and saturation distribution in a CO_2 storage project using a Surrogate Reservoir Model (SRM). Greenhouse Gas Sci Technol. 4:1–27.

Span, R.; Wagner, W. (1996), A New Equation of State for Carbon Dioxide Covering the Fluid Region from the Triple-Point Temperature to 1100 K

at Pressures up to 800 MPa. *Journal of Physical and Chemical Reference Data*, 25, 1509–1597.

Wagner, W. P.; Pruss, A. (2002), The IAPWS Formulation 1995 for the Thermodynamic Properties of Ordinary Water Substance for General and Scientific Use. *Journal of Physical and Chemical Reference Data*, 31, 387–535.

Wainwright, H.; Finsterle, S.; Zhou, Q.; Birkholzer, J. (2012) Modeling the Performance of Large-Scale CO_2 Storage Systems: A Comparison of Different Sensitivity Analysis Methods, NRAPTRS-III-002-2012; NRAP Technical Report Series; U.S. Department of Energy, National Energy Technology Laboratory: Morgantown, WV.

Wang, Z.; Small, M.J.; Karamalidis, A.K. (2013), Multimodel predictive system for carbon dioxide solubility in saline formation waters. *Environ. Sci. Technol.* 47, 1407–1415.

Zhang, Y.; Sahinidis, N.V. (2013), Uncertainty Quantification in CO_2 Sequestration Using Surrogate Models from Polynomial Chaos Expansion, Industrial & Engineering Chemistry Research, 52(9).